

RAJ

**DETERMINING THE EFFECT OF MODAL TRUNCATION AND
MODAL ERRORS IN
COMPONENT MODE SYNTHESIS METHODS**

by

Timothy W. Widrick

The George Washington University

Thesis directed by

Dr. Robert Tolson

Professor of Engineering and Applied Science

July 1, 1992

ABSTRACT

Structural models are growing larger and more complex and, hence, their finite element representations consume more time for model verification and analysis. A technique being used to reduce model complexity and development time while still retaining model fidelity is the method of component mode synthesis (CMS).

The first concern of this research is determining the effect of component modal truncation in component mode synthesis. This is an important concern in CMS since it is the truncation of modes that reduces model complexity. The truncation of modes was studied by using MSC/NASTRAN and applying three different CMS methods, namely a fixed-interface, a free-interface, and a hybrid-interface method, to a space station model (HMB-2R) having over 4500 degrees of freedom. It was found that the hybrid-interface (which mimicked the physical boundary conditions) and the fixed-interface method both performed well while the free-interface method gave less accurate results.

The second concern of this research is to determine the effect of component level errors on the system mode shapes and frequencies when using component mode synthesis. This is to simulate a real situation where each component model does have errors. The effect of these errors was studied by first adding errors to the components of a two dimensional version of HMB-2R and then using the Craig-Bampton method of CMS to calculate the system mode shapes and frequencies. It was found that the errors at the component level are significantly magnified at the system level, particularly for the fundamental system mode. However, these results depend on the validity of the method used to alter the mass and stiffness matrices of each component.

TABLE OF CONTENTS

ABSTRACT	ii
TABLE OF CONTENTS	iii
LIST OF FIGURES	v
LIST OF TABLES	viii
NOMENCLATURE	ix
I. INTRODUCTION	1
II. PRELIMINARY CONCEPTS AND DEFINITIONS	4
2.1 Component Modes	6
III. A GENERALIZED PROCEDURE OF COMPONENT MODE SYNTHESIS	9
3.1 Extending to N Components	13
3.2 Extending to Forced Systems	13
IV. TWO COMPONENT MODE SYNTHESIS METHODS	14
4.1 The Craig-Bampton Method	14
4.2 The Craig-Chang Method	25
4.3 Differences in the Craig-Bampton and Craig-Chang Methods	39
V. COMPONENT MODE SYNTHESIS ON HMB WITH MSC/NASTRAN	40
5.1 Hybrid Case	43
5.2 Free Case	49
5.3 Fixed Case	53
5.4 Conclusions	57
VI. ERROR STUDY WITH BEAM MODEL IN MATLAB	58
6.1 Model Development	59
6.2 The Craig-Bampton Method on the Beam Model	59
6.3 The Error Study	63
VII. CONCLUDING REMARKS	72
REFERENCES	75
A. NORMAL, CONSTRAINT, AND ATTACHMENT MODES	77
A.1 Normal Modes	77
A.2 Constraint Modes	78
A.3 Attachment Modes for Constrained Components	81

A.4 Attachment Modes for Unconstrained Components	82
A.5 Inertia Relief Attachment Modes	84
A.6 Residual Attachment Modes for Both Constrained and Unconstrained Components	88
B. DERIVATION OF CONSTRAINT EQUATION (4.12)	91
C. HMB-2R FLEXIBLE MODE SHAPES UP TO 50 HZ	93
D. THE FINITE ELEMENT METHOD	99
E. BEAM MODEL FLEXIBLE MODE SHAPES UP TO 100 HZ	102
F. THE ANALYTICAL MODEL IMPROVEMENT METHOD	104

LIST OF FIGURES

Figure 2.1: (a) Full structural system; (b) components α and β of the structure.	4
Figure 4.1: The full system for <i>Example 1</i>	16
Figure 4.2: The full system for <i>Example 2</i>	31
Figure 5.1: The HMB-2R finite element model.	40
Figure 5.2: Nodes on HMB-2R used for calculating <i>MCC</i>	43
Figure 5.3: Stick-figure of HMB-2R.	44
Figure 5.4: Restraining of components for hybrid runs.	44
Figure 5.5: Component restraint for the fixed case.	53
Figure 6.1: The beam model similar to HMB-2R.	58
Figure 6.2: Results of using the best case errors (0.5% on eigenvalues and 1% on modes). (a) Errors on both; (b) errors on modes; (c) errors on eigenvalues.	65
Figure 6.3: Results of using the worst case errors (2.5% on eigenvalues and 5% on modes). (a) Errors on both; (b) errors on modes; (c) errors on eigenvalues.	66
Figure 6.4: Results of adding errors to the main truss only.	68
Figure 6.5: Results of adding errors to the outboard truss only.	68
Figure 6.6: Results of errors to the alpha joint only.	69
Figure 6.7: Results of adding errors to the EPS only.	69
Figure 6.8: Results of adding errors to Fwd PV only.	69
Figure 6.9: Results of adding errors to Aft PV only.	70
Figure 6.10: Results of adding errors to the TCS only.	70
Figure A.1: A cantilevered beam substructure.	78
Figure A.2: Normal modes of the constrained component.	78

Figure A.3: Constraint modes of cantilever beam.	80
Figure A.4: Attachment modes of the constrained component.	82
Figure A.5: One choice of coordinates for the unrestrained beam.	84
Figure C.1: HMB-2R mode shape one, 4.66 Hz.	93
Figure C.2: HMB-2R mode shape two, 5.97 Hz.	93
Figure C.3: HMB-2R mode shape three, 7.54 Hz.	93
Figure C.4: HMB-2R mode shape four, 10.8 Hz.	94
Figure C.5: HMB-2R mode shape five, 11.9 Hz.	94
Figure C.6: HMB-2R mode shape six, 12.5 Hz.	94
Figure C.7: HMB-2R mode shape seven, 13.2 Hz.	95
Figure C.8: HMB-2R mode shape eight, 13.8 Hz.	95
Figure C.9: HMB-2R mode shape nine, 14.3 Hz.	95
Figure C.10: HMB-2R mode shape ten, 15.5 Hz.	96
Figure C.11: HMB-2R mode shape eleven, 21.3 Hz.	96
Figure C.12: HMB-2R mode shape twelve, 24.7 Hz.	96
Figure C.13: HMB-2R mode shape thirteen, 27.0 Hz.	97
Figure C.14: HMB-2R mode shape fourteen, 33.7 Hz.	97
Figure C.15: HMB-2R mode shape fifteen, 38.2 Hz.	97
Figure C.16: HMB-2R mode shape sixteen, 40.2 Hz.	98
Figure C.17: HMB-2R mode shape seventeen, 43.1 Hz.	98
Figure C.18: HMB-2R mode shape eighteen, 49.7 Hz.	98
Figure D.1: The degrees of freedom for this finite element.	99
Figure E.1: Beam model mode shape one, 4.66 Hz.	102

Figure E.2: Beam model mode shape two, 24.1 Hz.	102
Figure E.3: Beam model mode shape three, 26.9 Hz.	102
Figure E.4: Beam model mode shape four, 34.5 Hz.	102
Figure E.5: Beam model mode shape five, 38.9 Hz.	102
Figure E.6: Beam model mode shape six, 50.6 Hz.	102
Figure E.7: Beam model mode shape seven, 58.6 Hz.	103
Figure E.8: Beam model mode shape eight, 70.5 Hz.	103
Figure E.9: Beam model mode shape nine, 93.8 Hz.	103
Figure E.10: Beam model mode shape ten, 95.5 Hz.	103

LIST OF TABLES

Table 5.1: HMB-2R frequency data for hybrid cases.	44
Table 5.2: Summary of component frequency data for the hybrid case.	45
Table 5.3: Hybrid run data for HMB-2R.	45
Table 5.4: Frequency results for hybrid cases.	46
Table 5.5: Percent frequency errors for hybrid cases.	47
Table 5.6: Percent <i>MCC</i> error for hybrid cases.	47
Table 5.7: HMB-2R frequency data for free cases.	50
Table 5.8: Summary of component frequency data for the free case.	50
Table 5.9: Free run data for HMB-2R.	51
Table 5.10: Frequency results for free cases.	51
Table 5.11: Percent frequency errors for free cases.	52
Table 5.12: Percent <i>MCC</i> errors for free cases.	52
Table 5.13: HMB-2R frequency data for fixed cases.	54
Table 5.14: Summary of component frequency data for fixed case.	54
Table 5.15: Fixed case data for HMB-2R.	55
Table 5.16: Frequency results for fixed cases.	55
Table 5.17: Percent frequency errors for fixed cases.	56
Table 5.18: Percent <i>MCC</i> errors for fixed cases.	56
Table 6.1: Frequency data for beam model.	60
Table 6.2: Run data for the beam model.	61
Table 6.3: Frequency results for beam model cases.	61
Table 6.4: Percent frequency errors for beam model cases.	62
Table 6.5: Percent <i>MCC</i> error for beam cases.	62

NOMENCLATURE

Symbols	Meaning
α, β	Designates a component in the two component example.
$\mu^\alpha, \kappa^\alpha$	Transformed mass and stiffness matrices for component α .
μ, κ	Matrices with all the component μ 's, or κ 's, on the diagonal.
ω	Natural frequency of a component.
ω_s	Natural frequency of the full <i>system</i> .
Λ	Diagonal matrix of squared component natural frequencies.
Λ_s	Diagonal matrix of squared <i>system</i> natural frequencies.
Ψ	Matrix of component modes.
Ψ_c	Component <i>constraint</i> mode matrix.
Ψ_a	Component <i>attachment</i> mode matrix.
Ψ_r	Component <i>rigid-body</i> mode matrix.
ϕ	One component normal mode.
Φ	Matrix of component normal modes.
Φ_e	Matrix of component <i>elastic</i> normal modes.
Φ_k	Truncated matrix of component normal modes (<i>k</i> for <i>kept</i>).
$\Phi_{s,g}$	<i>System</i> mode shape matrix in generalized coordinates.
Φ_s	<i>System</i> mode shape matrix in global coordinates.
ρ	Designates any component in a system; material density.
σ	Lagrange multipliers.
ζ	Refers to either a component of p or of σ in the Lagrangian.
A	Cross-sectional <i>area</i> .

C	<i>Constraint</i> matrix used in the Lagrangian (not constraint modes).
E	<i>Elastic</i> modulus.
f	<i>Force</i> vector.
f_e	<i>Equilibrated</i> force vector.
g	Constrained component flexibility matrix (k^{-1}).
G	Flexibility matrix for constrained or unconstrained components.
G_e	Component <i>elastic</i> flexibility matrix.
G_d	Component residual flexibility matrix.
I	Cross-sectional area moment of <i>inertia</i> .
L	The <i>Lagrangian</i> ; element <i>length</i> .
MCC	<i>Modal correlation coefficient</i> .
M_o, K_o	Mass and stiffness matrices for the full (<i>original</i>) structural system.
M, K	Synthesized mass and stiffness matrices for the full system.
m, k	Component mass and stiffness matrices.
p	Generalized coordinates.
P	<i>Projection</i> matrix.
q	Linearly independent generalized coordinates (a subset of p).
Q	Generalized force in the Lagrangian.
R	<i>Reaction</i> forces.
S	A transformation matrix to go from p coordinates to q coordinates.
T, U	Kinetic and potential energy.
u_i	<i>Interior</i> coordinates of a component.
u_j	Coordinates at the <i>joint</i> of a component.

- u** Component physical coordinates.
- δW** Virtual *work*.
- x** Full structural system physical coordinates (global coordinates).

I. INTRODUCTION

Component mode synthesis (CMS) is a method of analyzing a full structural system by dividing the system into distinct components (or substructures), analyzing the components separately, and then mathematically combining (or synthesizing) the components to get the system results. Component mode synthesis can be used for numerous types of analysis including solving the eigenvalue problem, finding steady-state or transient response of a system, calculating stress, etc.

There are several reasons for using component mode synthesis. With very complex structures, such as Space Station Freedom, it can be very difficult to develop a full finite element model in a timely manner since the major components are built in different locations. In situations like this, each location can develop a model for their own component which will later be put into the full system model via CMS. This has the added benefits of being able to have each component model test verified by the manufacturer and increasing the probability of recognizing potential substructure problems, such as nonlinearities and significant dynamic characteristics, at an earlier stage.¹ Also with Space Station Freedom, the fact that it would not be completely assembled on Earth necessitates that the system results be obtained by mathematically combining the components; component mode synthesis is ideal for this application.

Also, depending on the model and the computer, it may be inefficient, if not impossible, to do an analysis of the full structural model in one computer run; however, since CMS breaks the model into substructures to do much of the analysis and discards unwanted or unneeded information (truncates modes) before synthesizing, it can be used to solve this problem.

Pioneering work in component mode synthesis was done in the 1960's by Hurty.² Since then, several different variations of CMS, which are discussed in more detail in section II, have been developed. In nearly all papers that introduce a new method, including the references given in this document, is a study of how many component modes can be truncated while still obtaining acceptable results. Indeed, the truncation of modes is one of the things that make CMS methods useful, and the results of such a study may determine whether that method is used in practice or not. Some papers, such as reference 3, compare modal truncation using different methods. However, in nearly all these references, the truncation study is done on very simple structures such as a 2-D truss or a simple beam. One exception is the study in reference 1 where the authors used a CMS method on the Viking Orbiter. Another exception is the study in reference 4 where the authors applied one method of CMS to a space station model (this study is discussed further in section V).

To complement these works, this document presents two studies. The first study applies *three* different CMS methods to a 3-D space station model that has over 4500 degrees of freedom. The goal of this study is to determine the effect of component modal truncation on the system frequencies and mode shapes when using component mode synthesis. MSC/NASTRAN, a finite element program, will be used for this study. Each method will be analyzed to determine the number of vibrational modes needed for acceptable results. The primary difference in these three methods is the choice of boundary conditions imposed on the interface (or *joint*) coordinates: one method restrains them; another method allows them to move freely; and the third method restrains only a chosen portion to simulate the actual physical conditions.

The second study considers a different aspect of using component mode synthesis: that of errors in component models. The goal of this study is to determine the effects of component modeling errors on the system mode shapes and frequencies. This is to simulate a real situation in which component mode synthesis is used to obtain the system results after each component model has been test verified. Errors are added to the mode shapes and eigenvalues of each component before they are synthesized. To accomplish this with MSC/NASTRAN requires knowledge of a special programming language designed for use in MSC/NASTRAN. Since time did not permit the author to learn this language and develop a suitable database of results from which to draw conclusions, MATLAB, a matrix manipulation program, is used. The errors are added to the components of a 2-D finite element beam model, developed within MATLAB, that has similarities to the space station model.

II. PRELIMINARY CONCEPTS AND DEFINITIONS

The simple spring mass system shown in Figure 2.1 will be used to mathematically introduce component mode synthesis. In this case, the full structural system is divided into two substructures, α and β . The coordinates (or degrees of freedom) u are subscripted with i if they are *interior* to the component or j if they are at the *joint*.

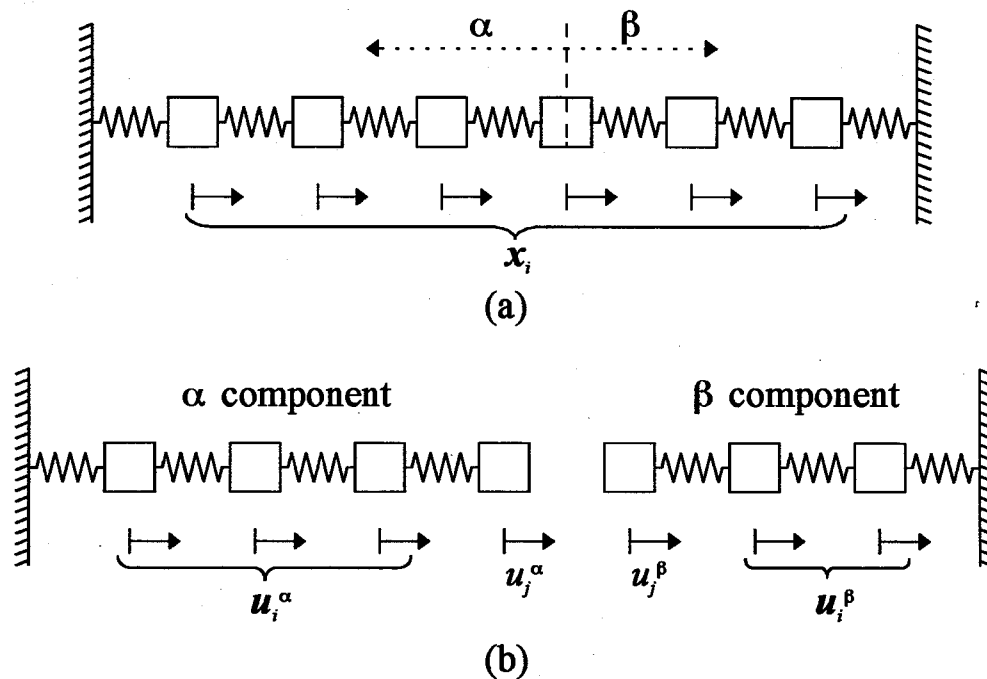


Figure 2.1: (a) Full structural system; (b) components α and β of the structure.

The equation of motion for the full system is written as

$$M_o \ddot{x} + K_o x = f_o \quad (2.1)$$

where the subscript o stands for the *original*, or full, structural system. When referring to system mass and stiffness matrices, capital letters will be used; for substructure mass and stiffness matrices, lower case letters will be used. When M and K are shown without any subscript, it means that these are the *synthesized* system matrices which will not be

equal to M_o and K_o . The x vector represents the physical coordinates of the full structural system while u is used for substructures.

The equation of motion for a component, α in this case, is written as

$$m^\alpha \ddot{u}^\alpha + k^\alpha u^\alpha = f^\alpha \quad (2.2)$$

To make equation (2.2) more useful, it is partitioned so that the interior degrees of freedom are grouped ahead of the joint degrees of freedom, or

$$\begin{bmatrix} m_{ii} & m_{ij} \\ m_{ji} & m_{jj} \end{bmatrix}^\alpha \begin{Bmatrix} \ddot{u}_i \\ \ddot{u}_j \end{Bmatrix}^\alpha + \begin{bmatrix} k_{ii} & k_{ij} \\ k_{ji} & k_{jj} \end{bmatrix}^\alpha \begin{Bmatrix} u_i \\ u_j \end{Bmatrix}^\alpha = \begin{Bmatrix} f_i \\ f_j \end{Bmatrix}^\alpha \quad (2.3)$$

The goal of component mode synthesis in this study, to get the system natural frequencies and mode shapes in physical space, is accomplished in part through information derived from equation (2.3). Conceptually, the dynamics of the component is contained in this information. It is important to note that solving equation (2.3) provides few directly useful results since the motion of the substructure as a part of the full system is still unknown.

Most component mode synthesis methods use a Ritz approximation for u , the unknown, in the form

$$u^\rho = \Psi^\rho p^\rho, \quad \rho = \alpha, \beta \quad (2.4)$$

where Ψ is a matrix of preselected component modes, and p is a vector of generalized coordinates. *The selection of Ψ is the fundamental difference between the various CMS methods* and will be discussed later. In an attempt to make clear the concept behind component mode synthesis, the approach to the problem is outlined:

- Divide the structure into components.
- Choose Ψ for each component. The choice of modes in Ψ is somewhat intuitive and depends on the boundary conditions of each component. It is here that the total model size can be significantly reduced by truncating component modes.
- Using the Ψ 's, m 's, and k 's, form the system mass and stiffness matrices (M and K).
- Solve the eigenvalue problem $(K - \omega_i^2 M)p_i = 0$ which gives the system eigenvalues (natural frequencies) and eigenvectors (mode shapes) in generalized coordinates. The subscript i on p indicates that this is a *total* p vector, made up of all component p 's (such as p^p in equation (2.4)).
- Use equation (2.4) to transform the modes into component physical space.
- Use coordinate transformations to get mode shapes in global coordinates.

In this document, the truncation of modes is first examined in *Example 1* where it is found that keeping the lower frequency modes is important. For different applications, however, it may happen that some higher frequency modes are more important than some lower modes. For example, Spanos and Tsuha⁵ showed that when control of a flexible multibody spacecraft is of interest, some higher frequency modes can be important because of actuator effects and sensor locations. They also provided a mathematical rationale for choosing which modes are important and which ones can be truncated for such a case.

2.1 Component Modes

The modes that make up Ψ for each component can be put in two categories:

those for constrained components and those for unconstrained components. The categorization depends not only on the system, but also on the method of component mode synthesis. For example, if a method restrains all joint coordinates, then all sets of component modes are for constrained components regardless of the physical boundary conditions. Such a method is called a *fixed-interface* method. On the other hand, if the system is unconstrained and the method of component mode synthesis does not restrain joint coordinates, then unconstrained component modes result. This type of method is called a *free-interface* method. There also exist the so-called *hybrid-interface* methods which restrain a portion of the joint coordinates.⁶

Component modes are predominantly of the following types: *normal modes*, *constraint modes*, and *attachment modes*. Normal modes are dynamic vibrational modes while constraint and attachment modes are static deflection shapes. However, any mode that is thought to be important in getting more accurate results may be used. Such modes have been called *imposed modes*.¹ Additionally, recent methods have introduced modes that can be used instead of, or as a supplement to, normal modes. These modes have been called *boundary flexibility vectors*, *static Ritz vectors*, or *Lanczos vectors*.^{7,8} Not all methods use all types of modes; the Craig-Bampton method (a fixed-interface type) discussed in section IV uses only normal and constraint modes. One method that takes a totally different approach to component mode synthesis and does not use any of these modes was developed by Suarez and Singh;⁹ they proposed an *exact* method in which they synthesize the components by solving the eigenvalue problem after each consecutive connection of each joint coordinate.

See **Appendix A** for developments and diagrams of normal, constraint, and

attachment component modes for both constrained and unconstrained components. The developments are similar to that given by Craig³ where there are also examples of their calculation. In this document, the examples are of component mode synthesis methods, but examples of component mode calculation are given if they are pertinent. Also, all diagrams of component modes are calculated and plotted from a ten-node finite element cantilevered beam.

III. A GENERALIZED PROCEDURE OF COMPONENT MODE SYNTHESIS³

The following development is for undamped, free vibration. Classical damping can be easily built into the following procedure as was shown by Craig¹⁰ who also gives an overview of component mode synthesis techniques. To derive the system equation of motion, Lagrange's equation of motion with the generalized force term will be used. However, since there are constraints that must be satisfied, such as compatible joint displacements, the Lagrangian (kinetic energy minus potential energy) will be augmented to include these constraints. This is accomplished through the use of undetermined multipliers.¹¹

For simplicity, let the system be composed of only two components, α and β , as in Figure 2.1. The physical displacements of joint coordinates are constrained by

$$u_j^\alpha = u_j^\beta \quad (3.1)$$

In a more general case, the joint coordinates of all components would be transformed into global coordinates where the displacement compatibility constraints are enforced. Constraints such as the one in equation (3.1) can be written in terms of the system generalized coordinates p (see equation (3.8) for the definition of p) and then combined in the matrix form

$$Cp = 0 \quad (3.2)$$

A detailed approach of forming this equation for the Craig-Bampton method will be demonstrated in section IV. In this form, this constraint will be handled via undetermined multipliers as stated above.

For a free vibration problem, another constraint, that of force compatibility at the joints, is given as

$$f_j^\alpha + f_j^\beta = 0 \quad (3.3)$$

This constraint will be used to show that the generalized force term in Lagrange's equation of motion is zero.

Now, with these ideas in mind, the augmented Lagrangian is

$$L = T - U + \sigma^T C p \quad (3.4)$$

where T and U are, respectively, the system kinetic and potential energies, and σ is the vector of undetermined multipliers.

The kinetic and potential energies of the complete system can be written as

$$T = \frac{1}{2} (\dot{u}^\alpha)^T m^\alpha \dot{u}^\alpha + \frac{1}{2} (\dot{u}^\beta)^T m^\beta \dot{u}^\beta = \frac{1}{2} (\dot{p}^\alpha)^T \mu^\alpha \dot{p}^\alpha + \frac{1}{2} (\dot{p}^\beta)^T \mu^\beta \dot{p}^\beta \quad (3.5)$$

$$U = \frac{1}{2} (u^\alpha)^T k^\alpha u^\alpha + \frac{1}{2} (u^\beta)^T k^\beta u^\beta = \frac{1}{2} (p^\alpha)^T \kappa^\alpha p^\alpha + \frac{1}{2} (p^\beta)^T \kappa^\beta p^\beta \quad (3.6)$$

where

$$\mu^\alpha \equiv \Psi^{\alpha T} m^\alpha \Psi^\alpha, \quad \kappa^\alpha \equiv \Psi^{\alpha T} k^\alpha \Psi^\alpha, \quad \text{etc.} \quad (3.7)$$

The form of the kinetic and potential energies are simplified by the definitions

$$p \equiv \begin{Bmatrix} p^\alpha \\ p^\beta \end{Bmatrix}, \quad \mu \equiv \begin{bmatrix} \mu^\alpha & \mathbf{0} \\ \mathbf{0} & \mu^\beta \end{bmatrix}, \quad \kappa \equiv \begin{bmatrix} \kappa^\alpha & \mathbf{0} \\ \mathbf{0} & \kappa^\beta \end{bmatrix} \quad (3.8)$$

Making use of the block diagonal form of μ and κ , T and U are written

$$T = \frac{1}{2} \dot{p}^T \mu \dot{p} \quad (3.9)$$

$$U = \frac{1}{2} p^T \kappa p \quad (3.10)$$

Writing out the Lagrangian now gives

$$L = \frac{1}{2} \dot{p}^T \mu \dot{p} - \frac{1}{2} p^T \kappa p + \sigma^T C p \quad (3.11)$$

which will be substituted into Lagrange's equation of motion

$$\frac{d}{dt} \left(\frac{\partial L}{\partial \dot{\zeta}_s} \right) - \frac{\partial L}{\partial \zeta_s} = Q_s \quad (3.12)$$

where ζ_s refers to either the generalized coordinates, p_s , or the Lagrange multipliers, σ_s , and Q_s is the “generalized force.”

Before substituting equation (3.11) into equation (3.12), the generalized force term will be shown to be zero by showing that the virtual work (δW) is zero. Using equations (3.1) and (3.3) and the fact that forces are exerted only at the joints, δW is

$$\begin{aligned}\delta W &= (\delta \mathbf{u}_j^\alpha)^T \mathbf{f}_j^\alpha + (\delta \mathbf{u}_j^\beta)^T \mathbf{f}_j^\beta \\ &= (\delta \mathbf{u}_j^\alpha)^T (\mathbf{f}_j^\alpha + \mathbf{f}_j^\beta) \\ &= 0\end{aligned}\tag{3.13}$$

and therefore $Q_s = 0$.

With this result, equation (3.12) is evaluated with $\zeta_s = p_s$ giving

$$\mu \ddot{\mathbf{p}} + \kappa \mathbf{p} = \mathbf{C}^T \boldsymbol{\sigma}\tag{3.14}$$

subject to $\mathbf{C}\mathbf{p} = \mathbf{0}$. To solve these two coupled equations, most methods introduce a linear transform of the form

$\mathbf{p} = \mathbf{S}\mathbf{q}$	(3.15)
-------------------------------------	---------------

where \mathbf{S} is a non-square transformation matrix and \mathbf{q} is a vector whose elements are a *linearly independent* subset of \mathbf{p} . In this case, linear independence just means that there are no redundant coordinates. The idea behind this transformation is to get the system equation of motion (equation (3.14)) in terms of \mathbf{q} , where, by the definition of \mathbf{q} , there can be no constraints.

Before transforming the equation of motion, a formula for the calculation of \mathbf{S} will be derived. First partition \mathbf{p} into *linearly independent* coordinates (\mathbf{p}_l) and *dependent* coordinates (\mathbf{p}_d). (Note that $\mathbf{q} = \mathbf{p}_l$.) Partitioning \mathbf{C} in a corresponding manner and rewriting $\mathbf{C}\mathbf{p} = \mathbf{0}$ gives

$$Cp = [C_{dl} \ C_{dd}] \begin{Bmatrix} p_l \\ p_d \end{Bmatrix} = [C_{dl} \ C_{dd}] \begin{Bmatrix} q \\ p_d \end{Bmatrix} = \mathbf{0} \quad (3.16)$$

Solving for p yields

$$p = \begin{Bmatrix} q \\ p_d \end{Bmatrix} = \begin{bmatrix} I_n \\ -C_{dd}^{-1} C_{dl} \end{bmatrix} q = Sq \quad (3.17)$$

Therefore,

$$S = \begin{bmatrix} I_n \\ -C_{dd}^{-1} C_{dl} \end{bmatrix} \quad (3.18)$$

The derivation of the desired system equation of motion can now be completed.

Substituting $p = Sq$ into $Cp = \mathbf{0}$ gives, since the elements of q are independent,

$$CS = \mathbf{0} \quad (3.19)$$

Substituting $p = Sq$ into equation (3.14) and premultiplying by S^T gives the sought after equation of motion

$$M\ddot{q} + Kq = \mathbf{0} \quad (3.20)$$

where the system mass and stiffness matrices have been defined by

$$M = S^T \mu S, \quad K = S^T \kappa S \quad (3.21)$$

Also, the fact that $S^T C^T = \mathbf{0}$ has been used.

3.1 Extending to N Components

To extend the above development to n components, only equation (3.8) needs modification. The “new” equation (3.8) is

$$p \equiv \begin{Bmatrix} p^1 \\ p^2 \\ p^3 \\ \vdots \\ p^n \end{Bmatrix}, \quad \mu \equiv \begin{bmatrix} \mu^1 & 0 & 0 & 0 & \dots & 0 \\ 0 & \mu^2 & 0 & 0 & \dots & 0 \\ 0 & 0 & \mu^3 & 0 & \dots & 0 \\ \vdots & & & \ddots & & \vdots \\ 0 & 0 & \dots & 0 & \mu^{n-1} & 0 \\ 0 & 0 & 0 & \dots & 0 & \mu^n \end{bmatrix}, \quad \kappa \equiv \begin{bmatrix} \kappa^1 & 0 & 0 & 0 & \dots & 0 \\ 0 & \kappa^2 & 0 & 0 & \dots & 0 \\ 0 & 0 & \kappa^3 & 0 & \dots & 0 \\ \vdots & & & \ddots & & \vdots \\ 0 & 0 & \dots & 0 & \kappa^{n-1} & 0 \\ 0 & 0 & 0 & \dots & 0 & \kappa^n \end{bmatrix} \quad (3.22)$$

3.2 Extending to Forced Systems

The extension of the previous development to forced systems is done by recalculating the virtual work. Since there are externally applied forces, the virtual work is given as

$$\begin{aligned} \delta W &= (\delta u^\alpha)^T f^\alpha + (\delta u^\beta)^T f^\beta \\ &= (\delta p^\alpha)^T (\Psi^\alpha)^T f^\alpha + (\delta p^\beta)^T (\Psi^\beta)^T f^\beta \\ &= \delta p^T \Psi^T f \end{aligned} \quad (3.23)$$

where

$$\Psi \equiv \begin{bmatrix} \Psi^\alpha & 0 \\ 0 & \Psi^\beta \end{bmatrix}, \quad f \equiv \begin{Bmatrix} f^\alpha \\ f^\beta \end{Bmatrix} \quad (3.24)$$

Equation (3.14) is derived as before and in this case there will be another term. Since the virtual work is not zero, Q_s is not zero, and equation (3.14) is modified to be

$$\mu \ddot{p} + \kappa p = C^T \sigma + \Psi^T f \quad (3.25)$$

The rest of the derivation is the same and new system equation of motion is

$$M \ddot{q} + Kq = S^T \Psi^T f \quad (3.26)$$

IV. TWO COMPONENT MODE SYNTHESIS METHODS

4.1 The Craig-Bampton Method^{3,12}

As mentioned previously, the Craig-Bampton method of component mode synthesis is a fixed-interface method. Also, the matrix Ψ is made up of only normal and constraint modes which, as discussed in section A.2, make up a linearly independent set of modes. In free-interface methods, such as the Craig-Chang method³, special precautions are taken to ensure this property.

Since Ψ is made up of only linearly independent normal and constraint modes, it is assumed that any displacements can be written as a linear combination of these modes. Therefore equation (2.4), $\mathbf{u}^p = \Psi^p \mathbf{p}^p$, is rewritten in the form

$$\mathbf{u}^p = \Phi_k^p \mathbf{p}_k^p + \Psi_c^p \mathbf{p}_c^p \quad (4.1)$$

for component p . From this equation and the following definition for \mathbf{p}_c , the matrix Ψ^p will be constructed.

Define the constraint generalized coordinates \mathbf{p}_c to be the physical displacements of the joints \mathbf{u}_j or, $\mathbf{p}_c = \mathbf{u}_j$. This important definition renders the constraint equation $C\mathbf{p} = \mathbf{0}$ trivial to form (see equation (4.6)). Now, since the normal modes are fixed-interface modes, the matrix Ψ^p is constructed and equation (4.1) is rewritten in the partitioned form

$$\begin{Bmatrix} \mathbf{u}_i \\ \mathbf{u}_j \end{Bmatrix}^p = \begin{bmatrix} \Phi_{ik} & \Psi_{ic} \\ \mathbf{0} & I \end{bmatrix}^p \begin{Bmatrix} \mathbf{p}_k \\ \mathbf{p}_c \end{Bmatrix}^p \quad (4.2)$$

where, from equation (A.5),

$$\Psi_{ic}^{\rho} = -(\mathbf{k}_{ii}^{\rho})^{-1} \mathbf{k}_{ij}^{\rho} \quad (4.3)$$

From equation (3.7), μ and κ for component ρ are given by

$$\mu^{\rho} = (\Psi^{\rho})^T \mathbf{m}^{\rho} \Psi^{\rho} = \begin{bmatrix} \Phi_{ik}^T & \mathbf{0}^T \\ \Psi_{ic}^T & \mathbf{I} \end{bmatrix}^{\rho} \begin{bmatrix} \mathbf{m}_{ii} & \mathbf{m}_{ij} \\ \mathbf{m}_{ji} & \mathbf{m}_{jj} \end{bmatrix}^{\rho} \begin{bmatrix} \Phi_{ik} & \Psi_{ic} \\ \mathbf{0} & \mathbf{I} \end{bmatrix}^{\rho} \quad (4.4)$$

and

$$\kappa^{\rho} = (\Psi^{\rho})^T \mathbf{k}^{\rho} \Psi^{\rho} = \begin{bmatrix} \Phi_{ik}^T & \mathbf{0}^T \\ \Psi_{ic}^T & \mathbf{I} \end{bmatrix}^{\rho} \begin{bmatrix} \mathbf{k}_{ii} & \mathbf{k}_{ij} \\ \mathbf{k}_{ji} & \mathbf{k}_{jj} \end{bmatrix}^{\rho} \begin{bmatrix} \Phi_{ik} & \Psi_{ic} \\ \mathbf{0} & \mathbf{I} \end{bmatrix}^{\rho} \quad (4.5)$$

The full μ and κ are then given by equation (3.22).

For convenience, the rest of the development assumes there are only two components as in Figure 2.1. The constraint $C\mathbf{p} = \mathbf{0}$ can then be written as

$$\begin{bmatrix} \mathbf{0} & \mathbf{I} & \mathbf{0} & \vdots & -\mathbf{I} \end{bmatrix} \begin{Bmatrix} \mathbf{p}_k^{\alpha} \\ \mathbf{p}_c^{\alpha} \\ \mathbf{p}_k^{\beta} \\ \dots \\ \mathbf{p}_c^{\beta} \end{Bmatrix} = \mathbf{0} \quad (4.6)$$

For this method, it is simple to find S just by forming $\mathbf{p} = S\mathbf{q}$. This yields

$$\begin{Bmatrix} \mathbf{p}_k^{\alpha} \\ \mathbf{p}_c^{\alpha} \\ \mathbf{p}_k^{\beta} \\ \mathbf{p}_c^{\beta} \end{Bmatrix} = \begin{bmatrix} \mathbf{I} & \mathbf{0} & \mathbf{0} \\ \mathbf{0} & \mathbf{0} & \mathbf{I} \\ \mathbf{0} & \mathbf{I} & \mathbf{0} \\ \mathbf{0} & \mathbf{0} & \mathbf{I} \end{bmatrix} \begin{Bmatrix} \mathbf{p}_k^{\alpha} \\ \mathbf{p}_k^{\beta} \\ \mathbf{p}_c^{\alpha} \end{Bmatrix} \quad (4.7)$$

where the vector \mathbf{q} is chosen so that the normal mode coordinates \mathbf{p}_k are grouped ahead

of the joint coordinates p_c . Note that equation (3.17) could be used to calculate an S and then rearranged to give this form of S .

The system mass and stiffness matrices, given in equation (3.21), are used to solve the eigenvalue problem. The eigenvectors are then converted from generalized coordinates to physical space by using equation (4.2) as will be shown in *Example 1*. Finally, coordinate transformations, if necessary, are performed to put the mode shapes in global coordinates.

In *Example 1*, the highest frequency mode will be deleted from the α component before the synthesis begins. Part (b) of this example will look at what happens when, instead of the highest frequency mode, the lowest frequency mode is deleted. Note that if no modes are truncated, the Craig-Bampton method is exact.

Example 1: The Craig-Bampton method.

Problem:

For the system shown in Figure 4.1:

- (a) Determine the effect of truncating the highest frequency mode from α .
- (b) Truncate the lowest frequency mode instead of the highest.

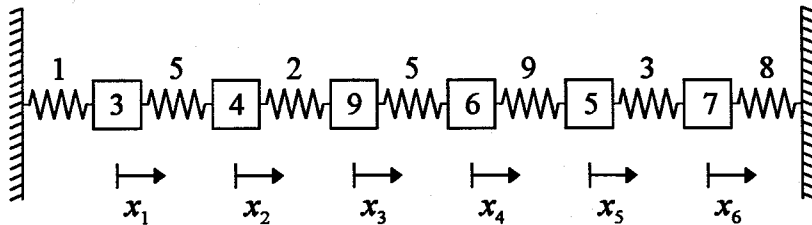
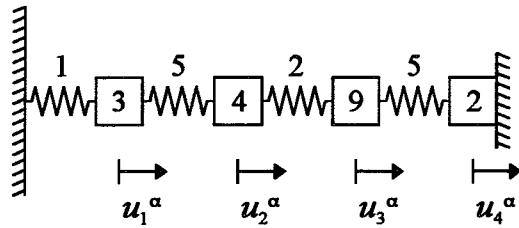


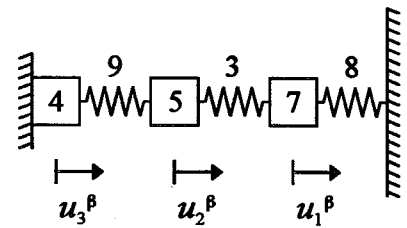
Figure 4.1: The full system for *Example 1*.

Solution:

(a) Choose component α to be:



and β to be:



Note that the fourth mass is divided such that $m_4^\alpha + m_3^\beta = m_4$.

Component α :

The equation of motion is

$$\begin{bmatrix} 3 & 0 & 0 & 0 \\ 0 & 4 & 0 & 0 \\ 0 & 0 & 9 & 0 \\ 0 & 0 & 0 & 2 \end{bmatrix} \begin{Bmatrix} \ddot{u}_1 \\ \ddot{u}_2 \\ \ddot{u}_3 \\ \ddot{u}_4 \end{Bmatrix}^\alpha + \begin{bmatrix} 6 & -5 & 0 & 0 \\ -5 & 7 & -2 & 0 \\ 0 & -2 & 7 & -5 \\ 0 & 0 & -5 & 5 \end{bmatrix} \begin{Bmatrix} u_1 \\ u_2 \\ u_3 \\ u_4 \end{Bmatrix}^\alpha = \begin{Bmatrix} 0 \\ 0 \\ 0 \\ 0 \end{Bmatrix} \quad (\text{e1.1})$$

Normal Modes:

To calculate the normal modes, coordinate u_4^α , since it is restrained, is partitioned out leaving

$$\begin{bmatrix} 3 & 0 & 0 \\ 0 & 4 & 0 \\ 0 & 0 & 9 \end{bmatrix} \begin{Bmatrix} \ddot{u}_1 \\ \ddot{u}_2 \\ \ddot{u}_3 \end{Bmatrix}^\alpha + \begin{bmatrix} 6 & -5 & 0 \\ -5 & 7 & -2 \\ 0 & -2 & 7 \end{bmatrix} \begin{Bmatrix} u_1 \\ u_2 \\ u_3 \end{Bmatrix}^\alpha = \begin{Bmatrix} 0 \\ 0 \\ 0 \end{Bmatrix} \quad (\text{e1.2})$$

or, symbolically,

$$m_{ii}^\alpha \ddot{u}_i^\alpha + k_{ii}^\alpha u_i^\alpha = 0 \quad (\text{e1.3})$$

Solving the eigenvalue problem $(k_{ii}^\alpha - \omega^2 m_{ii}^\alpha) \phi^\alpha = 0$ and normalizing Φ^α such that

$$(\Phi^\alpha)^T m_{ii}^\alpha \Phi^\alpha = I \text{ gives}$$

$$\Lambda^\alpha = \begin{bmatrix} 0.2963 & 0 & 0 \\ 0 & 0.8877 & 0 \\ 0 & 0 & 3.3437 \end{bmatrix} \quad (\text{e1.4})$$

and

$$\Phi^\alpha = \begin{bmatrix} 0.3300 & -0.2174 & 0.4209 \\ 0.3373 & -0.1451 & -0.3394 \\ 0.1557 & 0.2933 & 0.0294 \end{bmatrix} \quad (\text{e1.5})$$

Constraint Modes:

Using equation (4.3), Ψ_{ic}^α is

$$\Psi_{ic}^\alpha = -k_u^{\alpha-1} k_y^\alpha = - \begin{bmatrix} 6 & -5 & 0 \\ -5 & 7 & -2 \\ 0 & -2 & 7 \end{bmatrix}^{-1} \begin{Bmatrix} 0 \\ 0 \\ -5 \end{Bmatrix} = \begin{Bmatrix} 0.5263 \\ 0.6316 \\ 0.8947 \end{Bmatrix} \quad (\text{e1.6})$$

Therefore, by equation (4.2), after truncating the highest frequency normal mode the component mode matrix Ψ^α is,

$$\Psi^\alpha = \begin{bmatrix} 0.3300 & -0.2174 & 0.5263 \\ 0.3373 & -0.1451 & 0.6316 \\ 0.1557 & 0.2933 & 0.8947 \\ 0 & 0 & 1 \end{bmatrix} \quad (\text{e1.7})$$

Using equations (4.4) and (4.5), μ^α and κ^α are calculated to be

$$\mu^\alpha = \begin{bmatrix} 1 & 0 & 2.6270 \\ 0 & 1 & 1.6518 \\ 2.6270 & 1.6518 & 11.6316 \end{bmatrix} \quad (\text{e1.8})$$

$$\kappa^\alpha = \begin{bmatrix} 0.2963 & 0 & 0 \\ 0 & 0.8877 & 0 \\ 0 & 0 & 0.5263 \end{bmatrix} \quad (\text{e1.9})$$

Component β :

Following the same development as for α , the equation of motion is

$$\begin{bmatrix} 7 & 0 & 0 \\ 0 & 5 & 0 \\ 0 & 0 & 4 \end{bmatrix} \begin{Bmatrix} \ddot{u}_1 \\ \ddot{u}_2 \\ \ddot{u}_3 \end{Bmatrix}^\beta + \begin{bmatrix} 11 & -3 & 0 \\ -3 & 12 & -9 \\ 0 & -9 & 9 \end{bmatrix} \begin{Bmatrix} u_1 \\ u_2 \\ u_3 \end{Bmatrix}^\beta = \begin{Bmatrix} 0 \\ 0 \\ 0 \end{Bmatrix} \quad (\text{e1.10})$$

Normal Modes:

In this case coordinate u_3^β , since it is restrained, is partitioned out leaving

$$\begin{bmatrix} 7 & 0 \\ 0 & 5 \end{bmatrix} \begin{Bmatrix} \ddot{u}_1 \\ \ddot{u}_2 \end{Bmatrix}^\beta + \begin{bmatrix} 11 & -3 \\ -3 & 12 \end{bmatrix} \begin{Bmatrix} u_1 \\ u_2 \end{Bmatrix}^\beta = \begin{Bmatrix} 0 \\ 0 \end{Bmatrix} \quad (\text{e1.11})$$

Solving the eigenvalue problem gives

$$\Lambda^\beta = \begin{bmatrix} 1.3309 & 0 \\ 0 & 2.6405 \end{bmatrix} \quad (\text{e1.12})$$

and

$$\Phi^\beta = \begin{bmatrix} 0.3415 & -0.1620 \\ 0.1917 & 0.4041 \end{bmatrix} \quad (\text{e1.13})$$

Constraint Modes:

Ψ_{ic}^β is

$$\Psi_{ic}^\beta = \begin{Bmatrix} 0.2195 \\ 0.8049 \end{Bmatrix} \quad (\text{e1.14})$$

The component mode matrix Ψ^β is

$$\Psi^\beta = \begin{bmatrix} 0.3415 & -0.1620 & 0.2195 \\ 0.1917 & 0.4041 & 0.8049 \\ 0 & 0 & 1 \end{bmatrix} \quad (\text{e1.15})$$

μ^β and κ^β are calculated to be

$$\mu^\beta = \begin{bmatrix} 1 & 0 & 1.2960 \\ 0 & 1 & 1.3772 \\ 1.2690 & 1.3772 & 7.5764 \end{bmatrix} \quad (\text{e1.16})$$

and

$$\kappa^\beta = \begin{bmatrix} 1.3309 & 0 & 0 \\ 0 & 2.6405 & 0 \\ 0 & 0 & 1.7561 \end{bmatrix} \quad (\text{e1.17})$$

Synthesis:

Now that the necessary data for both components have been calculated, the synthesis can begin. Equation (4.7), $p = Sq$, for this problem is

$$\begin{bmatrix} p_1^\alpha \\ p_2^\alpha \\ u_4^\alpha \\ p_1^\beta \\ p_2^\beta \\ u_3^\beta \end{bmatrix} = S \begin{bmatrix} p_1^\alpha \\ p_2^\alpha \\ p_1^\beta \\ p_2^\beta \\ u_4^\alpha \end{bmatrix} \quad (\text{e1.18})$$

since $p_c = u_j$ for each component. Forming S from equation (e1.18) gives

$$S = \begin{bmatrix} 1 & 0 & 0 & 0 & 0 \\ 0 & 1 & 0 & 0 & 0 \\ 0 & 0 & 0 & 0 & 1 \\ 0 & 0 & 1 & 0 & 0 \\ 0 & 0 & 0 & 1 & 0 \\ 0 & 0 & 0 & 0 & 1 \end{bmatrix} \quad (\text{e1.19})$$

Now, μ and κ are constructed according to equation (3.8). For example purposes, μ is written out giving

$$\mu = \begin{bmatrix} 1 & 0 & 2.6270 & 0 & 0 & 0 \\ 0 & 1 & 1.6518 & 0 & 0 & 0 \\ 2.6270 & 1.6518 & 11.6316 & 0 & 0 & 0 \\ 0 & 0 & 0 & 1 & 0 & 1.2960 \\ 0 & 0 & 0 & 0 & 1 & 1.3772 \\ 0 & 0 & 0 & 1.2960 & 1.3772 & 7.5764 \end{bmatrix} \quad (\text{e1.20})$$

Finally, the system mass and stiffness matrices are calculated by equation (3.21) giving

$$M = \begin{bmatrix} 1 & 0 & 0 & 0 & 2.6270 \\ 0 & 1 & 0 & 0 & 1.6518 \\ 0 & 0 & 1 & 0 & 1.2960 \\ 0 & 0 & 0 & 1 & 1.3772 \\ 2.6270 & 1.6518 & 1.2960 & 1.3772 & 19.2080 \end{bmatrix} \quad (\text{e1.21})$$

and

$$K = \begin{bmatrix} 0.2963 & 0 & 0 & 0 & 0 \\ 0 & 0.8877 & 0 & 0 & 0 \\ 0 & 0 & 1.3309 & 0 & 0 \\ 0 & 0 & 0 & 2.6405 & 0 \\ 0 & 0 & 0 & 0 & 2.2824 \end{bmatrix} \quad (\text{e1.22})$$

Solving for the eigenvalues and mode shapes gives

$$\Lambda_s = \begin{bmatrix} 0.0984 & 0 & 0 & 0 & 0 \\ 0 & 0.4693 & 0 & 0 & 0 \\ 0 & 0 & 1.0727 & 0 & 0 \\ 0 & 0 & 0 & 1.7191 & 0 \\ 0 & 0 & 0 & 0 & 4.1275 \end{bmatrix} \quad (\text{e1.23})$$

and

$$\Phi_{s,g} = \begin{bmatrix} 0.7860 & -0.9540 & -0.3115 & 0.4022 & 0.5026 \\ 0.1239 & 0.2479 & -0.8219 & 0.4328 & 0.3737 \\ 0.0623 & 0.0945 & 0.4621 & 0.7272 & 0.3397 \\ 0.0321 & 0.0398 & 0.0809 & -0.3256 & 0.6789 \\ 0.6016 & 0.1338 & 0.0858 & -0.1267 & -0.1776 \end{bmatrix} \quad (\text{e1.24})$$

where the subscript g indicates that this is still in generalized coordinates. In this case, each mode is normalized such that its magnitude is one. To transform the mode shapes to physical space, equation (4.2) is used for one component at a time. Writing this equation for the α component gives

$$u^\alpha = \Psi^\alpha \begin{Bmatrix} p_1 \\ p_2 \\ u_4 \end{Bmatrix} \quad (\text{e1.25})$$

Therefore, from the order of the generalized coordinates (on the right hand side of equation (e1.18)), it is recognized that to get the “ α part” of Φ_s , the first, second, third, and fifth rows of $\Phi_{s,g}$ must be premultiplied by Ψ^α . Using the same logic, the “ β part” is calculated by premultiplying the third, fourth, and fifth rows of $\Phi_{s,g}$ by Ψ^β . For illustration purposes, the α part is written out:

$$\Phi_{s_x} = \Psi^\alpha \begin{bmatrix} 0.7860 & -0.9540 & -0.3115 & 0.4022 & 0.5026 \\ 0.1239 & 0.2479 & -0.8219 & 0.4328 & 0.3737 \\ 0.6016 & 0.1338 & 0.0858 & -0.1267 & -0.1776 \end{bmatrix} \quad (\text{e1.26})$$

After calculating both parts, the mode shapes are then rearranged to put them in the same order as in Figure 4.1. In this simple example, this rearranging is all that is required to transform the component physical coordinates to global coordinates. Specifically, Φ_s is made of (and in this order): rows one and two of the α part, then either row three of the α part or row three of the β part (they are the same since they both correspond to coordinate x_4), and then rows two and one of the β part. Thus, the mode shape matrix in global coordinates (x) space is

$$\Phi_s = \begin{bmatrix} 0.1697 & 0.3309 & 0.1289 & -0.0331 & -0.0140 \\ 0.1938 & 0.3032 & 0.0728 & -0.0084 & 0.0050 \\ 0.2154 & -0.0487 & -0.2265 & 0.0899 & 0.0459 \\ 0.1859 & -0.1485 & 0.0913 & -0.1495 & -0.2816 \\ 0.1573 & -0.1574 & 0.2026 & -0.1110 & 0.3116 \\ 0.0458 & -0.0612 & 0.1741 & 0.3225 & -0.0522 \end{bmatrix} \quad (\text{e1.27})$$

To facilitate the comparison of the results to the exact, the above mode shape matrix was normalized with respect to the full system mass matrix M_o given below.

The exact eigenvalues and mode shapes are calculated by solving the full structural system eigenvalue problem. The full system equation of motion is

$$M_o \ddot{x} + K_o x = 0 \quad (\text{e1.28})$$

where

$$M_o = \begin{bmatrix} 3 & 0 & 0 & 0 & 0 & 0 \\ 0 & 4 & 0 & 0 & 0 & 0 \\ 0 & 0 & 9 & 0 & 0 & 0 \\ 0 & 0 & 0 & 6 & 0 & 0 \\ 0 & 0 & 0 & 0 & 5 & 0 \\ 0 & 0 & 0 & 0 & 0 & 7 \end{bmatrix}, \quad K_o = \begin{bmatrix} 6 & -5 & 0 & 0 & 0 & 0 \\ -5 & 7 & -2 & 0 & 0 & 0 \\ 0 & -2 & 7 & -5 & 0 & 0 \\ 0 & 0 & -5 & 14 & -9 & 0 \\ 0 & 0 & 0 & -9 & 12 & -3 \\ 0 & 0 & 0 & 0 & -3 & 11 \end{bmatrix} \quad (\text{e1.29})$$

Solving the eigenvalue problem and normalizing the modes with respect to M_o yields

$$\Lambda_o = \begin{bmatrix} 0.0984 & 0 & 0 & 0 & 0 & 0 \\ 0 & 0.4693 & 0 & 0 & 0 & 0 \\ 0 & 0 & 1.0727 & 0 & 0 & 0 \\ 0 & 0 & 0 & 1.7190 & 0 & 0 \\ 0 & 0 & 0 & 0 & 3.3423 & 0 \\ 0 & 0 & 0 & 0 & 0 & 4.1308 \end{bmatrix} \quad (\text{e1.30})$$

and

$$\Phi_o = \begin{bmatrix} 0.1698 & 0.3305 & 0.1297 & -0.0360 & -0.4207 & 0.0133 \\ 0.1937 & 0.3035 & 0.0721 & -0.0061 & 0.3388 & -0.0170 \\ 0.2154 & -0.0487 & -0.2264 & 0.0897 & -0.0273 & 0.0478 \\ 0.1859 & -0.1485 & 0.0913 & -0.1495 & -0.0096 & -0.2816 \\ 0.1573 & -0.1574 & 0.2026 & -0.1110 & 0.0216 & 0.3109 \\ 0.0458 & -0.0612 & 0.1741 & 0.3225 & -0.0052 & -0.0521 \end{bmatrix} \quad (\text{e1.31})$$

A comparison of the results given by the Craig-Bampton method (in equations (e1.23) and (e1.27)) to the exact results (given in equations (e1.30) and (e1.31)), show that the first four frequencies and mode shapes are very accurately reproduced by the method. Therefore, if only the first four modes were of interest, this may suffice. ■

(b) Since this part is identical to part (a), except for which mode is truncated, the intermediate steps are omitted and only the final results are given:

$$\Lambda_s = \begin{bmatrix} 0.1149 & 0 & 0 & 0 & 0 \\ 0 & 1.0055 & 0 & 0 & 0 \\ 0 & 0 & 1.5171 & 0 & 0 \\ 0 & 0 & 0 & 3.1462 & 0 \\ 0 & 0 & 0 & 0 & 3.3459 \end{bmatrix} \quad (\text{e1.32})$$

and

$$\Phi_s = \begin{bmatrix} 0.1044 & 0.2539 & 0.1314 & 0.1620 & 0.4047 \\ 0.1312 & 0.1884 & 0.1118 & 0.0893 & -0.3520 \\ 0.2131 & -0.2286 & -0.0254 & 0.0295 & 0.0259 \\ 0.2204 & 0.0705 & 0.0934 & 0.1226 & -0.0145 \\ 0.1881 & 0.1351 & -0.0437 & -0.3787 & 0.0325 \\ 0.0554 & 0.1023 & -0.3445 & 0.1031 & -0.0079 \end{bmatrix} \quad (\text{e1.33})$$

A comparison of these results to the exact reveals that large errors are caused by deleting the lowest frequency mode from α . In fact, the results are so poor that it is hard to tell which synthesized mode corresponds to which exact mode. With part (a) results

(where the highest frequency mode was deleted from α), however, this is not a problem. Therefore, although it is unclear exactly how many of the upper frequency modes can be truncated, it is evident that keeping the lower frequency modes is important. ■■

4.2 The Craig-Chang Method^{3,21}

The Craig-Chang method of component mode synthesis is a free-interface method that uses, for an unconstrained component, rigid-body modes, normal modes, and residual inertia relief attachment modes. Or, if the component is constrained, the method uses normal modes and residual attachment modes. In the following development, it will be assumed that the component is unconstrained; if it is constrained, simply leave out the rigid-body modes and use residual attachment modes in place of residual inertia relief attachment modes. See **Appendix A** for component mode descriptions.

Define the A set of coordinates for a component to be the *joint* coordinates; the rest of the coordinates are divided into the R set, a statically determinate set that restrains the component against rigid-body motion, and the W set. Equation (2.4), $\mathbf{u}^p = \Psi^p \mathbf{p}^p$, can be written in the partitioned form

$$\mathbf{u}^p = \begin{Bmatrix} \mathbf{u}_w \\ \mathbf{u}_j \\ \mathbf{u}_r \end{Bmatrix}^p = \begin{bmatrix} \Phi_{wk} & \Psi_{wr} & \Psi_{wd} \\ \Phi_{jk} & \Psi_{jr} & \Psi_{jd} \\ \Phi_{rk} & \Psi_{rr} & \Psi_{rd} \end{bmatrix}^p \begin{Bmatrix} \mathbf{p}_k \\ \mathbf{p}_r \\ \mathbf{p}_d \end{Bmatrix}^p \quad (4.8)$$

where Φ_k are the kept free-interface elastic normal modes, Ψ_r are the rigid-body modes, and Ψ_d are the residual inertia relief attachment modes. For convenience, the equations for calculating the rigid-body modes and attachment modes are summarized from sections

A.5 and A.6:

$$\Psi_d = G_d F \quad (4.9)$$

where for **unconstrained components**:

$$\begin{aligned} G_d &= P^T G P - \Phi_k \Lambda_{kk}^{-1} \Phi_k^T \\ F &= \begin{bmatrix} \mathbf{0}_{wj} \\ I_{jj} \\ \mathbf{0}_{rj} \end{bmatrix} \\ G &= \begin{bmatrix} g_{ww} & g_{wj} & \mathbf{0}_{wr} \\ g_{jw} & g_{jj} & \mathbf{0}_{jr} \\ \mathbf{0}_{rw} & \mathbf{0}_{rj} & \mathbf{0}_{rr} \end{bmatrix}, \quad g = \begin{bmatrix} g_{ww} & g_{wj} \\ g_{jw} & g_{jj} \end{bmatrix} = \begin{bmatrix} k_{ww} & k_{wj} \\ k_{jw} & k_{jj} \end{bmatrix}^{-1}, \quad k = \begin{bmatrix} k_{ww} & k_{wj} & k_{wr} \\ k_{jw} & k_{jj} & k_{jr} \\ k_{rw} & k_{rj} & k_{rr} \end{bmatrix} \\ P &= I - m \Psi_r \Psi_r^T \\ \Psi_r &= \begin{bmatrix} -g \begin{bmatrix} k_{wr} \\ k_{jr} \end{bmatrix} \\ I_{rr} \end{bmatrix}, \quad \Psi_r^T m \Psi_r = I_{rr} \end{aligned} \quad (4.10)$$

and for **constrained components**:

$$\begin{aligned} G_d &= G - \Phi_k \Lambda_{kk}^{-1} \Phi_k^T \\ F &= \begin{bmatrix} \mathbf{0}_{wj} \\ I_{jj} \end{bmatrix} \\ G &= \begin{bmatrix} g_{ww} & g_{wj} \\ g_{jw} & g_{jj} \end{bmatrix}, \quad \begin{bmatrix} g_{ww} & g_{wj} \\ g_{jw} & g_{jj} \end{bmatrix} = k^{-1} = \begin{bmatrix} k_{ww} & k_{wj} \\ k_{jw} & k_{jj} \end{bmatrix}^{-1} \end{aligned} \quad (4.11)$$

An important quality of the Craig-Chang method is the generalized coordinates chosen to be the independent set: only the rigid-body and kept normal mode coordinates are retained. This is theoretically possible because of the free interface; all physical degrees of freedom are represented in the Ritz approximation even if only normal mode coordinates are kept. In contrast, fixed interface methods, such as the Craig-Bampton

method, must keep component modes present that will allow non-zero interface displacements. *However, leaving out the attachment mode coordinates means the method cannot be exact.* The maximum order of synthesized system is equal to the total number of physical coordinates minus the total number of joint coordinates. At first glance, one might be inclined to leave the attachment mode coordinates in the independent set, which is possible, to at least start off with an exact method. However, this property of the Craig-Chang method is a potential benefit, especially for systems having a large number of joint coordinates. Leaving out the attachment mode coordinates reduces the system order further than just the truncation of normal modes alone. Also, by the method the attachment modes are calculated, it is noted that *normal modes must be truncated*; the minimum number of truncated modes must equal the number of joint coordinates for the component.

In **Appendix B** is a derivation of a constraint (given in equation (4.12)) that allows the attachment mode coordinates to be removed from the independent set. *This constraint is an approximation allowed by neglecting the inertia effects of the attachment modes.* The constraint is

$$P_d^\alpha + P_d^\beta = \mathbf{0} \quad (4.12)$$

As shown below, the attachment mode coordinates are removed from the independent set by enforcing equation (4.12), along with the joint displacement compatibility constraint, in $Cp = \mathbf{0}$.

The rest of the derivation follows section **III** for the most part. μ^p and κ^p are calculated from equation (3.7) where Ψ^p is given in equation (4.8). Both m^p and k^p are

both partitioned as k^p was in equation (4.10).

Since the coordinates p_d^p are chosen to be the dependent coordinates, for a two component system,

$$p = \begin{Bmatrix} p_d^\alpha \\ p_d^\beta \\ p_k^\alpha \\ p_r^\alpha \\ p_k^\beta \\ p_r^\beta \end{Bmatrix} = \begin{Bmatrix} p_d^\alpha \\ p_d^\beta \\ q \end{Bmatrix}, \quad q = \begin{Bmatrix} p_k^\alpha \\ p_r^\alpha \\ p_k^\beta \\ p_r^\beta \end{Bmatrix} \quad (4.13)$$

This ordering of p is chosen so that $C_{d\delta}$ given below, is nonsingular.

The constraint equation, $Cp = 0$, is used to enforce both compatible joint displacements $u_j^\alpha = u_j^\beta$ (equation (3.1)) and equation (4.12). Equation (4.8) is used to write the joint displacement equation in terms of the generalized coordinates giving

$$\Phi_{jk}^\alpha p_k^\alpha + \Psi_{jr}^\alpha p_r^\alpha + \Psi_{jd}^\alpha p_d^\alpha = \Phi_{jk}^\beta p_k^\beta + \Psi_{jr}^\beta p_r^\beta + \Psi_{jd}^\beta p_d^\beta \quad (4.14)$$

Therefore, $Cp = 0$ can be written as

$$Cp = [C_{dd} \ C_{d\delta}] \begin{Bmatrix} p_d^\alpha \\ p_d^\beta \\ p_k^\alpha \\ p_r^\alpha \\ p_k^\beta \\ p_r^\beta \end{Bmatrix} = \begin{bmatrix} \Psi_{jd}^\alpha & -\Psi_{jd}^\beta & \Phi_{jk}^\alpha & \Psi_{jr}^\alpha & -\Phi_{jk}^\beta & -\Psi_{jr}^\beta \\ I & I & 0 & 0 & 0 & 0 \end{bmatrix} \begin{Bmatrix} p_d^\alpha \\ p_d^\beta \\ p_k^\alpha \\ p_r^\alpha \\ p_k^\beta \\ p_r^\beta \end{Bmatrix} = 0 \quad (4.15)$$

Extracting out the matrices C_{dd} and C_{dl} gives

$$C_{dd} = \begin{bmatrix} \Psi_{jd}^\alpha & -\Psi_{jd}^\beta \\ \mathbf{I} & \mathbf{I} \end{bmatrix}, \quad C_{dl} = \begin{bmatrix} \Phi_{jk}^\alpha & \Psi_{jr}^\alpha & -\Phi_{jk}^\beta & -\Psi_{jr}^\beta \\ \mathbf{0} & \mathbf{0} & \mathbf{0} & \mathbf{0} \end{bmatrix} \quad (4.16)$$

From equation (3.18), S can be written as

$$S = \begin{bmatrix} -C_{dd}^{-1}C_{dl} \\ \mathbf{I}_l \end{bmatrix} \quad (4.17)$$

μ and κ are constructed according to the order of the generalized coordinates p .

For example, for a two component system,

$$\mu = \begin{bmatrix} \mu_{dd}^\alpha & \mathbf{0} & \mathbf{0} & \mathbf{0} & \mathbf{0} & \mathbf{0} \\ \mathbf{0} & \mu_{dd}^\beta & \mathbf{0} & \mathbf{0} & \mathbf{0} & \mathbf{0} \\ \mathbf{0} & \mathbf{0} & \mu_{kk}^\alpha & \mathbf{0} & \mathbf{0} & \mathbf{0} \\ \mathbf{0} & \mathbf{0} & \mathbf{0} & \mu_{rr}^\alpha & \mathbf{0} & \mathbf{0} \\ \mathbf{0} & \mathbf{0} & \mathbf{0} & \mathbf{0} & \mu_{kk}^\beta & \mathbf{0} \\ \mathbf{0} & \mathbf{0} & \mathbf{0} & \mathbf{0} & \mathbf{0} & \mu_{rr}^\beta \end{bmatrix}, \quad \kappa = \begin{bmatrix} \kappa_{dd}^\alpha & \mathbf{0} & \mathbf{0} & \mathbf{0} & \mathbf{0} & \mathbf{0} \\ \mathbf{0} & \kappa_{dd}^\beta & \mathbf{0} & \mathbf{0} & \mathbf{0} & \mathbf{0} \\ \mathbf{0} & \mathbf{0} & \kappa_{kk}^\alpha & \mathbf{0} & \mathbf{0} & \mathbf{0} \\ \mathbf{0} & \mathbf{0} & \mathbf{0} & \kappa_{rr}^\alpha & \mathbf{0} & \mathbf{0} \\ \mathbf{0} & \mathbf{0} & \mathbf{0} & \mathbf{0} & \kappa_{kk}^\beta & \mathbf{0} \\ \mathbf{0} & \mathbf{0} & \mathbf{0} & \mathbf{0} & \mathbf{0} & \kappa_{rr}^\beta \end{bmatrix} \quad (4.18)$$

The synthesized mass and stiffness matrices are calculated from equation (3.21),

or written again here,

$$M = S^T \mu S, \quad K = S^T \kappa S \quad (4.19)$$

The synthesized system equation of motion is

$$M\ddot{q} + Kq = \mathbf{0} \quad (4.20)$$

As before, the eigenvalue problem is solved in generalized coordinates and then the mode shapes are transformed back into physical space using equation (4.8). However, equation (4.8) needs the attachment mode coordinates as well as the normal mode and

rigid-body mode coordinates. A simple way to go from q coordinates to p coordinates is to multiply the mode shapes by the S matrix. Then equation (4.8) can be used for each component to put the mode shapes in component physical coordinates; they can then be transformed to global coordinates if necessary. This procedure, except for the need to calculate the attachment mode coordinates, is identical to that given in *Example 1*.

In *Example 2*, a slightly different system from the one in *Example 1* is considered: the support on the right hand side is removed. Since the α component is constrained, that part of the example shows the calculation and use of *residual attachment modes*; the β component on the other hand, since it is unrestrained, demonstrates using *rigid-body* and *residual inertia relief attachment modes*. The highest frequency mode is truncated from each component.

Example 2: The Craig-Chang method.

Problem:

For the system shown in Figure 4.2, the Craig-Chang method will be used to find the system natural frequencies and mode shapes. Only the highest frequency mode will be truncated from both components. The exact answer will be given for comparison.

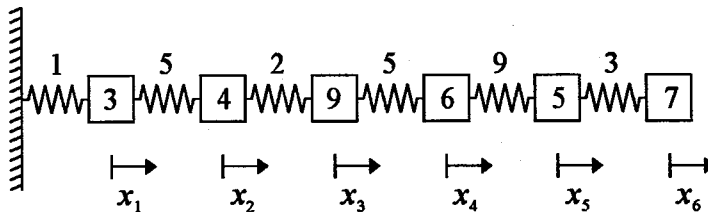
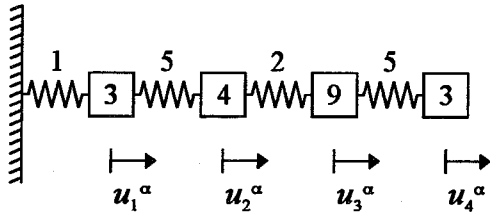


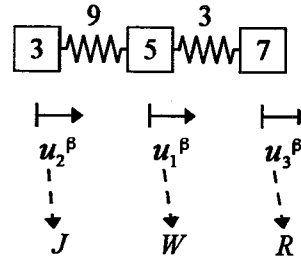
Figure 4.2: The full system for *Example 2*.

Solution:

Choose component α to be:



and β to be:



Note that now the fourth mass is halved whereas for the Craig-Bampton method it was not. For this method it was found, by trial and error, that halving gave the best results.

Component α :

The equation of motion is

$$\begin{bmatrix} 3 & 0 & 0 & 0 \\ 0 & 4 & 0 & 0 \\ 0 & 0 & 9 & 0 \\ 0 & 0 & 0 & 3 \end{bmatrix} \begin{bmatrix} \ddot{u}_1 \\ \ddot{u}_2 \\ \ddot{u}_3 \\ \ddot{u}_4 \end{bmatrix}^\alpha + \begin{bmatrix} 6 & -5 & 0 & 0 \\ -5 & 7 & -2 & 0 \\ 0 & -2 & 7 & -5 \\ 0 & 0 & -5 & 5 \end{bmatrix} \begin{bmatrix} u_1 \\ u_2 \\ u_3 \\ u_4 \end{bmatrix}^\alpha = \begin{bmatrix} 0 \\ 0 \\ 0 \\ 0 \end{bmatrix} \quad (\text{e2.1})$$

Normal Modes:

Solving the eigenvalue problem and normalizing the mode shapes gives

$$\Lambda^\alpha = \begin{bmatrix} 0.0382 & 0 & 0 & 0 \\ 0 & 0.5295 & 0 & 0 \\ 0 & 0 & 2.2776 & 0 \\ 0 & 0 & 0 & 3.3492 \end{bmatrix} \quad (\text{e2.2})$$

$$\Phi^\alpha = \begin{bmatrix} 0.1645 & -0.3543 & 0.0762 & -0.4183 \\ 0.1936 & -0.3126 & -0.0127 & 0.3386 \\ 0.2516 & 0.1227 & -0.1770 & -0.0372 \\ 0.2575 & 0.1799 & 0.4830 & 0.0369 \end{bmatrix} \quad (\text{e2.3})$$

Since the highest frequency mode is being truncated

$$\Lambda_k^\alpha = \begin{bmatrix} 0.0382 & 0 & 0 \\ 0 & 0.5295 & 0 \\ 0 & 0 & 2.2776 \end{bmatrix} \quad (\text{e2.4})$$

and

$$\Phi_k^\alpha = \begin{bmatrix} 0.1645 & -0.3543 & 0.0762 \\ 0.1936 & -0.3126 & -0.0127 \\ 0.2516 & 0.1227 & -0.1770 \\ 0.2575 & 0.1799 & 0.4830 \end{bmatrix} \quad (\text{e2.5})$$

Residual Attachment Modes:

Equations (4.11) are used since this component is restrained. Since there is only one joint coordinate, F is simply

$$F^\alpha = \begin{Bmatrix} 0 \\ 0 \\ 0 \\ 1 \end{Bmatrix} \quad (\text{e2.6})$$

The residual flexibility matrix G_d is calculated giving

$$G_d^\alpha = (k^\alpha)^{-1} - [\Phi_k \Lambda_k^{-1} \Phi_k^T]^\alpha = \begin{bmatrix} 0.0522 & -0.0432 & 0.0046 & -0.0046 \\ -0.0432 & 0.0342 & -0.0038 & 0.0037 \\ 0.0046 & -0.0038 & 0.0004 & -0.0004 \\ -0.0046 & 0.0037 & -0.0004 & 0.0004 \end{bmatrix} \quad (\text{e2.7})$$

Then, by equation (4.9), the residual attachment mode is

$$\Psi_d^\alpha = G_d^\alpha F^\alpha = \begin{Bmatrix} -0.0046 \\ 0.0037 \\ -0.0004 \\ 0.0004 \end{Bmatrix} \quad (\text{e2.8})$$

Note that the residual attachment mode is a multiple of the truncated mode. This

is expected since the attachment mode was derived to be linearly independent of kept modes and to contain information on *all* deleted modes, only one in this case.

Therefore, from equation (B.2), the component mode matrix for α is

$$\Psi^\alpha = \begin{bmatrix} 0.1645 & -0.3543 & 0.0762 & -0.0046 \\ 0.1936 & -0.3126 & -0.0127 & 0.0037 \\ 0.2516 & 0.1227 & -0.1770 & -0.0004 \\ 0.2575 & 0.1799 & 0.4830 & 0.0004 \end{bmatrix} \quad (\text{e2.9})$$

From equation (3.7),

$$\mu^\alpha = \begin{bmatrix} 1 & 0 & 0 & 0 \\ 0 & 1 & 0 & 0 \\ 0 & 0 & 1 & 0 \\ 0 & 0 & 0 & 0.0001 \end{bmatrix}, \quad \kappa^\alpha = \begin{bmatrix} 0.0382 & 0 & 0 & 0 \\ 0 & 0.5295 & 0 & 0 \\ 0 & 0 & 2.2776 & 0 \\ 0 & 0 & 0 & 0.0004 \end{bmatrix} \quad (\text{e2.10})$$

Component β :

Based on the partitioning of the stiffness (and mass) matrix in equation (4.10) and the coordinates chosen (see the figure of the β component), the equation of motion is

$$\begin{bmatrix} 5 & 0 & 0 \\ 0 & 3 & 0 \\ 0 & 0 & 7 \end{bmatrix} \begin{Bmatrix} \bar{u}_1 \\ \bar{u}_2 \\ \bar{u}_3 \end{Bmatrix}^\beta + \begin{bmatrix} 12 & -9 & -3 \\ -9 & 9 & 0 \\ -3 & 0 & 3 \end{bmatrix} \begin{Bmatrix} u_1 \\ u_2 \\ u_3 \end{Bmatrix}^\beta = \begin{Bmatrix} 0 \\ 0 \\ 0 \end{Bmatrix} \quad (\text{e2.11})$$

Normal Modes:

Solving the eigenvalue problem and normalizing the mode shapes gives

$$\Lambda^\alpha = \begin{bmatrix} 0.0000 & 0 & 0 \\ 0 & 0.7612 & 0 \\ 0 & 0 & 5.0674 \end{bmatrix} \quad (\text{e2.12})$$

and

$$\Phi^\alpha = \begin{bmatrix} 0.2582 & 0.2132 & 0.2965 \\ 0.2582 & 0.2856 & -0.4302 \\ 0.2582 & -0.2747 & -0.0274 \end{bmatrix} \quad (\text{e2.13})$$

Note that this set of normal modes includes the rigid-body mode. Therefore, the set of *elastic* natural frequencies and normal modes are given by

$$\Lambda_e^\alpha = \begin{bmatrix} 0.7612 & 0 \\ 0 & 5.0674 \end{bmatrix} \quad (\text{e2.14})$$

and

$$\Phi_e^\alpha = \begin{bmatrix} 0.2132 & 0.2965 \\ 0.2856 & -0.4302 \\ -0.2747 & -0.0274 \end{bmatrix} \quad (\text{e2.15})$$

Truncating the highest frequency mode leaves

$$\Lambda_k^\alpha = 0.7612 \quad (\text{e2.16})$$

and

$$\Phi_k^\alpha = \begin{bmatrix} 0.2132 \\ 0.2856 \\ -0.2747 \end{bmatrix} \quad (\text{e2.17})$$

Rigid-Body Modes:

To calculate the rigid-body mode, either the equation given in (4.10) may be used or, since it was calculated along with the normal modes, it may simply be retrieved from there. Either way, the result is

$$\Psi_r^\alpha = \begin{bmatrix} 0.2582 \\ 0.2582 \\ 0.2582 \end{bmatrix} \quad (\text{e2.18})$$

Residual Inertia Relief Attachment Modes:

Equations (4.10) are used since this component is unrestrained. Since there

is only one joint coordinate, F is simply

$$F^{\beta} = \begin{Bmatrix} 0 \\ 1 \\ 0 \end{Bmatrix} \quad (\text{e2.19})$$

The matrices P and G are calculated giving

$$P^{\beta} = \begin{bmatrix} 0.6667 & -0.3333 & -0.3333 \\ -0.2000 & 0.8000 & -0.2000 \\ -0.4667 & -0.4667 & 0.5333 \end{bmatrix}, \quad G^{\beta} = \begin{bmatrix} 0.3333 & 0.3333 & 0 \\ 0.3333 & 0.4444 & 0 \\ 0 & 0 & 0 \end{bmatrix} \quad (\text{e2.20})$$

The residual flexibility matrix G_d can be calculated yielding

$$G_d^{\beta} = \begin{bmatrix} 0.0173 & -0.0252 & -0.0016 \\ -0.0252 & 0.0365 & 0.0023 \\ -0.0016 & 0.0023 & 0.0001 \end{bmatrix} \quad (\text{e2.21})$$

Then, by equation (4.9), the residual attachment mode is

$$\Psi_d^{\beta} = G_d^{\beta} F^{\beta} = \begin{Bmatrix} -0.0252 \\ 0.0365 \\ 0.0023 \end{Bmatrix} \quad (\text{e2.22})$$

As may be expected from component α , the residual inertia relief attachment mode is a multiple of the truncated normal mode.

Assembling the component mode matrix, from equation (B.2),

$$\Psi^{\beta} = \begin{bmatrix} 0.2132 & 0.2582 & -0.0252 \\ 0.2856 & 0.2582 & 0.0365 \\ -0.2747 & 0.2582 & 0.0023 \end{bmatrix} \quad (\text{e2.23})$$

From equation (3.7),

$$\mu^{\beta} = \begin{bmatrix} 1 & 0 & 0 \\ 0 & 1 & 0 \\ 0 & 0 & 0.0072 \end{bmatrix}, \quad \kappa^{\beta} = \begin{bmatrix} 0.7612 & 0 & 0 \\ 0 & 0 & 0 \\ 0 & 0 & 0.0365 \end{bmatrix} \quad (\text{e2.24})$$

Synthesis:

The generalized coordinates are given as

$$p = \begin{Bmatrix} P_{d_1}^\alpha \\ P_{d_1}^\beta \\ P_{k_1}^\alpha \\ P_{k_2}^\alpha \\ P_{k_3}^\alpha \\ P_{k_1}^\beta \\ P_{r_1}^\beta \end{Bmatrix}, \quad q = \begin{Bmatrix} p_{k_1}^\alpha \\ p_{k_2}^\alpha \\ p_{k_3}^\alpha \\ p_{k_1}^\beta \\ p_{r_1}^\beta \end{Bmatrix} \quad (\text{e2.25})$$

To find the matrix S which is needed to transform p coordinates to q coordinates, the matrices C_{dd} and C_{dl} are needed. From equation (4.16),

$$C_{dd} = \begin{bmatrix} 0.0004 & -0.0365 \\ & 1 & & & \\ & & 1 & & \end{bmatrix} \quad (\text{e2.26})$$

and, since the β component has a rigid-body mode,

$$C_{dl} = \begin{bmatrix} \Phi_{jk}^\alpha & -\Phi_{jk}^\beta & -\Psi_{jr}^\beta \\ \mathbf{0} & \mathbf{0} & \mathbf{0} \end{bmatrix} = \begin{bmatrix} -0.2575 & -0.1799 & 0.4830 & -0.2856 & -0.2582 \\ & 0 & 0 & 0 & 0 \\ & & 0 & 0 & 0 \end{bmatrix} \quad (\text{e2.27})$$

Now, S can be calculated from equation (4.17) giving

$$S = \begin{bmatrix} 6.9736 & 4.8705 & -13.0786 & 7.7340 & 6.9914 \\ -6.9736 & -4.8705 & 13.0786 & -7.7340 & -6.9914 \\ & 1 & 0 & 0 & 0 \\ & 0 & 1 & 0 & 0 \\ & 0 & 0 & 1 & 0 \\ & 0 & 0 & 0 & 1 \\ & 0 & 0 & 0 & 0 & 1 \end{bmatrix} \quad (\text{e2.28})$$

The matrices μ and κ are constructed according to equation (4.18). For illustration, κ is given as

$$\kappa = \begin{bmatrix} 0.0004 & 0 & 0 & 0 & 0 & 0 & 0 \\ 0 & 0.0365 & 0 & 0 & 0 & 0 & 0 \\ 0 & 0 & 0.0382 & 0 & 0 & 0 & 0 \\ 0 & 0 & 0 & 0.5295 & 0 & 0 & 0 \\ 0 & 0 & 0 & 0 & 2.2776 & 0 & 0 \\ 0 & 0 & 0 & 0 & 0 & 0.7612 & 0 \\ 0 & 0 & 0 & 0 & 0 & 0 & 0 \end{bmatrix} \quad (\text{e2.29})$$

The synthesized mass and stiffness matrices are calculated from equation (4.19):

$$M = \begin{bmatrix} 1.3564 & 0.2489 & -0.6684 & 0.3953 & 0.3573 \\ 0.2489 & 1.1739 & -0.4669 & 0.2761 & 0.2496 \\ -0.6684 & -0.4669 & 2.2536 & -0.7413 & -0.6702 \\ 0.3953 & 0.2761 & -0.7413 & 1.4384 & 0.3963 \\ 0.3573 & 0.2496 & -0.6702 & 0.3963 & 1.3582 \end{bmatrix} \quad (\text{e2.30})$$

and

$$K = \begin{bmatrix} 1.8342 & 1.2544 & -3.3683 & 1.9918 & 1.8006 \\ 1.2544 & 1.4056 & -2.3525 & 1.3911 & 1.2576 \\ -3.3683 & -2.3525 & 8.5945 & -3.7356 & -3.3769 \\ 1.9918 & 1.3911 & -3.7356 & 2.9702 & 1.9969 \\ 1.8006 & 1.2576 & -3.3769 & 1.9969 & 1.8052 \end{bmatrix} \quad (\text{e2.31})$$

Solution of the eigenvalue problem yields

$$\Lambda_j = \begin{bmatrix} 0.0183 & 0 & 0 & 0 & 0 \\ 0 & 0.3002 & 0 & 0 & 0 \\ 0 & 0 & 0.6001 & 0 & 0 \\ 0 & 0 & 0 & 1.3132 & 0 \\ 0 & 0 & 0 & 0 & 4.0862 \end{bmatrix} \quad (\text{e2.32})$$

and

$$\Phi_s = \begin{bmatrix} 0.1052 & 0.2557 & 0.2653 & 0.0982 & -0.0687 \\ 0.1251 & 0.2610 & 0.2226 & 0.0384 & 0.0490 \\ 0.1702 & 0.1170 & -0.1507 & -0.2064 & 0.0422 \\ 0.1826 & -0.0038 & -0.1373 & 0.1830 & -0.2808 \\ 0.1873 & -0.0701 & -0.0749 & 0.2394 & 0.3092 \\ 0.1957 & -0.2341 & 0.1871 & -0.1160 & -0.0361 \end{bmatrix} \quad (e2.33)$$

where the mode shapes have already been transformed into physical space and normalized with respect to the full system mass matrix. This transformation is identical to that in *Example 1* except the mode shape matrix was first premultiplied by S to get the modes in p coordinates. For comparison, the exact solution is

$$\Lambda_o = \begin{bmatrix} 0.0183 & 0 & 0 & 0 & 0 & 0 \\ 0 & 0.3002 & 0 & 0 & 0 & 0 \\ 0 & 0 & 0.6001 & 0 & 0 & 0 \\ 0 & 0 & 0 & 1.3132 & 0 & 0 \\ 0 & 0 & 0 & 0 & 3.3422 & 0 \\ 0 & 0 & 0 & 0 & 0 & 4.1158 \end{bmatrix} \quad (e2.34)$$

and

$$\Phi_o = \begin{bmatrix} 0.1052 & 0.2558 & 0.2652 & 0.0965 & 0.4207 & 0.0138 \\ 0.1251 & 0.2609 & 0.2227 & 0.0398 & -0.3388 & -0.0176 \\ 0.1702 & 0.1170 & -0.1507 & -0.2066 & 0.0271 & 0.0485 \\ 0.1826 & -0.0038 & -0.1373 & 0.1831 & 0.0105 & -0.2843 \\ 0.1873 & -0.0701 & -0.0749 & 0.2393 & -0.0221 & 0.3108 \\ 0.1957 & -0.2341 & 0.1871 & -0.1159 & 0.0033 & -0.0361 \end{bmatrix} \quad (e2.35)$$

Comparing the results, it is seen that the Craig-Chang method performed well on the first four modes. As with the previous example, if only the first four modes were of interest, this may suffice. ■ ■

4.3 Differences in the Craig-Bampton and Craig-Chang Methods

The primary difference in these two methods of component mode synthesis is that *the Craig-Bampton method is a fixed-interface type while the Craig-Chang method is a free-interface type*. This categorization alone may be enough for choosing one method above the other. For example, if the free-interface boundary most closely represents the actual physical conditions, the Craig-Chang method should be used. (This idea is discussed further in section V.)

Another notable distinction is the fact that *the Craig-Bampton method is exact if all normal modes are retained whereas the Craig-Chang method is not*. The reason that the Craig-Chang method is not exact arises from the choice of independent generalized coordinates: only normal and rigid-body coordinates are retained which, as discussed previously, can significantly reduce the synthesized model order for systems with large numbers of joint coordinates. However, the cost is to lose accuracy. Note that the Craig-Chang method can be modified to include the attachment mode coordinates; this would make it exact if only the minimum number of normal modes were truncated.

A third, important difference between these two methods is that the Craig-Chang method uses *inertia relief modes* to account for elasticity of deleted normal modes; there is no such provision in the Craig-Bampton method. An advantage of using these modes is that they may improve convergence; a disadvantage is that their calculation is computationally more intensive than the calculation of constraint modes (which are used in the Craig-Bampton method).

V. COMPONENT MODE SYNTHESIS ON HMB WITH MSC/NASTRAN

In an effort to determine the effect of substructure modal truncation, three types of component mode synthesis, standard in version 67 of MSC/NASTRAN, were applied to a finite element model of HMB-2R. HMB-2R is a dynamically scaled laboratory space-station model developed at the NASA-Langley Research Center.⁴ The finite element model of the particular configuration studied has over 4500 degrees of freedom and is shown in Figure 5.1. This model was divided into eight components: the main truss, the outboard truss, the alpha joint, the electrical power system (EPS), the forward and aft photo-voltaic arrays (Fwd PV and Aft PV), the thermal control system (TCS), and the AWP pallet (which, in the figure, is on the back side of the main truss).

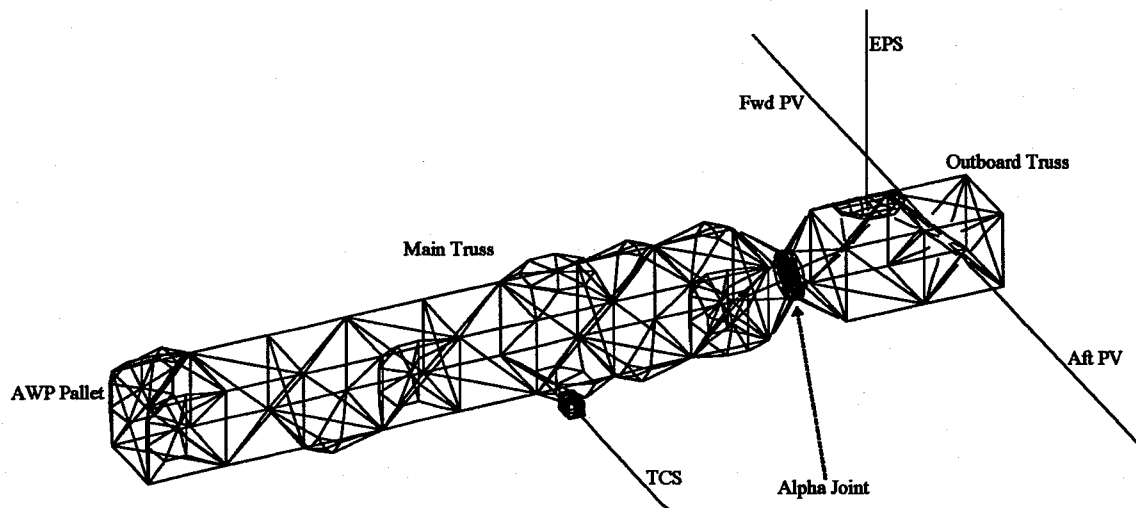


Figure 5.1: The HMB-2R finite element model.

In reference 4, the authors have done a limited component mode synthesis study with a slightly different configuration. They used the Craig-Bampton method to study the effect of truncating modes while keeping the same number of modes from each component. They found that accurate frequency results were obtained for all modes at least up to the lowest upper frequency kept from any component.

The purpose of this section is also to study the effect of truncating modes, but with two differences: 1) three types of component mode synthesis will be investigated, namely a *fixed-interface*, a *free-interface*, and a *hybrid-interface* type; and 2) the number of modes kept from one component is not necessarily equal to the number kept for another component. The approach taken here was to keep modes from each component up to a certain frequency (50 Hz in this case) and deviate from there; the manner of deviation will first be shown in section 5.1. The reason for using 50 Hz is to have some variety; that is, some components have frequencies in this range and some do not (as will be seen in the next sub-section). A similar approach was used to study a simple beam structure in reference 13 but with the focus primarily on free-interface methods.

The method of component mode synthesis implemented in MSC/NASTRAN was developed by Herting.¹⁴ A benefit of this method is that the choice of interface (joint) boundary conditions during normal mode calculation is completely arbitrary. For example, the user can have all joint coordinates fixed as in the Craig-Bampton method, or all free as in the Craig-Chang method. In fact, Herting states that when all joint coordinates are fixed, the method produces exactly the same matrices as the Craig-Bampton method. He goes on to state that other studies^{15,16} have shown that this method gives identical results to the Craig-Chang method when free boundary conditions are used. He concludes by recommending the use of boundary conditions that most closely represent the physical boundary conditions. For instance, if an antenna is attached to an aircraft, a fixed boundary should be used for the antenna and a free boundary for the aircraft.

To evaluate the results in each case, both the synthesized frequency and the mode

shapes were compared to the exact. The parameter used to compare the mode shapes in this study will be called the modal correlation coefficient (*MCC*). The *MCC* is defined as the absolute value of the dot product of the approximate mode shape with the exact mode divided by their magnitudes, or, if ϕ_a is the approximate mode and ϕ_e is the exact,

$$MCC = \frac{|\phi_a^T \phi_e|}{\|\phi_a\| \|\phi_e\|}, \quad 0 \leq MCC \leq 1 \quad (5.1)$$

If the *MCC* is unity, the approximate mode matches the exact mode; if it equals zero, the approximate mode is orthogonal to the exact mode. The *MCC* is used to correlate the approximate modes with the exact modes and to order them in the same order as the exact modes; the approximate frequencies, therefore, may not be in strictly ascending order. This parameter is the square root of the Modal Assurance Criterion (*MAC*) used in other studies.⁴

For the HMB-2R structure, forty one nodes (out of over 800 possible nodes) with six degrees of freedom each were chosen to represent the mode shape. Identified by their MSC/NASTRAN grid point number, the chosen nodes are shown in Figure 5.2.

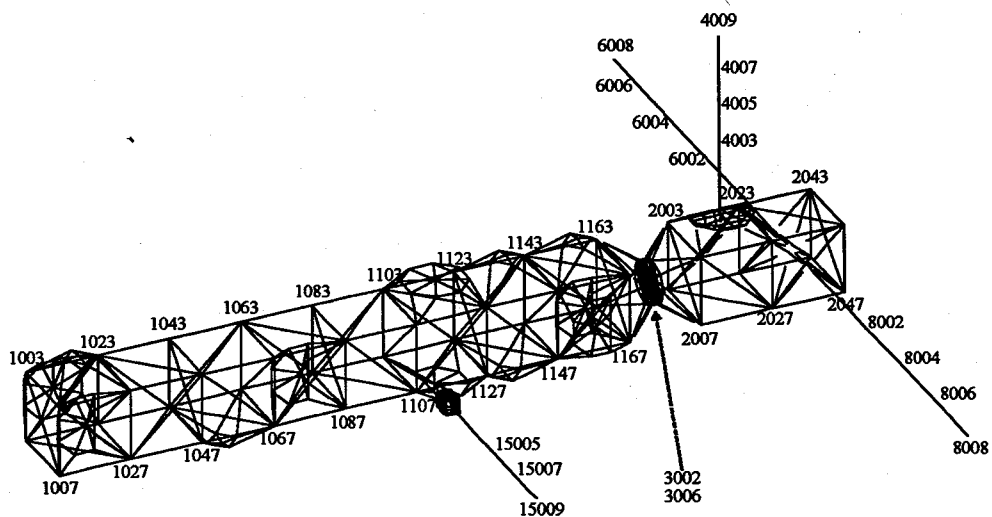


Figure 5.2: Nodes on HMB-2R used for calculating *MCC*.

5.1 Hybrid Case

To show the boundary conditions that were used, HMB-2R is redrawn as a “stick-figure” in Figure 5.3. The boundary conditions are shown in Figure 5.4 where the shaded cross-hatchings represent the fixed coordinates during normal mode analysis. The criterion for this selection is to try to get as close as possible to the physical conditions while attempting to simulate possible test configurations where it is assumed that each component is cantilevered at one end.

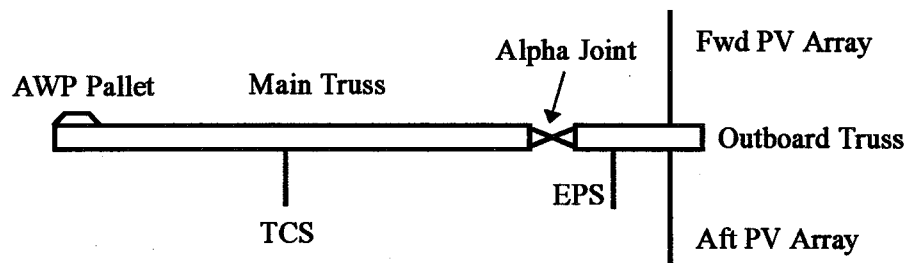


Figure 5.3: Stick-figure of HMB-2R.

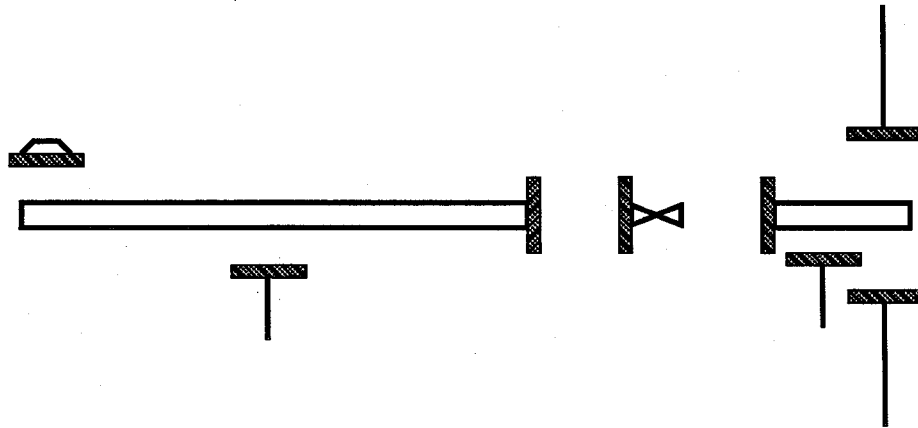


Figure 5.4: Restraining of components for hybrid runs.

The frequency data (in Hz) for the full system and for each component are shown in Table 5.1. Note that not all frequency data are included; each component listing includes only one or two frequencies beyond 50 Hz. The system frequencies listed are “exact,” that is, they were calculated by solving the complete system eigenvalue problem.

Frequency Number	Full System	Main Truss	Outboard Truss	Alpha Joint	EPS	Fwd PV	Aft PV	TCS	AWP Pallet
1	4.656	4.872	41.23	114.9	44.32	20.13	20.13	42.87	69.50
2	5.972	4.950	55.50		44.32	20.13	20.13	42.87	72.86
3	7.538	17.80			344.3	168.7	168.7	452.7	
4	10.83	19.93			344.3	168.7	168.7	467.3	
5	11.86	25.19							
6	12.47	34.19							
7	13.23	35.83							
8	13.84	40.12							
9	14.32	47.23							
10	15.45	53.32							
11	21.35	59.86							
12	24.73								
13	26.95								
14	33.68								
15	38.21								
16	40.22								
17	43.09								
18	49.73								

Table 5.1: HMB-2R frequency data for hybrid cases.

A summary of component frequency data is given in Table 5.2. These data were used to determine what set of cases would be studied.

Component	Number of modes below 50 Hz	Lowest frequency (Hz)	Next frequency (after 50 Hz)
Main truss	9	4.872	53.32
Outboard truss	1	41.23	55.50
Alpha joint	0	114.9	115.1
EPS	2	44.32 (2)*	344.3
Fwd PV array	2	20.13 (2)	168.7
Aft PV array	2	20.13 (2)	168.7
TCS	2	42.87 (2)	452.7
AWP pallet	0	69.50	72.9

* There are two modes at this frequency.

Table 5.2: Summary of component frequency data for the hybrid case.

From information in Table 5.2, a set of nine cases were selected. Table 5.3 shows the number of kept normal modes for each component in each case. Case one is the “control-case,” keeping all component modes up to 50 Hz. Cases two through five vary the number of normal modes kept for the main truss while holding all others constant. Case six deletes the one mode from the outboard truss. Cases seven and eight delete the number of modes kept from the appendages in two steps. Case nine is simply the control-case except with a minimum of one mode kept for each component.

Component	Number of normal modes kept for each component in hybrid case:								
	one	two	three	four	five	six	seven	eight	nine
Main truss	9	6	3	0	15	9	9	9	9
Outboard truss	1	1	1	1	1	0	1	1	1
Alpha joint	0	0	0	0	0	0	0	0	1
EPS	2	2	2	2	2	2	1	0	2
Fwd PV array	2	2	2	2	2	2	1	0	2
Aft PV array	2	2	2	2	2	2	1	0	2
TCS	2	2	2	2	2	2	1	0	2
AWP pallet	0	0	0	0	0	0	0	0	1

Table 5.3: Hybrid run data for HMB-2R.

Results:

The frequency results, percent frequency errors, and percent *MCC* errors for each case are shown in Tables 5.4 through 5.6, respectively. In some cases, the modes were switched according to the highest *MCC*. To simplify viewing, all errors above five percent are highlighted.

Frequency Number	Exact Frequency	Frequency results for hybrid case:								
		1	2	3	4	5	6	7	8	9
1	4.656	4.657	4.657	4.658	4.658	4.656	4.657	4.663	4.740	4.656
2	5.972	5.973	5.974	5.974	5.975	5.973	5.974	6.076	6.097	5.973
3	7.538	7.542	7.544	7.549	7.558	7.541	7.543	7.682	7.690	7.542
4	10.83	10.84	10.84	10.86	10.88	10.84	10.84	10.99	11.18	10.83
5	11.86	11.86	11.86	11.86	11.88	11.86	11.86	11.97	12.82	11.86
6	12.47	12.48	12.48	12.49	12.49	12.48	12.48	12.75	14.09	12.47
7	13.23	13.23	13.23	13.24	13.25	13.23	13.24	13.66	16.75	13.23
8	13.84	13.84	13.84	13.86	13.91	13.84	13.84	16.59	14.92	13.84
9	14.32	14.35	14.35	14.60	14.92	14.35	14.35	14.39	14.59	14.35
10	15.45	15.47	15.47	15.72	15.95	15.46	15.47	15.46	15.55	15.46
11	21.35	21.48	21.58	21.79	22.52	21.45	21.50	22.24	22.28	21.48
12	24.73	24.82	25.03	25.21	30.39	24.80	24.83	25.25	25.30	24.82
13	26.95	27.34	27.87	28.01	27.45	27.22	27.34	27.58	28.49	27.28
14	33.68	34.67	35.09	36.31	36.55	34.25	34.67	34.68	35.46	34.67
15	38.21	38.51	41.63	45.96	47.65	38.47	38.51	38.58	38.95	38.41
16	40.22	41.31	44.12	44.42	44.28	40.99	41.34	41.65	41.87	41.20
17	43.09	43.99	44.46	44.23		43.50	44.00	47.20	48.72	43.99
18	49.73									

Table 5.4: Frequency results for hybrid cases.

Frequency Number	Percent frequency errors for hybrid case:								
	1	2	3	4	5	6	7	8	9
1	0.02	0.03	0.05	0.05	0.02	0.02	0.15	1.81	0.01
2	0.02	0.02	0.04	0.04	0.02	0.02	1.74	2.08	0.02
3	0.06	0.08	0.15	0.26	0.04	0.06	1.90	2.02	0.06
4	0.14	0.14	0.29	0.50	0.13	0.14	1.53	3.23	0.04
5	0.01	0.02	0.05	0.16	0.01	0.01	0.92	8.09	0.01
6	0.04	0.04	0.12	0.15	0.03	0.04	2.21	12.98	0.02
7	0.01	0.01	0.03	0.13	0.01	0.03	3.24	26.89	0.01
8	0.06	0.06	0.17	0.57	0.05	0.06	19.94	7.81	0.06
9	0.19	0.22	1.92	4.15	0.18	0.19	0.46	1.86	0.17
10	0.10	0.15	1.77	3.21	0.09	0.11	0.07	0.64	0.09
11	0.64	1.09	2.08	5.56	0.49	0.70	4.18	4.36	0.64
12	0.35	1.20	1.94	22.85	0.29	0.39	2.11	2.29	0.34
13	1.45	3.42	3.95	1.84	0.99	1.45	2.32	5.73	1.23
14	2.94	4.19	7.81	8.54	1.71	2.94	2.97	5.30	2.94
15	0.79	8.96	26.28	24.69	0.68	0.79	0.96	1.94	0.52
16	2.70	9.70	10.42	10.08	1.89	2.78	3.55	4.09	2.43
17	2.09	3.17	2.63		0.94	2.10	9.52	13.05	2.07

Table 5.5: Percent frequency errors for hybrid cases.

Frequency Number	Percent MCC errors for hybrid case:								
	1	2	3	4	5	6	7	8	9
1	0.00	0.00	0.00	0.00	0.00	0.00	0.02	0.03	0.00
2	0.00	0.00	0.00	0.00	0.00	0.00	0.13	0.12	0.00
3	0.00	0.00	0.00	0.00	0.00	0.00	0.22	0.23	0.00
4	0.00	0.00	0.03	0.11	0.00	0.00	1.05	3.43	0.00
5	0.00	0.00	0.01	0.05	0.00	0.00	2.25	22.47	0.00
6	0.00	0.00	0.01	0.02	0.00	0.00	1.89	33.12	0.00
7	0.00	0.00	0.01	0.09	0.00	0.00	22.45	36.78	0.00
8	0.01	0.01	0.06	0.82	0.01	0.01	40.95	78.47	0.01
9	0.02	0.02	1.85	3.27	0.01	0.02	13.05	26.30	0.02
10	0.00	0.00	1.07	0.97	0.00	0.00	25.89	26.41	0.00
11	0.02	0.05	0.36	2.23	0.01	0.02	1.87	2.02	0.02
12	0.02	0.17	0.48	36.27	0.01	0.02	1.81	1.80	0.01
13	0.03	0.30	0.40	25.88	0.04	0.03	0.53	1.48	0.02
14	0.32	0.53	2.73	2.26	0.18	0.32	0.34	2.28	0.32
15	0.35	28.01	28.40	13.90	0.29	0.34	0.51	3.96	0.23
16	1.10	50.52	18.64	73.46	0.86	1.16	1.40	2.38	0.96
17	0.75	12.67	5.58		0.29	0.77	3.59	4.52	0.69

Table 5.6: Percent MCC error for hybrid cases.

Discussion:

Notice that the eighteenth exact mode (at 49.7 Hz) was not recovered in any of these cases. Since component mode synthesis always gives a higher estimate of the frequency, the synthesized eighteenth frequency was, in all these cases, above the cut-off value of 50 Hz. If it were important to recover this mode, the eigenvalue solver would have to be set to a higher frequency.

Hybrid case one, where all component normal modes up to 50 Hz were kept, the maximum frequency error was 2.94% and the maximum *MCC* error was 1.1%, which would be acceptable results for most applications. Cases two through four, where main truss modes were progressively truncated, show increasing errors in the higher frequencies with a maximum frequency error of 24.7% in case four. However, even in case four where there are no main truss modes, the errors for the first eight modes were still less than one percent. This reveals that the main truss contributes to the lower frequency modes *mostly* through its static deflection shapes (such as constraint and attachment modes). Indeed, the ninth mode is the first mode in which the main truss exhibits significant motion (see **Appendix C** where figures of the system mode shapes up to 50 Hz are given). Case five, which adds an extra main truss mode, reduces the maximum frequency error to 1.89% and the maximum *MCC* error to 0.86%. This demonstrates that higher frequency dynamics (above 50 Hz) of a component have an effect on the lower frequency dynamics (below 50 Hz) of the system. The sixth case demonstrates that truncating the outboard truss normal mode only slightly affect the results, resulting in the same maximum frequency error as case one and only increasing the maximum *MCC* error by six hundredths of a percent. This shows that the static deflection shapes of the

outboard truss are more important than its dynamic normal modes in the range of interest. On the contrary, the appendage normal modes are shown to be very important to the accuracy of the results in cases seven and eight. It is interesting to note that truncating the appendage normal modes most adversely affect modes five through eight and to a slightly lesser degree, modes nine and ten. This is because these modes are primarily appendage modes as can be seen in **Appendix C**. Case nine, which includes the first normal mode from both the alpha joint and the pallet, demonstrate that this information is of little importance, resulting in the same maximum frequency error as case one and only decreasing the maximum *MCC* error fourteen hundredths of a percent. An overall trend, observable in cases one through four, is that if component modes are kept up to at least twice the desired frequency (which would be 25 Hz for case one, about 17 Hz for case two, etc.), the errors are less than one percent.

5.2 Free Case

The boundary conditions for this case are totally free which means each component has rigid-body modes. In the normal modes analysis, however, they were not included and each normal mode set consists only of *flexible* normal modes. The reason for stating this is to make it clear that it is the number of these modes that are varied, not the number of rigid-body modes. The frequency data are given in Table 5.7.

Frequency Number	Full System	Main Truss	Outboard Truss	Alpha Joint	EPS	Fwd PV	Aft PV	TCS	AWP Pallet
1	4.656	20.78	79.97	105.2	266.7	150.0	150.0	466.8	241.0
2	5.972	21.93	84.74	124.2	266.7	150.0	150.0	466.8	241.4
3	7.538	29.20			854.2	456.3	456.3		
4	10.83	41.74			854.2	456.3	456.3		
5	11.86	44.87							
6	12.47	50.78							
7	13.23	56.92							
8	13.84	62.35							
9	14.32	67.37							
10	15.45	67.89							
11	21.35	68.62							
12	24.73								
13	26.95								
14	33.68								
15	38.21								
16	40.22								
17	43.09								
18	49.73								

Table 5.7: HMB-2R frequency data for free cases.

A summary of component frequency data is given in Table 5.8.

Component	Number of modes below 50 Hz	Lowest frequency (Hz)	Next frequency (after 50 Hz)
Main truss	6	20.78	56.92
Outboard truss	0	80.0	84.74
Alpha joint	0	105.2	124.2
EPS	0	266.7 (2)*	854.2
Fwd PV array	0	150.0 (2)	456.3
Aft PV array	0	150.0 (2)	456.3
TCS	0	466.8 (2)	not calculated
AWP pallet	0	241.0	241.4

* There are two modes at this frequency.

Table 5.8: Summary of component frequency data for the free case.

Because of a requirement in MSC/NASTRAN, the control-case is *not* the number of modes below 50 Hz. For numerical reasons, at least one normal mode has to be

retained from each component. The set of cases selected is shown in Table 5.9.

Component	Number of normal modes kept for each component in free case:			
	one	two	three	four
Main truss	6	3	1	6
Outboard truss	1	1	1	1
Alpha joint	1	1	1	1
EPS	1	1	1	2
Fwd PV array	1	1	1	2
Aft PV array	1	1	1	2
TCS	1	1	1	2
AWP pallet	1	1	1	1

Table 5.9: Free run data for HMB-2R.

Results:

The results are shown in the same format as before in Tables 5.10 through 5.13.

Frequency Number	Exact Frequency	Frequency results for free case:			
		1	2	3	4
1	4.656	4.722	4.722	4.723	4.703
2	5.972	6.054	6.054	6.054	6.044
3	7.538	7.684	7.686	7.687	7.635
4	10.83	11.17	11.17	11.21	11.05
5	11.86	12.66	12.66	12.67	12.46
6	12.47	13.70	13.70	13.73	13.39
7	13.23	14.69	14.69	14.77	13.94
8	13.84	14.42	14.44	14.50	14.52
9	14.32	15.43	15.45	15.68	14.97
10	15.45	16.08	16.10	16.17	15.89
11	21.35	22.10	22.14	22.60	21.91
12	24.73	25.10	25.12	27.59	25.08
13	26.95	28.84	29.33	31.37	28.39
14	33.68	34.79	35.56	36.86	34.74
15	38.21	39.02	43.10	44.19	38.92
16	40.22	41.42	48.51	48.01	41.20
17	43.09	47.95	47.96		46.29
18	49.73				

Table 5.10: Frequency results for free cases.

Frequency Number	Percent frequency errors for free case:			
	1	2	3	4
1	1.43	1.43	1.44	1.03
2	1.36	1.37	1.37	1.19
3	1.93	1.96	1.97	1.28
4	3.13	3.13	3.52	2.05
5	6.73	6.75	6.83	5.11
6	9.86	9.87	10.06	7.32
7	10.99	11.04	11.59	5.38
8	4.21	4.36	4.84	4.95
9	7.70	7.83	9.51	4.52
10	4.10	4.19	4.64	2.84
11	3.51	3.73	5.89	2.66
12	1.48	1.56	11.55	1.41
13	7.02	8.82	16.40	5.34
14	3.31	5.60	9.46	3.15
15	2.11	12.81	15.65	1.86
16	2.97	20.59	19.36	2.43
17	11.26	11.28		7.42

Table 5.11: Percent frequency errors for free cases.

Frequency Number	Percent <i>MCC</i> errors for free case:			
	1	2	3	4
1	0.02	0.02	0.02	0.01
2	0.06	0.06	0.06	0.03
3	0.23	0.23	0.23	0.07
4	4.03	4.03	3.71	1.62
5	12.14	12.10	12.53	12.55
6	17.20	17.19	17.25	12.65
7	28.94	29.64	33.39	19.06
8	45.85	47.53	55.16	30.17
9	55.90	54.68	39.02	34.04
10	27.16	25.60	15.56	4.83
11	1.03	1.13	2.62	0.24
12	0.30	0.43	31.89	0.21
13	0.86	1.50	18.55	0.24
14	0.55	3.29	3.13	0.37
15	3.11	6.30	10.23	1.60
16	3.70	10.00	75.64	1.76
17	3.02	2.56		0.91

Table 5.12: Percent *MCC* errors for free cases.

Discussion:

Comparison of these errors to those of the hybrid cases reveal that the free case results are considerably less accurate. The errors seem to be more evenly distributed throughout the range than in the hybrid case, but are higher on the average. In fact, *all* the frequency errors are above one percent — even for the first frequency. This indicates that a large number of component modes would have to be retained to achieve a high degree of accuracy up to 50 Hz.

5.3 Fixed Case

The fixed case boundary conditions are shown in Figure 5.5 and the frequency data subject to those conditions are given in Table 5.13.

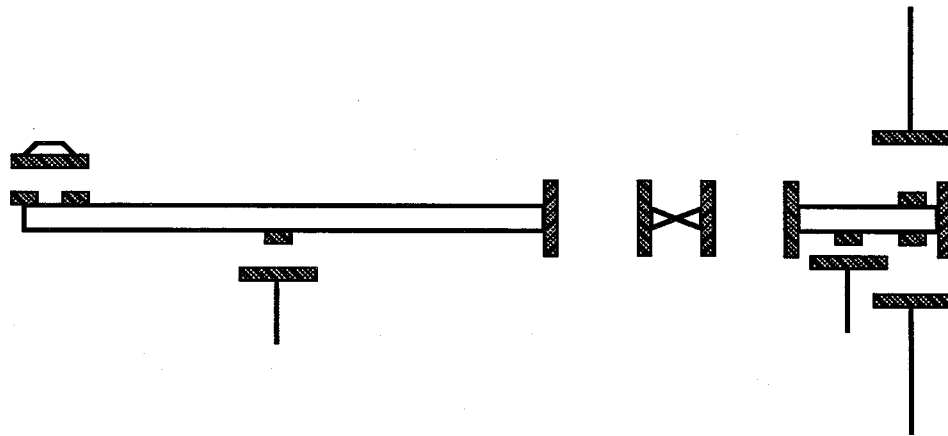


Figure 5.5: Component restraint for the fixed case.

Frequency Number	Full System	Main Truss	Outboard Truss	Alpha Joint	EPS	Fwd PV	Aft PV	TCS	AWP Pallet
1	4.656	28.55	75.57	139.4	44.32	20.13	20.13	42.87	69.50
2	5.972	32.42	89.26	139.7	44.32	20.13	20.13	42.87	72.86
3	7.538	37.08			344.3	168.7	168.7	452.7	
4	10.83	50.68			344.3	168.7	168.7	467.3	
5	11.86	54.52							
6	12.47	57.68							
7	13.23	60.69							
8	13.84								
9	14.32								
10	15.45								
11	21.35								
12	24.73								
13	26.95								
14	33.68								
15	38.21								
16	40.22								
17	43.09								
18	49.73								

Table 5.13: HMB-2R frequency data for fixed cases.

The summary of frequency data that was used to determine what set of cases would be used is given in Table 5.14 and the set of cases is shown in Table 5.15.

Component	Number of modes below 50 Hz	Lowest frequency (Hz)	Next frequency (after 50 Hz)
Main truss	4	28.55	54.52
Outboard truss	0	75.57	89.26
Alpha joint	0	139.4	139.7
EPS	2	44.32 (2)*	344.3
Fwd PV array	2	20.13 (2)	168.7
Aft PV array	2	20.13 (2)	168.7
TCS	2	42.87 (2)	452.7
AWP pallet	0	69.50	72.86

* There are two modes at this frequency.

Table 5.14: Summary of component frequency data for fixed case.

Component	Number of normal modes kept for each component in fixed case:					
	one	two	three	four	five	six
Main truss	4	2	0	4	4	4
Outboard truss	0	0	0	0	0	1
Alpha joint	0	0	0	0	0	1
EPS	2	2	2	1	0	2
Fwd PV array	2	2	2	1	0	2
Aft PV array	2	2	2	1	0	2
TCS	2	2	2	1	0	2
AWP pallet	0	0	0	0	0	1

Table 5.15: Fixed case data for HMB-2R.

Results:

As before, the results are shown in Tables 5.16 through 5.18.

Frequency Number	Exact Frequency	Frequency results for fixed case:					
		1	2	3	4	5	6
1	4.656	4.657	4.658	4.658	4.739	4.740	4.656
2	5.972	5.974	5.975	5.975	5.986	6.098	5.974
3	7.538	7.545	7.557	7.558	7.573	7.693	7.545
4	10.83	10.85	10.85	10.88	11.03	11.19	10.84
5	11.86	11.86	11.86	11.88	12.34	12.82	11.86
6	12.47	12.48	12.49	12.49	14.89	14.10	12.48
7	13.23	13.24	13.24	13.25	13.39	16.77	13.24
8	13.84	13.85	13.85	13.91	14.10	14.93	13.85
9	14.32	14.37	14.50	14.92	14.58	14.60	14.37
10	15.45	15.50	15.88	15.95	15.77	15.58	15.50
11	21.35	21.52	21.60	22.54	21.99	22.33	21.51
12	24.73	25.07	25.36	30.40	25.31	25.56	25.06
13	26.95	27.85	28.20	27.45	29.00	29.08	27.79
14	33.68	34.86	36.14	36.55	35.79	35.81	34.86
15	38.21	41.75	42.41	47.65	41.75	41.81	41.55
16	40.22	41.59	48.49	44.28	42.40	42.55	41.34
17	43.09	44.49	44.32		44.62	49.25	44.45
18	49.73						

Table 5.16: Frequency results for fixed cases.

Frequency Number	Percent frequency errors for fixed case:					
	1	2	3	4	5	6
1	0.03	0.05	0.05	1.80	1.82	0.02
2	0.03	0.04	0.04	0.23	2.10	0.03
3	0.09	0.25	0.26	0.47	2.06	0.09
4	0.21	0.21	0.50	1.85	3.32	0.11
5	0.04	0.04	0.16	4.09	8.11	0.03
6	0.10	0.11	0.15	19.37	13.05	0.09
7	0.03	0.03	0.14	1.22	26.74	0.02
8	0.11	0.11	0.57	1.92	7.91	0.11
9	0.33	1.26	4.16	1.80	1.96	0.31
10	0.33	2.80	3.22	2.10	0.82	0.32
11	0.81	1.18	5.58	3.03	4.61	0.78
12	1.38	2.54	22.89	2.35	3.34	1.33
13	3.33	4.64	1.86	7.60	7.90	3.11
14	3.51	7.31	8.54	6.26	6.33	3.51
15	9.26	10.99	24.69	9.27	9.41	8.75
16	3.40	20.55	10.08	5.40	5.79	2.77
17	3.24	2.84		3.54	14.28	3.14

Table 5.17: Percent frequency errors for fixed cases.

Frequency Number	Percent <i>MCC</i> errors for fixed case:					
	1	2	3	4	5	6
1	0.00	0.00	0.00	0.03	0.03	0.00
2	0.00	0.00	0.00	0.01	0.12	0.00
3	0.00	0.00	0.00	0.02	0.23	0.00
4	0.01	0.01	0.11	4.09	3.36	0.00
5	0.00	0.00	0.05	27.23	22.37	0.00
6	0.00	0.01	0.02	47.71	33.04	0.00
7	0.00	0.00	0.08	1.87	37.29	0.00
8	0.02	0.03	0.81	12.23	79.35	0.02
9	0.07	2.11	3.24	11.67	26.26	0.07
10	0.01	1.24	0.96	2.04	27.24	0.01
11	0.02	0.14	2.20	0.55	1.90	0.02
12	0.34	0.66	36.05	0.72	1.62	0.38
13	0.36	0.67	25.80	1.45	1.58	0.39
14	0.55	4.69	2.26	2.26	2.27	0.53
15	17.03	14.54	13.90	38.10	35.16	27.26
16	15.23	18.89	73.45	23.23	22.10	16.38
17	3.11	2.78		1.87	4.38	2.48

Table 5.18: Percent *MCC* errors for fixed cases.

Discussion:

The fixed case exhibits some of the same traits as the hybrid case. Truncating main truss modes primarily affected the higher frequency modes. Truncating appendage modes was again detrimental to modes five through eight but also to the higher frequency modes. Overall however, the errors for the fixed case, though lower than the errors for the free case, are higher than the errors for the hybrid case.

However, if these results are compared to the hybrid case by using a criterion different than cut-off frequency, namely the number of modes kept, one may arrive at a different conclusion. Comparing fixed case one with hybrid case two shows that the fixed case gave better results with fewer normal modes. Also, fixed case two, with fewer modes, resulted in approximately the same accuracy as hybrid case three.

5.4 Conclusions

With the HMB-2R structure, the chosen components, and the method of component mode synthesis built into MSC/NASTRAN, it is seen that both the hybrid case and the fixed case performed well. If the criterion for judging the results is the cut-off frequency, then the hybrid method is better; if, on the other hand, the criterion for judging the results is the number of modes kept, the fixed method is better. Under either criterion, the free case performed the worst.

In the range of interest, the relatively stiff outboard truss, alpha joint, and pallet contribute mostly through their static deflection shapes, not their normal modes. The dynamics of the main truss are important to the higher frequency modes but have little influence on the lower frequency modes. The appendage normal modes are very important contributors to modes in the middle of the spectrum but affect all modes.

VI. ERROR STUDY WITH BEAM MODEL IN MATLAB

The purpose of this section is to determine the effect on system results of errors in component modes and frequencies. This is to simulate a situation where the finite element model for each component, after it has been refined to agree with modal test data, is used for component mode synthesis. The Craig-Bampton method is used on a 2-D finite element beam model that has similarities to HMB-2R. This model is developed within MATLAB, a matrix manipulation program. With 46 three-degree-of-freedom nodes, the model has a total of 138 degrees of freedom and is shown in Figure 6.1. See **Appendix D** for a brief description of the finite element approach as applied to this model.

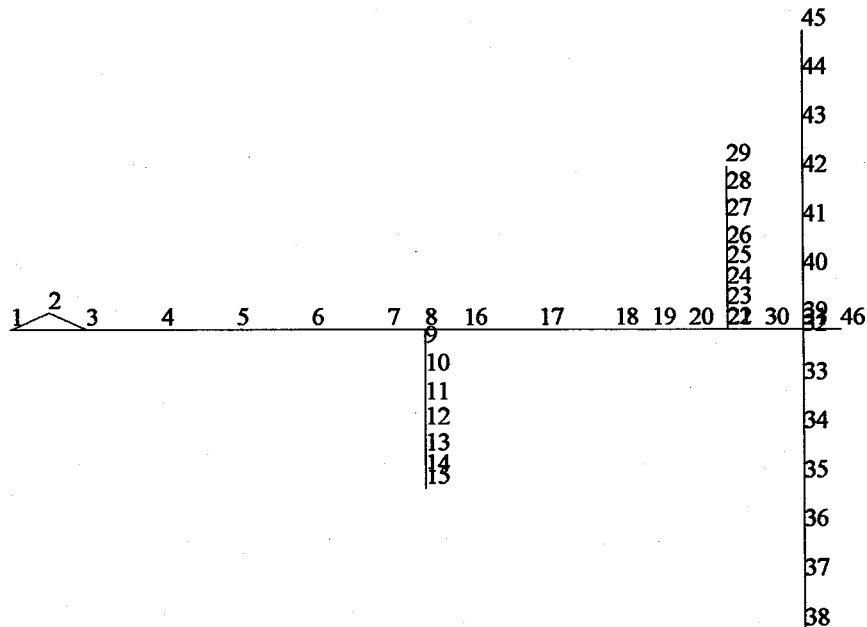


Figure 6.1: The beam model similar to HMB-2R.

After discussing the model derivation, a study similar to those done on HMB-2R will be done on this model to determine the number of component modes necessary for

acceptable results. Following this will be the error study.

6.1 Model Development

The beam model was developed using the same dimensions as the HMB-2R. The elements along the truss were chosen to be the same length as one bay in most cases; exceptions are when the element is half-length to allow for the connection of an appendage. The element properties, elastic modulus, area, density, etc. for the trusses were arrived at by starting with equivalent beam theory¹⁷ and ignoring the pallets. Once the truss was converted to a beam, the pallets were added by inspection. The appendages were already beams and therefore needed little modification. At this stage, the total system was “tuned” by changing the densities and inertias globally so that the fundamental frequency matched the HMB-2R fundamental frequency. The alpha joint properties were also adjusted individually so that its fundamental frequency matched the HMB-2R alpha joint’s fundamental frequency; the reason for choosing the alpha joint is discussed below. Final tuning was done so that both of previously mentioned criteria were met.

6.2 The Craig-Bampton Method on the Beam Model

The division of the beam model in preparation for the Craig-Bampton method of component mode synthesis was done somewhat differently than with HMB-2R. The reason for this is inherent in the model. For example, if the main truss were fixed at the attachment points of the pallet, the TCS, and the alpha joint as the Craig-Bampton method requires, it would consist of a series of doubly cantilevered beams that do not communicate with each other and hence have high natural frequencies. Two things were done to solve this problem: one, the joint coordinate between the main truss and the TCS

was moved down one node on the TCS; and two, the pallet is no longer a separate component but considered part of the main truss. (This is not deemed critical since the pallet in the HMB-2R model exhibited negligible dynamic characteristics in the range of interest.) The other appendages were altered in the same manner as the TCS, leaving only the alpha joint to be the same as in the HMB-2R model. This is the reason for tuning only this component to have the same fundamental frequency as its counterpart.

The frequency data are shown in Table 6.1 where the Aft PV is on the same side as the EPS. Because of the fewer modes in the 50 Hz range, this model will be studied up to 100 Hz. The fewer modes result because of the loss of torsion and out of the plane bending, which agrees with the fact that the beam model has approximately one third the number of modes below 50 Hz as the HMB-2R model. Figures of the mode shapes are given in **Appendix E**.

Frequency Number	Full System	Main Truss	Outboard Truss	Alpha Joint	EPS	Fwd PV	Aft PV	TCS
1	4.656	2.095	1218	139.4	82.58	42.78	42.78	76.82
2	24.14	11.08			517.7	268.2	268.2	481.5
3	26.94	44.69						
4	34.54	94.24						
5	38.85	128.2						
6	50.61							
7	58.60							
8	70.52							
9	93.83							
10	95.49							

Table 6.1: Frequency data for beam model.

The set of cases selected from the frequency data and the range of interest are shown in Table 6.2. The first case, as before, keeps only component modes in the range.

The second case truncates half of the main truss modes while case three truncates all appendage modes. Case four keeps all component modes below 300 Hz.

Component	Number of normal modes kept for each component in case:			
	1	2	3	4
Main Truss	4	2	4	5
Outboard Truss	0	0	0	0
Alpha Joint	0	0	0	1
EPS	1	1	0	1
Fwd PV	1	1	0	2
Aft PV	1	1	0	2
TCS	1	1	0	1

Table 6.2: Run data for the beam model.

Results:

The frequency results are given in Table 6.3. The frequency and *MCC* errors are given in Table 6.4 and Table 6.5 respectively.

Frequency Number	Exact Frequency	Frequency results of case:			
		1	2	3	4
1	4.656	4.656	4.656	4.672	4.656
2	24.14	24.15	25.46	24.40	24.14
3	26.94	26.94	27.04	30.88	26.94
4	34.54	34.56	34.67	40.53	34.55
5	38.85	38.94	40.28	43.37	38.87
6	50.61	50.69	51.10	60.68	50.63
7	58.60	58.65	67.91	68.52	58.63
8	70.52	71.46	93.57	87.26	70.61
9	93.83	94.01		94.25	93.93
10	95.49	96.38			95.93

Table 6.3: Frequency results for beam model cases.

Frequency Number	Percent frequency errors for case:			
	1	2	3	4
1	0.00	0.01	0.35	0.00
2	0.07	5.49	1.10	0.01
3	0.02	0.37	14.65	0.00
4	0.04	0.35	17.34	0.03
5	0.22	3.67	11.64	0.05
6	0.18	0.98	19.91	0.04
7	0.09	15.90	16.94	0.05
8	1.33	32.68	23.73	0.12
9	0.19		0.45	0.10
10	0.93			0.46

Table 6.4: Percent frequency errors for beam model cases.

Frequency Number	Percent <i>MCC</i> error for case:			
	1	2	3	4
1	0.00	0.00	0.00	0.00
2	0.00	2.71	1.67	0.00
3	0.00	0.74	6.52	0.00
4	0.00	0.52	11.74	0.00
5	0.00	1.62	6.83	0.00
6	0.01	1.07	15.69	0.00
7	0.02	45.94	58.50	0.00
8	0.04	29.07	14.59	0.00
9	0.77		59.50	0.17
10	0.12			0.02

Table 6.5: Percent *MCC* error for beam cases.

Discussion:

These results show some similarities to the HMB-2R model results. Keeping only

the modes in the 100 Hz range gave a maximum frequency error of 1.33% and a maximum *MCC* error of 0.77%. Truncation of main truss modes led to poor results in the upper frequencies while truncating appendage modes added large errors to nearly all modes. Keeping all modes up to 300 Hz led to very accurate results with a maximum frequency error of 0.46% and a maximum *MCC* error of 0.17%. To avoid confusing errors that are caused by component mode synthesis with the effects of adding component errors in the next section, the 300 Hz case will be used.

6.3 The Error Study

The goal of this section is to determine the effect of errors at the component level on final results. In general, errors were added to the mode shapes and eigenvalues of each component which were in turn used to update the mass and stiffness matrices. The approach used to add errors is discussed below. The updating was done (by using the Analytical Model Improvement (AMI) Method¹⁸) so that each component mass and stiffness matrix would be consistent with the modified mode shapes and frequencies. Since the constraint modes were calculated from the modified stiffness, they will have errors that simulate the real process. Component mode synthesis was then executed using the modified information. For an overview of the AMI method, see **Appendix F**.

The errors were added to *all* component modes and eigenvalues with random numbers that were uniformly distributed between the negative and positive of the maximum error. The reason for adding errors to all the modes (instead of just to the *kept* modes, for example) is to get as close as possible to a real situation. In a real situation none of the modes calculated from the finite element model of a structure would be exact. Before adding errors to the mode shapes, they were normalized to have a unit magnitude.

In all cases, the errors were added to the full length mode shapes (which bypasses the first step in the AMI procedure shown in **Appendix F**).

Two pairs of maximum errors were used in this study; one pair to represent a best case scenario and the other pair to represent a worst case scenario. The best case pair set a maximum error of one half percent for the eigenvalues and one percent for each element of the mode shapes. The worst case had a maximum error of two and a half percent for the eigenvalues and five percent for the modes. These numbers are based on experience of how accurately modes and frequencies can be measured.

There are two parts to this study: part one adds errors (both scenarios) to all components for each case, and part two adds the worst case errors to only one component for each case.

Part one results:

The results for part one are presented in an error bar format for both the percent frequency and percent *MCC* errors for each specific case. In each case, thirty computer runs were made to obtain a distribution. Shown on all plots are the maximum and minimum percent errors (*) for each frequency of interest. Also shown on each plot at each frequency are the mean value (in the middle of the bar) and one standard deviation above and below the mean (the ends of the bar).

The results using the best case errors are shown in Figure 6.2. In part (a), the errors were added to both eigenvalues and mode shapes; in part (b), errors were only added to the modes, while in part (c), errors were only added to the eigenvalues. The results for using the worst case errors are shown in Figure 6.3.

Contrary to what was done in the HMB-2R studies, the modes here are *not*

ordered by the values of the MCC 's. This will tend to increase the MCC errors. The reason for not ordering them is, in part, because of the large number of computer runs and in part because the approximate modes, in many cases, did not correlate well with any of the exact modes. The modes are in order of ascending frequencies.

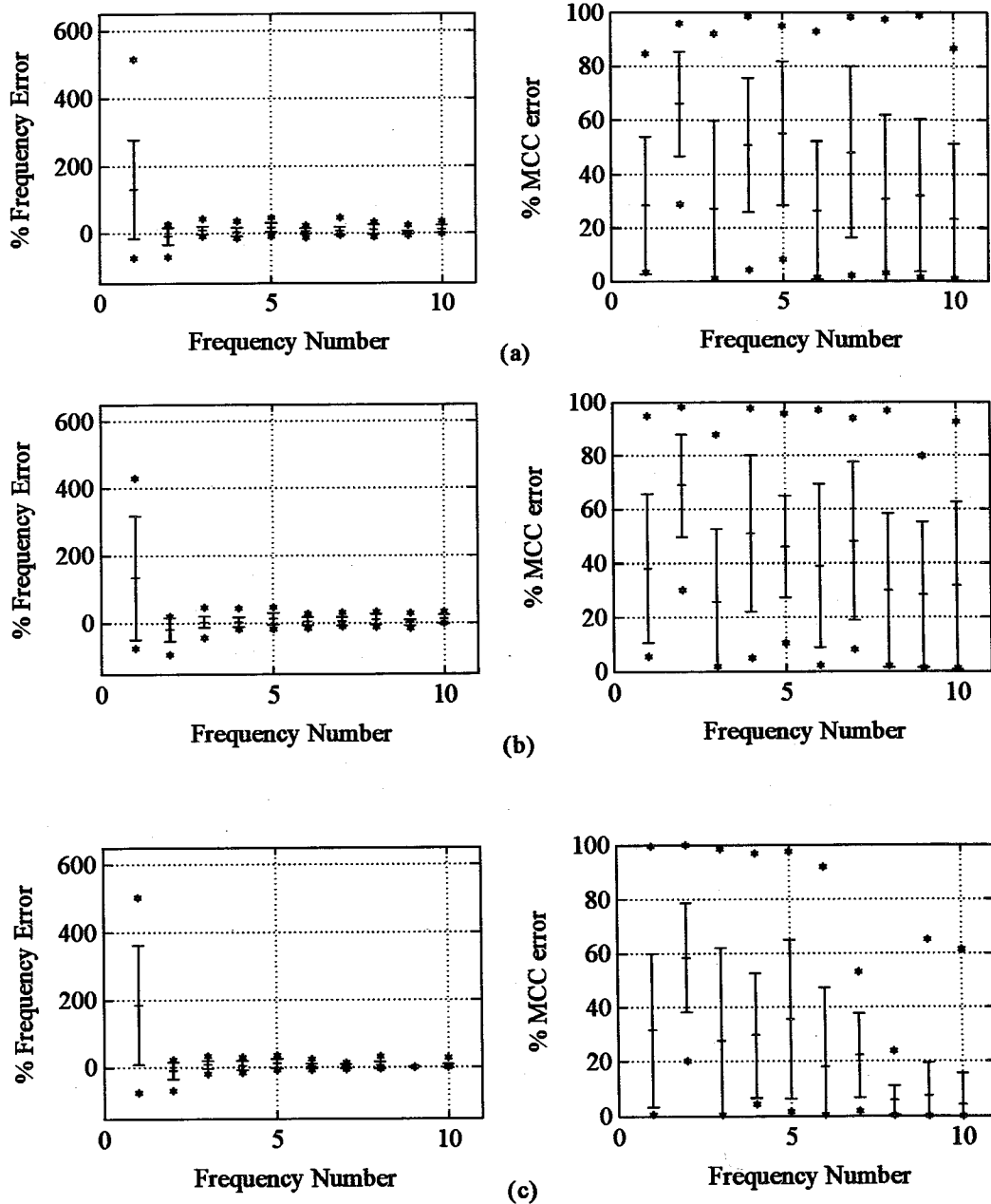


Figure 6.2: Results of using the best case errors (0.5% on eigenvalues and 1% on modes). (a) Errors on both; (b) errors on modes; (c) errors on eigenvalues.

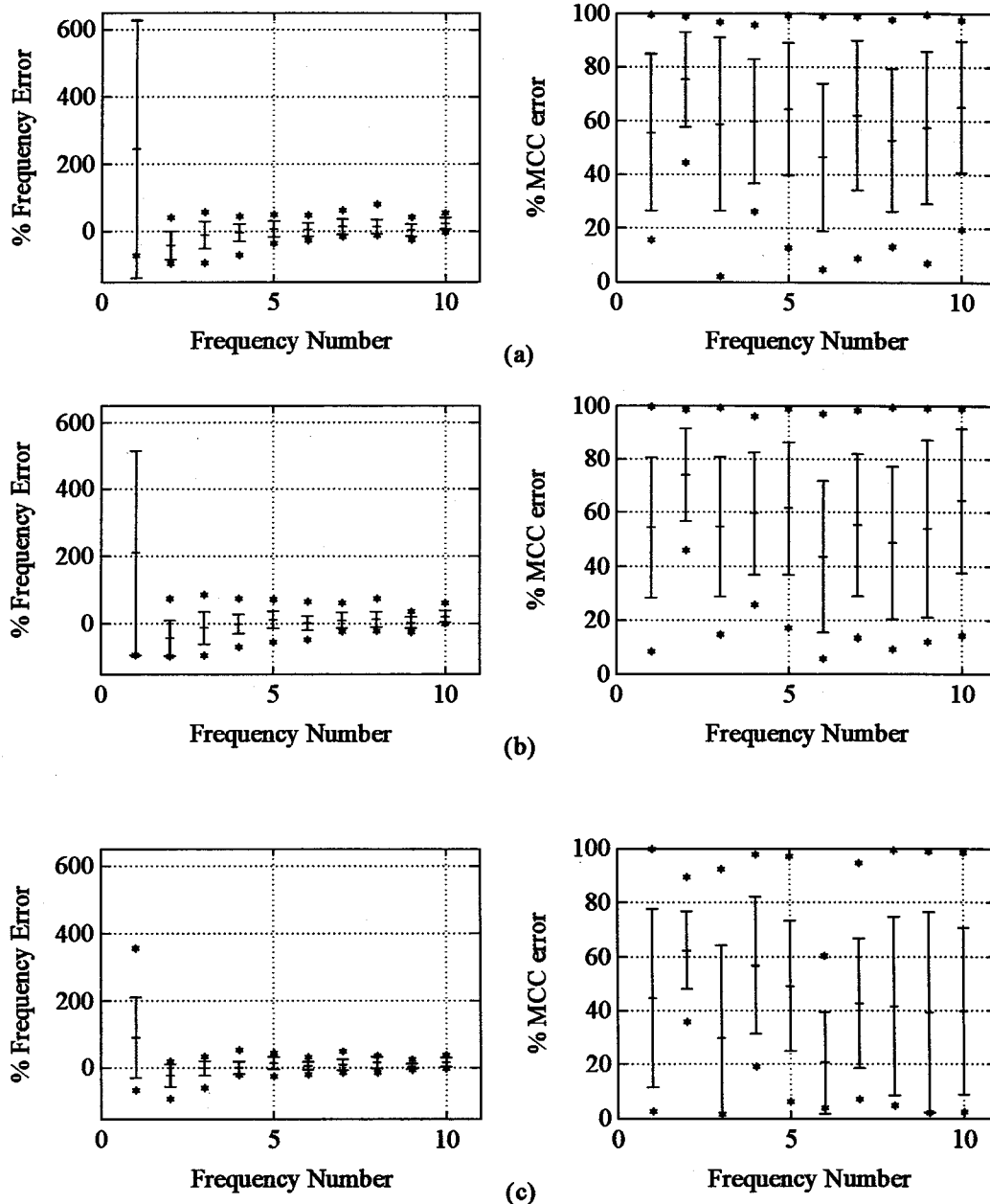


Figure 6.3: Results of using the worst case errors (2.5% on eigenvalues and 5% on modes). (a) Errors on both; (b) errors on modes; (c) errors on eigenvalues.

Discussion/Conclusions:

A prominent characteristic of all these results is that, in general, *errors at the component level are magnified at the system level*. It is important to note that the same magnification would have resulted regardless of CMS method used (provided that a

sufficient number of modes were retained); it is repeated that the Craig-Bampton method itself contributed only very small errors. The magnification of errors may in fact be caused by the AMI procedure (which was used to alter the mass and stiffness matrices so they were consistent with the erroneous modes and frequencies). This is discussed further in section VII where some implications are also considered.

Some of the frequencies have errors that are over one hundred times as large as the imposed errors. In particular, the greatest magnification is for the first system mode. This demonstrates that *the first mode for this beam model is extremely sensitive to errors in components*. Also, *the estimate for the fundamental frequency is biased high*.

It would appear, by comparing parts (b) and (c) in Figure 6.2 and in Figure 6.3, that the *errors in modes and frequencies contribute approximate equally to the system errors*. It is also interesting to note that these errors did not seem to add to each other.

Although in most cases the frequency errors tend to decrease as the frequency number increases, the *MCC* errors show this tendency only in part (c) of Figure 6.2. It is noted once again however that the modes were *not* ordered according to the *MCC* values which may have made the results look slightly worse. The high *MCC* errors indicate that *component modeling errors can cause the modes to be highly uncorrelated with the exact*.

Part two results:

An interesting way to follow errors from the component level to the system level is to add errors to one component for each case. The following seven figures, corresponding to the seven components, show the results of adding the worst case errors to both the modes and frequencies of the specified component. The plots of percent frequency error and percent *MCC* error are in the same format as before. Starting with the main truss, the results are shown in Figures 6.8 through 6.14.

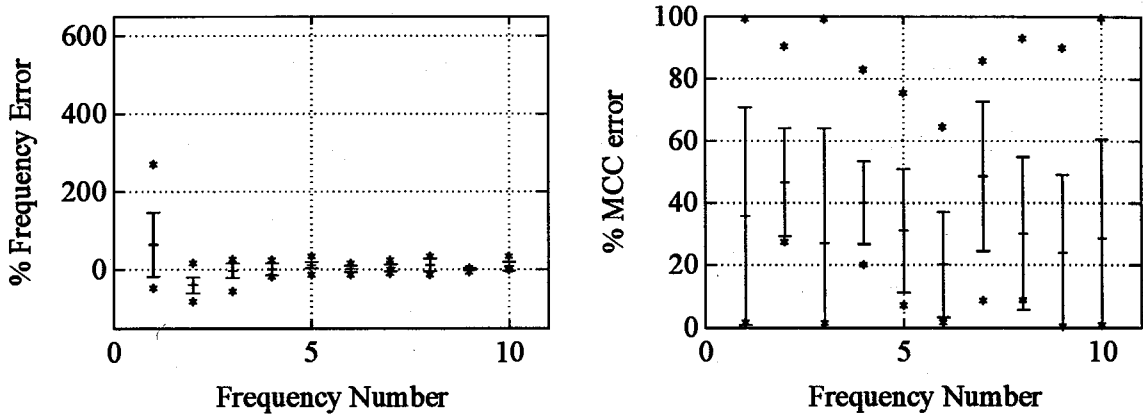


Figure 6.4: Results of adding errors to the **main truss** only.

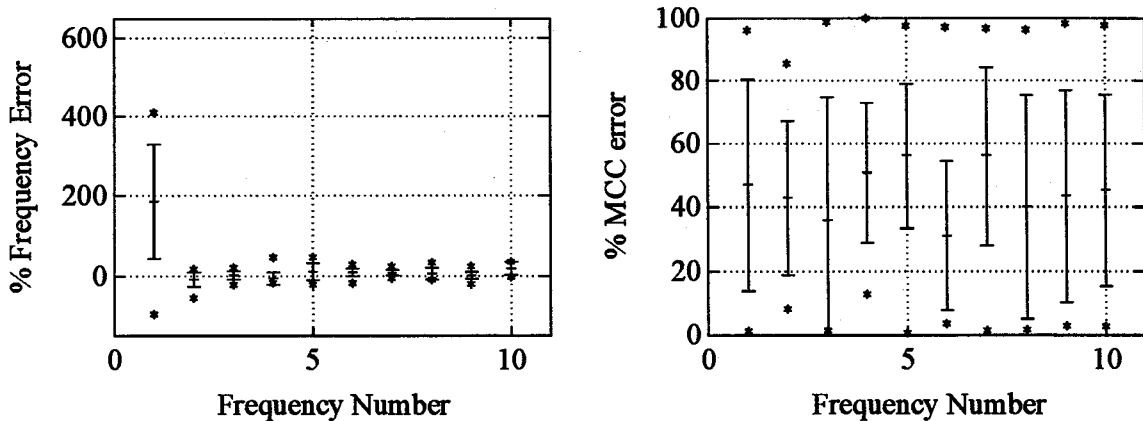


Figure 6.5: Results of adding errors to the **outboard truss** only.

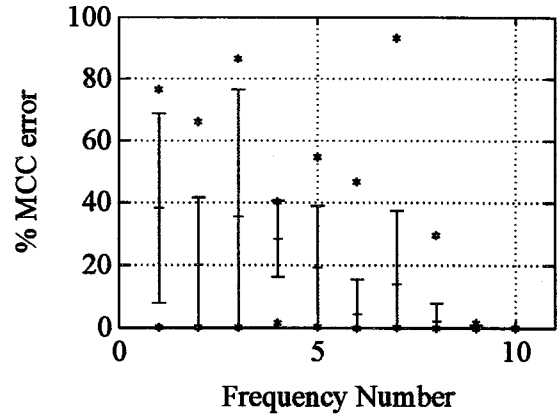
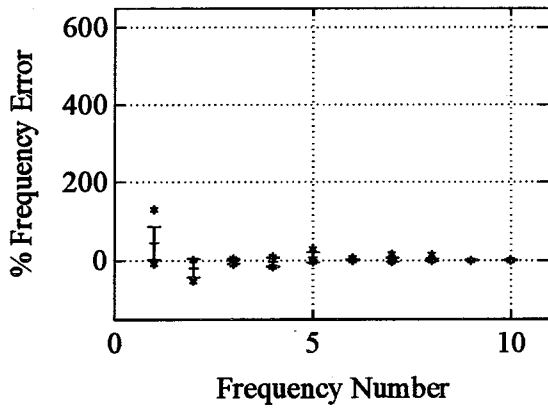


Figure 6.6: Results of errors to the alpha joint only.

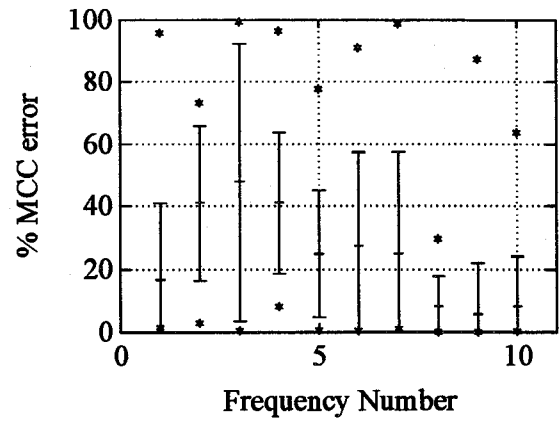
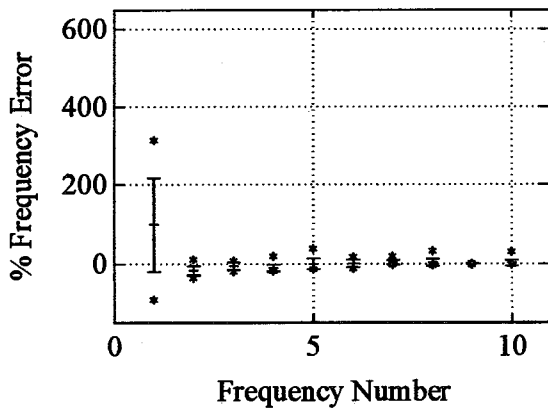


Figure 6.7: Results of adding errors to the EPS only.

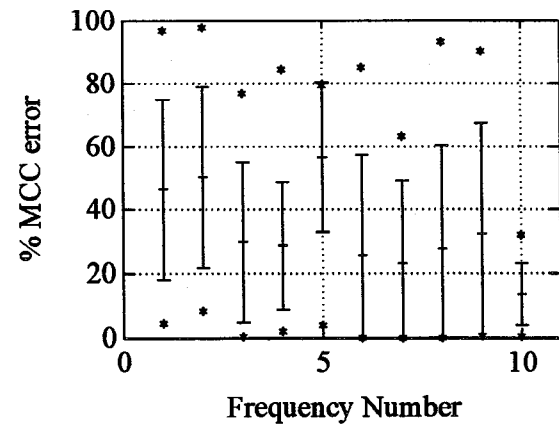
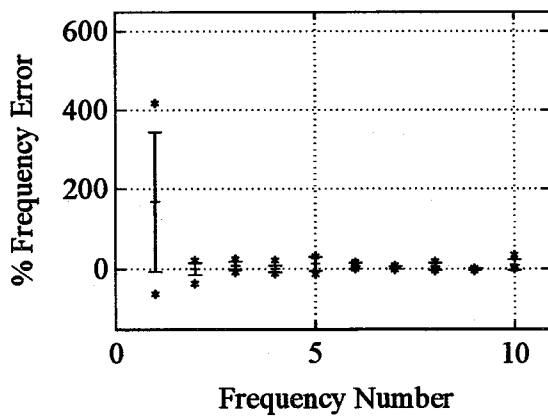


Figure 6.8: Results of adding errors to Fwd PV only.

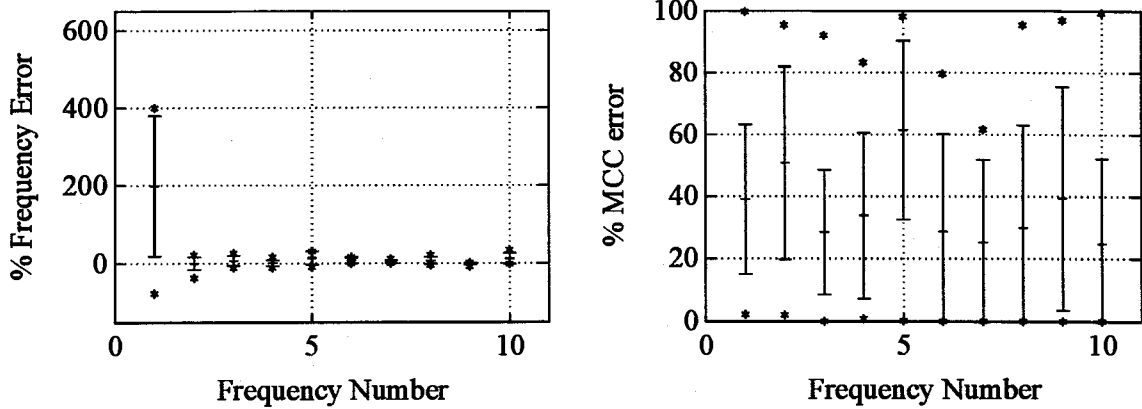


Figure 6.9: Results of adding errors to Aft PV only.

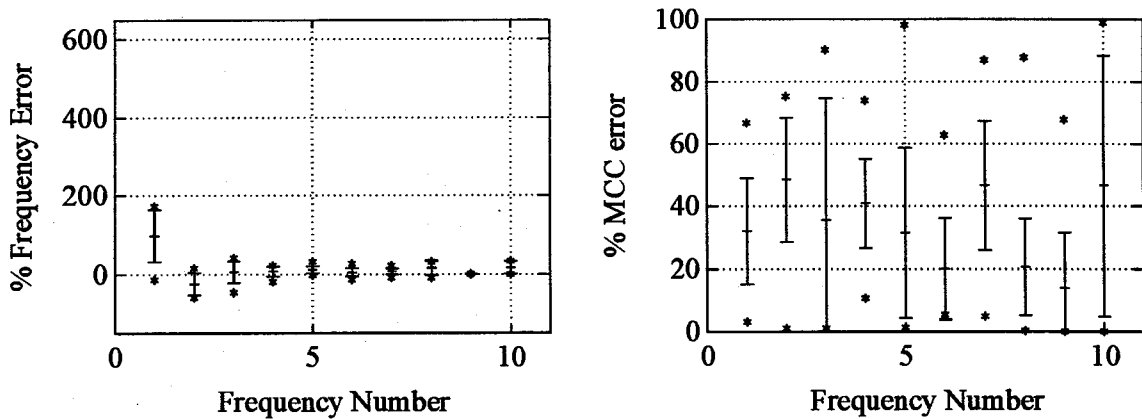


Figure 6.10: Results of adding errors to the TCS only.

Discussion/Conclusions:

As in part one, all these results show that errors are magnified at the system level. In addition, these results show that the errors are magnified even when only one component is erroneous. These results also show that the first mode is very sensitive to errors in any component and that this estimate is biased high. Note that since all normal modes for the outboard truss were truncated, all the errors for that case were caused by the modified mass and stiffness matrices.

A trend that is evident by comparing these results to the mode shape figures shown in **Appendix E** is that *errors in a component most affect the system modes where that component is a major factor*. For example, the main truss, the TCS, and the alpha joint cause the largest errors in mode two and, from Figure E.2, it is observed that these are the three most important components for that mode.

VII. CONCLUDING REMARKS

The first objective of this study was to determine the number of component modes necessary for accurate frequency and mode shape results when using component mode synthesis. This aspect was studied by using MSC/NASTRAN on a finite element space station model having over 4500 degrees of freedom. It was found that imposing hybrid component boundary conditions that most closely represented the actual physical boundary conditions, and keeping component modes up to twice the desired frequency, resulted in frequencies and MCC 's that were accurate to within one percent of the exact. When the fixed-interface method (the Craig-Bampton method) was used, keeping component modes up to twice the desired frequency led to larger errors than for the hybrid case. However, when the numbers of modes kept for both of these methods were compared, it was found that the fixed-interface method provided more accurate results with fewer modes. It is also noted that the fixed case boundary conditions were somewhat similar to the hybrid case. The free-interface method resulted in the largest errors: all frequency errors were above one percent in the cases studied. This is not a generalization of free-interface methods; in *Example 2* for instance, the free-interface method performed very well. The above results indicate that using boundary conditions that mimic the actual physical conditions is beneficial. This is logical since component mode synthesis methods are Ritz methods which, by their nature, give more accurate results as the assumed modes approach the actual modes.

The second objective was to determine the effect of errors at the component level on the system frequencies and mode shapes. For this study, the Craig-Bampton method was used on a 2-D version of the space station model mentioned above. It was found that

the errors in component modes and eigenvalues were significantly magnified (by over one hundred times in some cases) at the system level. The results also demonstrated the extreme sensitivity of the first mode to errors in any component and that this frequency estimate is biased high. By adding errors to component modes and eigenvalues separately, it was determined that errors in modes and errors in eigenvalues have approximately the same effect on system results. Finally, it was found that errors in a component most significantly affected the system modes in which that component was a major factor.

However, all these results depend on the validity of the AMI procedure which was used to modify the mass and stiffness matrices of each component. It may be that this method alters these matrices in an unrealistic manner which causes the magnification of errors. To enhance this research, a worthwhile topic of study would be to compare this method with other methods. It is believed by the author that the AMI procedure is the cause of the magnification and, more specifically, that it is the fact that *this procedure does not take precautions to conserve component mass* that causes the magnification. Perhaps if the AMI procedure was modified to ensure mass conservation, the results would be more reasonable. Or, if not, perhaps a method that changes the properties of the model (such as material density or the elastic modulus) would be more appropriate. If, however, the AMI procedure is the “best” method currently available or is not at fault, then these results indicate that, in terms of model accuracy, conducting tests on the full structural system and updating the corresponding finite element model is preferable to using a component-by-component approach.

Using the component-by-component approach together with the AMI procedure

has implications in control system design. First, the tendency to overestimate fundamental frequency is undesirable for control system design since it is important to have the controller “roll-off” before the first natural frequency. Second, the poor mode shape results indicate that sensors and actuators must be co-located for stability.

Another factor to consider is the model itself: perhaps errors in the components of a more complex structure would have less effect on the system results. Therefore, another extension of the error study would be to use a more complex, 3-D model.

To conclude, it is felt by the author that the performance of any method which uses test data to modify finite element models (such as the AMI procedure) should be evaluated within the component mode synthesis process. This is because these methods are very important in the application of component mode synthesis on real structures; also, a method that performs well in component mode synthesis would very likely perform very well for other applications.

REFERENCES

1. J. A. Garba, B. K. Wada, and J. C. Chen, "Experiences in using Modal Synthesis Within Project Requirements," *The Shock and Vibration Bulletin*, Bulletin 46, Part 5, pp. 213-230, August 1976.
2. W. C. Hurty, "Dynamic Analysis of Structural Systems Using Component Modes," *AIAA Journal*, vol. 3, pp. 678-685, 1965.
3. W. A. Benfield, C. S. Bodley, and G. Morosow, "Modal Synthesis Methods," *Symp. Substr. Testing and Synth.*, NASA Marshall Space Flight Center, 1972.
4. P. E. McGowan, H. E. Edighoffer, and J. W. Wallace, "Development of an Experimental Space Station Model for Structural Dynamics Research," NASA TM-102601, NASA-Langley Research Center, 1990.
5. J. T. Spanos and W. S. Tsuha, "Selection of Component Modes for the Simulation of Flexible Multibody Spacecraft," *Astrodynamics 1989*, AAS 89-438, vol. 71, part 2, pp. 855-877, 1990.
6. R. R. Craig, *Structural Dynamics*, John Wiley and Sons, New York, 1981.
7. A. A. Abdallah and A. A. Hucklebridge, "Boundary Flexibility Method of Component Mode Synthesis using Static Ritz Vectors," *Computers and Structures*, vol. 35, no. 1, pp. 51-61, 1990.
8. J. J. Allen, "A Component Synthesis Method Using Lanczos Vectors," *International Journal of Analytical and Experimental Modal Analysis*, vol. 4, pp. 33-38, April 1989.
9. L. E. Suarez and M. P. Singh, "An Exact Component Mode Synthesis Approach," *Earthquake Engineering and Structural Dynamics*, vol. 16, pp. 293-310, February 1988.
10. R. R. Craig, "Methods of Component Mode Synthesis," *Shock and Vibration Digest*, Naval Research Lab., Washington, DC, vol. 9, pp. 3-10, 1977.
11. L. Meirovitch, *Methods of Analytical Dynamics*, McGraw-Hill, 1970.
12. R. R. Craig and M. C. C. Bampton, "Coupling of Substructures for Dynamic Analysis," *AIAA Journal*, v. 6, pp. 1313-1319, 1968.
13. D. R. Martinez and D. L. Gregory, "A Comparison of Free Component Mode Synthesis Techniques Using MSC/NASTRAN," SANDIA 83-0025, 1984.
14. D. N. Herting, "A General Purpose, Multi-Stage, Component Modal Synthesis Method," *Finite Elements in Analysis and Design*, vol. 1, pp. 153-164, 1985.
15. D. N. Herting and M. J. Morgan, "Component Mode Synthesis," Section 4.7, *NASTRAN Theoretical Manual*, Level 17.5 Updates.

16. D. N. Herting, "Accuracy of Results with NASTRAN Model Synthesis," 7th NASTRAN Users' Colloquium Papers, NASA CP-2062, 1978.
17. A. K. Noor, M. S. Anderson, and W. H. Greene, "Continuum Models for Beam-Like and Plate-Like Lattice Structures," AIAA Paper 78-493, 1978.
18. A. Berman and E. J. Nagy, "Improvement of a Large Analytical Model Using Test Data," AIAA Journal, vol. 21, August 1983.
19. W. A. Benfield and R. F. Hruda, "Vibration Analysis of Structures by Component Mode Substitution," AIAA Journal, v. 9, pp. 1255-1261, 1971.
20. S. Goldenberg and M. Shapiro, "A Study of Modal Coupling Procedures for the Space Shuttle," NASA CR-112252, Grumman Aerospace Corp., Bethpage NY, 1972.
21. R. H. MacNeal, "A Hybrid Method of Component Mode Synthesis," Computers and Structures, vol 1, pp 581-601, 1971.
22. S. Rubin, "Improved Component-Mode Representation for Structural Dynamic Analysis," AIAA Journal, vol. 13, pp 995-1006, 1975.
23. R. R. Craig and C-J. Chang, "On the Use of Attachment Modes in Substructure Coupling for Dynamic Analysis," Paper 77-405, AIAA/ASME 18th Structures, Structural Dynamics, and Materials Conference, San Diego, CA 1977.
24. I. H. Shames and C. L. Dym, Energy and Finite Element Methods in Structural Mechanics, Hemisphere Publishing Corporation, 1985.
25. J. S. Przemieniecki, Theory of Matrix Structural Analysis, Dover, 1985.

APPENDICES

A. NORMAL, CONSTRAINT, AND ATTACHMENT MODES

A.1 Normal Modes

Normal modes are the vibrational modes obtained by solving the component eigenvalue problem and may be classified as *fixed-interface normal modes*, *free-interface normal modes*, or *hybrid-interface normal modes*. Also, some methods^{19,20} use *loaded interface normal modes*, where mass and stiffness is added to m_{jj} and k_{jj} for each component. The normal modes (ϕ) for each component are calculated by solving the component eigenvalue problem

$$(k - \omega^2 m)\phi = \mathbf{0} \quad (\text{A.1})$$

subject to any natural boundary conditions and the conditions the method imposes. If the component is unrestrained and the method uses free interfaces, rigid-body modes can result. They can be treated as part of the normal mode set or considered separately; in the Craig-Chang method in section IV they are considered separately.

When referring to a matrix of component normal modes, Φ will be used instead of the more general Ψ . It will be assumed that Φ is normalized with respect to m , or,

$$\Phi^T m \Phi = I, \quad \Phi^T k \Phi = \Lambda \equiv \text{diag}[\omega^2] \quad (\text{A.2})$$

Later, Φ_k will be used to denote a truncated set of normal modes with k standing for *kept*.

To visualize a normal mode, consider the cantilevered beam substructure shown in Figure A.1 where it is assumed that the joint node is on the right end.

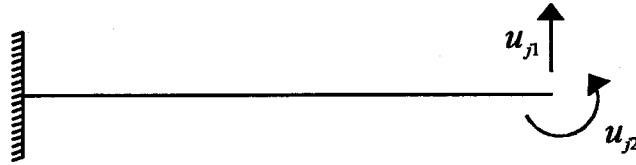


Figure A.1: A cantilevered beam substructure.

The fundamental normal mode for both a fixed-interface method and a free-interface method is shown in Figure A.2.

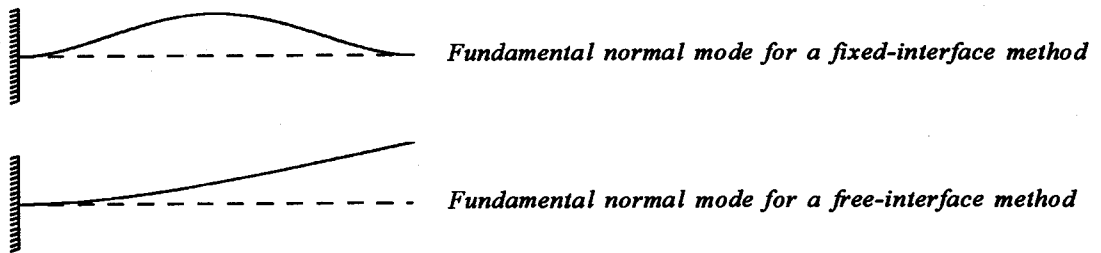


Figure A.2: Normal modes of the constrained component.

A.2 Constraint Modes

Let the physical coordinates of a component be divided into two sets, C , relative to which the constraint modes will be defined, and V , the complement of C . A constraint mode ψ_c is defined as the static deformation that results when a *unit deflection* is imposed on the j^{th} coordinate in set C while restraining the rest in that set and allowing the coordinates of set V to move freely. Mathematically, if m is the number of coordinates in C and the reactions on set C are denoted by R , for $j = 1,$

$$\begin{bmatrix} k_{vv} & k_{vc} \\ k_{cv} & k_{cc} \end{bmatrix} \begin{bmatrix} \psi_{v_1} \\ 1 \\ 0 \\ 0 \\ 0 \\ \vdots \\ 0 \end{bmatrix} = \begin{bmatrix} \mathbf{0}_{v_1} \\ R_{11} \\ R_{12} \\ R_{13} \\ \vdots \\ R_{1m} \end{bmatrix} \quad (\text{A.3})$$

defines the first constraint mode $\begin{bmatrix} \psi_{v_1} \\ 1 \\ 0 \\ 0 \\ 0 \\ \vdots \\ 0 \end{bmatrix}$ for component ρ . Therefore, the equation

$$\begin{bmatrix} k_{vv} & k_{vc} \\ k_{cv} & k_{cc} \end{bmatrix} \begin{bmatrix} \Psi_{vc} \\ I_{cc} \end{bmatrix} = \begin{bmatrix} \mathbf{0}_{vc} \\ R_{cc} \end{bmatrix} \quad (\text{A.4})$$

defines the set of constraint modes for the component. Solving for Ψ_{vc} gives

$$\Psi_{vc} = -k_{vv}^{-1} k_{vc} \quad (\text{A.5})$$

Thus, the constraint mode matrix for component ρ is

$$\Psi_c \equiv \begin{bmatrix} \Psi_{vc} \\ I_{cc} \end{bmatrix} = \begin{bmatrix} -k_{vv}^{-1} k_{vc} \\ I_{cc} \end{bmatrix} \quad (\text{A.6})$$

It is noted here that this definition is valid for either constrained or unconstrained

components, the only requirement being that for unconstrained components, k_{vv} is chosen such that it is nonsingular.

For the Craig-Bampton method, set C is made up of the joint coordinates and set V is composed of the interior coordinates. Under this condition, it is easy to visualize a constraint mode. For example, consider again the cantilevered beam shown in Figure A.1.

The joint node, on the right end, has two degrees of freedom. In other words, there are two joint coordinates, u_{j1} and u_{j2} , and therefore two constraint modes for this component. The constraint modes are shown in Figure A.3.

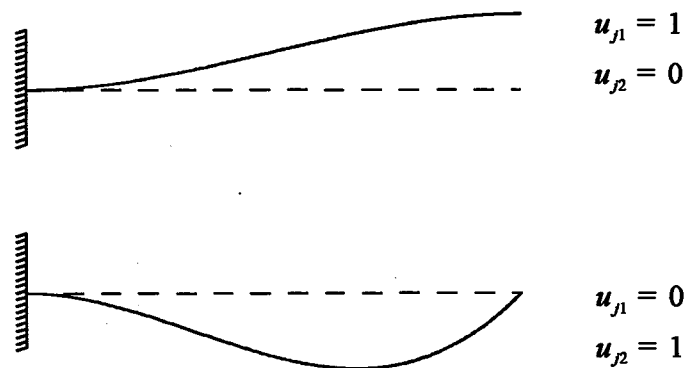


Figure A.3: Constraint modes of cantilever beam.

By definition, constraint modes are all linearly independent of each other. This is understandable since, in the above situation, each constraint mode moves a different joint coordinate while the remaining joint coordinates are restrained. Therefore all constraint modes will have zeros in each row corresponding to the joint coordinates except for one, making them all linearly independent of each other. They are also linearly independent of all normal modes for fixed interface methods for the same reason.

A.3 Attachment Modes for Constrained Components

Attachment modes will be defined relative to set A . Set W is the complement of A . An attachment mode ψ_a is defined as the static deflection of a component that results from exerting a *unit force* on one coordinate of set A while the remaining coordinates of A and the coordinates of W are unrestrained (except for any physical boundary conditions).

Letting n be the number of coordinates in A , for $j = 1$,

$$\begin{bmatrix} k_{ww} & k_{wa} \\ k_{aw} & k_{aa} \end{bmatrix} \begin{Bmatrix} \psi_{w_1} \\ \psi_{11} \\ \psi_{21} \\ \psi_{31} \\ \vdots \\ \psi_{n1} \end{Bmatrix} = \begin{Bmatrix} \mathbf{0}_{w_1} \\ 1 \\ 0 \\ 0 \\ \vdots \\ 0 \end{Bmatrix} \quad (\text{A.7})$$

defines the first attachment mode $\begin{Bmatrix} \psi_{w_1} \\ \psi_{11} \\ \psi_{21} \\ \psi_{31} \\ \vdots \\ \psi_{n1} \end{Bmatrix}$ for component ρ . Thus, the equation

$$\begin{bmatrix} k_{ww} & k_{wa} \\ k_{aw} & k_{aa} \end{bmatrix} \begin{bmatrix} \Psi_{wa} \\ \Psi_{aa} \end{bmatrix} = \begin{bmatrix} \mathbf{0}_{wa} \\ \mathbf{I}_{aa} \end{bmatrix} \quad (\text{A.8})$$

defines the set of attachment modes for the component. Let $\mathbf{g} \equiv \mathbf{k}^{-1}$. Solving for Ψ_a gives

$$\Psi_a \equiv \begin{bmatrix} \Psi_{wa} \\ \Psi_{aa} \end{bmatrix} = \begin{bmatrix} g_{ww} & g_{wa} \\ g_{aw} & g_{aa} \end{bmatrix} \begin{bmatrix} 0_{wa} \\ I_{aa} \end{bmatrix} = \begin{bmatrix} g_{wa} \\ g_{aa} \end{bmatrix} \quad (\text{A.9})$$

which is the attachment mode matrix. Since k^{-1} would not exist if the component was unconstrained, this definition only applies for constrained components.

For the same component as before, shown in Figure A.1, the attachment modes are shown in Figure A.4. For comparison, the fundamental normal mode for a free-interface method is also included.

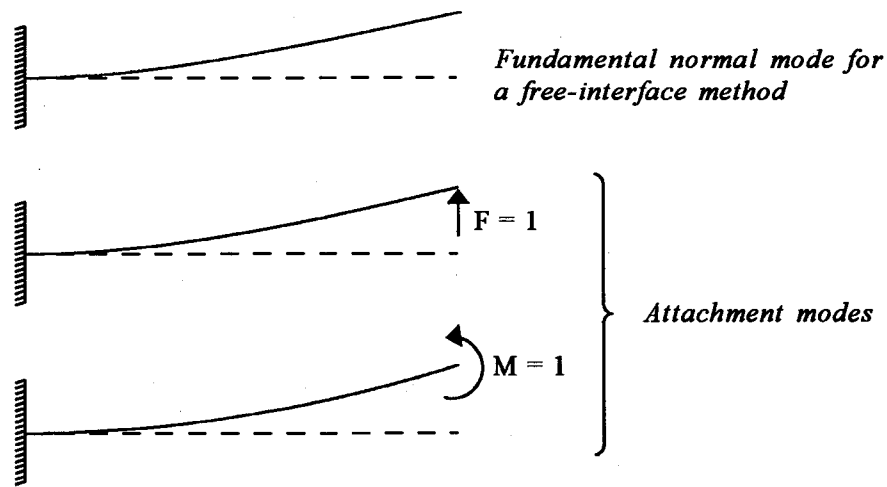


Figure A.4: Attachment modes of the constrained component.

As stated previously, these modes were actually calculated and plotted from a ten node finite element beam model. The reason for doing this is to show how similar these modes can be and to illustrate that *attachment modes may not be linearly independent of normal modes*. This problem is considered in section A.6.

A.4 Attachment Modes for Unconstrained Components

This section describes one possible way to define attachment modes for unconstrained components. Let the coordinates of the component be divided into three

sets: R , A , and W where R is a statically determinate set that is sufficient to prevent rigid-body motion. Again the attachment modes will be defined relative to set A . The component attachment mode matrix Ψ_a is then defined by

$$\begin{bmatrix} k_{ww} & k_{wa} & k_{wr} \\ k_{aw} & k_{aa} & k_{ar} \\ k_{rw} & k_{ra} & k_{rr} \end{bmatrix} \begin{bmatrix} \Psi_{wa} \\ \Psi_{aa} \\ \mathbf{0}_{ra} \end{bmatrix} = \begin{bmatrix} \mathbf{0}_{wa} \\ I_{aa} \\ R_{ra} \end{bmatrix} \quad (\text{A.10})$$

where R_{ra} are the reactions on the R set required to prevent rigid-body motion. Solving for the non-zero elements of Ψ_a gives

$$\begin{bmatrix} \Psi_{wa} \\ \Psi_{aa} \end{bmatrix} = \begin{bmatrix} k_{ww} & k_{wa} \\ k_{aw} & k_{aa} \end{bmatrix}^{-1} \begin{bmatrix} \mathbf{0}_{wa} \\ I_{aa} \end{bmatrix} = \begin{bmatrix} g_{ww} & g_{wa} \\ g_{aw} & g_{aa} \end{bmatrix} \begin{bmatrix} \mathbf{0}_{wa} \\ I_{aa} \end{bmatrix} = \begin{bmatrix} g_{wa} \\ g_{aa} \end{bmatrix} \quad (\text{A.11})$$

Therefore, one way to define an attachment mode matrix for unrestrained components is

$$\Psi_a \equiv \begin{bmatrix} \Psi_{wa} \\ \Psi_{aa} \\ \mathbf{0}_{ra} \end{bmatrix} = \begin{bmatrix} g_{wa} \\ g_{aa} \\ \mathbf{0}_{ra} \end{bmatrix} \quad (\text{A.12})$$

To visualize this type of attachment mode, consider the same beam component shown in Figure A.1 except with the support on the left removed. Then if the coordinates are chosen as shown in Figure A.5, the two attachment modes would look exactly like those shown in Figure A.4.

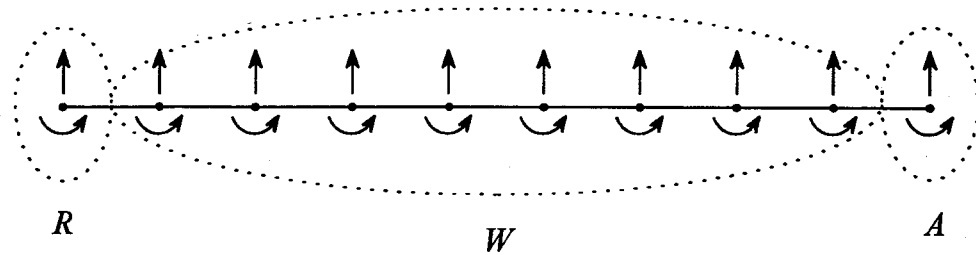


Figure A.5: One choice of coordinates for the unrestrained beam.

A.5 Inertia Relief Attachment Modes

This section looks at an alternative method of describing attachment modes for unconstrained components that was first used by MacNeal²¹ and Rubin.²² This development follows that of Craig^{3,23} who states that the reason for using these modes instead of those derived in section A.4 is the improved convergence by the mode-acceleration approach. Indeed, one may wonder about the effectiveness of the attachment modes defined in the previous section since an artificial restraint is imposed.

The idea here is to apply an equilibrated force vector f_e to a substructure that, in effect, cancels out the rigid-body d'Alembert force vector $m\ddot{u}$, caused by the original force. That is, subtract from the original force the inertial d'Alembert forces to get the equilibrated force (see equation (A.19)) and apply that to define the inertia relief attachment modes. The original force is the applied force that would have been used to define the attachment modes had there been no rigid-body motion to consider. The only difference in the original force used here and the one used in equation (A.10) is that now there will be no reaction forces since this is balanced by the inertial d'Alembert forces.

The rigid-body modes must first be calculated. It is true that these modes can belong to the set of normal modes, but they can also be considered a special case of

constraint modes. Let a component having n rigid-body modes be restrained at n statically determinate coordinates, the R set. Therefore, if V is the complement of R , from equation (A.6) the rigid-body modes are given by

$$\Psi_r = \begin{bmatrix} -k_{vv}^{-1}k_{vr} \\ I_{rr} \end{bmatrix} \quad (\text{A.13})$$

Also, let Ψ_r be normalized with respect to the mass matrix:

$$\Psi_r^T m \Psi_r = I_{rr} \quad (\text{A.14})$$

Assume that the component mode matrix Ψ is made up of these rigid-body modes and a complete set of *elastic* normal modes Φ_e . Equation (2.4), $u = \Psi p$, can then be written as a linear combination of the rigid-body coordinates p_r and the elastic coordinates p_e :

$$u = \Psi_r p_r + \Phi_e p_e \quad (\text{A.15})$$

where

$$\Phi_e^T m \Phi_e = I_{ee} \quad (\text{A.16})$$

Substituting equation (A.15) into the substructure equation of motion, equation (2.2), yields

$$m \Psi_r \ddot{p}_r + m \Phi_e \ddot{p}_e + k \Phi_e p_e = f \quad (\text{A.17})$$

since $k \Psi_r = \mathbf{0}$. Premultiplying equation (A.17) by Ψ_r^T and since the rigid-body modes are orthogonal to the elastic normal modes,

$$\ddot{p}_r = \Psi_r^T f \quad (\text{A.18})$$

From the definition, the equilibrated force vector is given as

$$f_e = f - m\ddot{u}_r \quad (\text{A.19})$$

Substituting $u_r = \Psi_r p_r$ and equation (A.18) into equation (A.19) yields

$$f_e = P f \quad (\text{A.20})$$

where

$$P \equiv I - m\Psi_r \Psi_r^T \quad (\text{A.21})$$

P is called the *projection matrix*.

Attachment modes $\bar{\Psi}_a$ can be defined by using equations (A.8) and (A.19):

$$\begin{bmatrix} k_{ww} & k_{wa} & k_{wr} \\ k_{aw} & k_{aa} & k_{ar} \\ k_{rw} & k_{ra} & k_{rr} \end{bmatrix} \begin{bmatrix} \bar{\Psi}_{wa} \\ \bar{\Psi}_{aa} \\ \mathbf{0}_{ra} \end{bmatrix} = \begin{bmatrix} P_{ww} & P_{wa} & P_{wr} \\ P_{aw} & P_{aa} & P_{ar} \\ P_{rw} & P_{ra} & P_{rr} \end{bmatrix} \begin{bmatrix} \mathbf{0}_{wa} \\ I_{aa} \\ \mathbf{0}_{ra} \end{bmatrix} = P F \quad (\text{A.22})$$

To solve for the attachment mode matrix, first write equation (A.22) in the form

$$\begin{bmatrix} k_{ww} & k_{wa} \\ k_{aw} & k_{aa} \end{bmatrix} \begin{bmatrix} \bar{\Psi}_{wa} \\ \bar{\Psi}_{aa} \end{bmatrix} = \begin{bmatrix} P_{ww} & P_{wa} \\ P_{aw} & P_{aa} \end{bmatrix} \begin{bmatrix} \mathbf{0}_{wa} \\ I_{aa} \end{bmatrix} \quad (\text{A.23})$$

giving

$$\begin{bmatrix} \bar{\Psi}_{wa} \\ \bar{\Psi}_{aa} \end{bmatrix} = \begin{bmatrix} g_{ww} & g_{wa} \\ g_{aw} & g_{aa} \end{bmatrix} \begin{bmatrix} P_{ww} & P_{wa} \\ P_{aw} & P_{aa} \end{bmatrix} \begin{bmatrix} \mathbf{0}_{wa} \\ I_{aa} \end{bmatrix} \quad (\text{A.24})$$

or

$$\bar{\Psi}_a \equiv \begin{bmatrix} \bar{\Psi}_{wa} \\ \bar{\Psi}_{aa} \\ \mathbf{0}_{ra} \end{bmatrix} = \begin{bmatrix} \mathbf{g}_{ww} & \mathbf{g}_{wa} & \mathbf{0}_{wr} \\ \mathbf{g}_{aw} & \mathbf{g}_{aa} & \mathbf{0}_{ar} \\ \mathbf{0}_{rw} & \mathbf{0}_{ra} & \mathbf{0}_{rr} \end{bmatrix} \begin{bmatrix} \mathbf{P}_{ww} & \mathbf{P}_{wa} & \mathbf{P}_{wr} \\ \mathbf{P}_{aw} & \mathbf{P}_{aa} & \mathbf{P}_{ar} \\ \mathbf{P}_{rw} & \mathbf{P}_{ra} & \mathbf{P}_{rr} \end{bmatrix} \begin{bmatrix} \mathbf{0}_{wa} \\ \mathbf{I}_{aa} \\ \mathbf{0}_{ra} \end{bmatrix} = \mathbf{GPF} \quad (\text{A.25})$$

\mathbf{G} is called the *flexibility matrix*.

The attachment mode matrix defined in equation (A.25) still has rigid-body contributions. To get a complete set of component inertial relief attachment modes $\hat{\Psi}_a$ that are orthogonal to the rigid-body modes with respect to the mass matrix, the equation

$$\Psi_r^T \mathbf{m} \hat{\Psi}_a = \mathbf{0} \quad (\text{A.26})$$

must be satisfied. This is easily done by choosing a \mathbf{C}_r defined by

$$\hat{\Psi}_a = \bar{\Psi}_a + \Psi_r \mathbf{C}_r \quad (\text{A.27})$$

such that equation (A.26) is satisfied. Premultiplying equation (A.27) by $\Psi_r^T \mathbf{m}$ gives

$$\Psi_r^T \mathbf{m} \hat{\Psi}_a = \Psi_r^T \mathbf{m} \bar{\Psi}_a + \Psi_r^T \mathbf{m} \Psi_r \mathbf{C}_r = \Psi_r^T \mathbf{m} \bar{\Psi}_a + \mathbf{C}_r \quad (\text{A.28})$$

Setting this equal to zero gives \mathbf{C}_r as

$$\mathbf{C}_r = -\Psi_r^T \mathbf{m} \bar{\Psi}_a \quad (\text{A.29})$$

Therefore, by equation (A.27),

$$\hat{\Psi}_a = \bar{\Psi}_a - \Psi_r \Psi_r^T \mathbf{m} \bar{\Psi}_a = (\mathbf{I} - \Psi_r \Psi_r^T \mathbf{m}) \bar{\Psi}_a = \mathbf{P}^T \bar{\Psi}_a \quad (\text{A.30})$$

The derivation of the inertia relief attachment modes is completed by substituting equation (A.25) into equation (A.30) giving

$$\hat{\Psi}_a = (\mathbf{P}^T \mathbf{G} \mathbf{P}) \mathbf{F} \quad (\text{A.31})$$

A.6 Residual Attachment Modes for Both Constrained and Unconstrained Components

Up to now, very little has been said about linear independence of attachment modes with respect to free-interface normal modes. As shown earlier in Figure A.4, attachment modes and normal modes can look very much alike. This section considers this aspect of choosing attachment modes. The following development is similar to that given by Craig.^{3,21} Also, throughout this section it will be assumed that the component is unconstrained unless stated otherwise; to go from equations for unconstrained components to equations for constrained components is trivial.

Consider once again equation (A.17). Premultiplying this by Φ_e^T gives

$$\ddot{\mathbf{p}}_e + \Lambda_{ee} \mathbf{p}_e = \Phi_e^T \mathbf{f} \quad (\text{A.32})$$

where Λ_{ee} is a diagonal matrix of non-zero eigenvalues. If the inertia term of these elastic modes is neglected,

$$\mathbf{p}_e = \Lambda_{ee}^{-1} \Phi_e^T \mathbf{f} \quad (\text{A.33})$$

This equation is then transformed into physical coordinates by premultiplying it by Φ_e :

$$\mathbf{u}_e = \Phi_e \mathbf{p}_e = \Phi_e \Lambda_{ee}^{-1} \Phi_e^T \mathbf{f} = \mathbf{G}_e \mathbf{f} \quad (\text{A.34})$$

where

$$\mathbf{G}_e = \Phi_e \Lambda_{ee}^{-1} \Phi_e^T \quad (\text{A.35})$$

\mathbf{G}_e is called the *elastic flexibility matrix*.

If \mathbf{f} is chosen to apply a unit load on one coordinate in the A set while all other elements are zero, the equation (A.34) actually defines one attachment mode that is

linearly independent of the rigid-body modes. This could be expanded to define a complete set of attachment modes that are orthogonal to the rigid-body modes:

$$U_e = G_e F, \quad F = \begin{bmatrix} \mathbf{0} \\ wa \\ I_{aa} \\ \mathbf{0} \\ ra \end{bmatrix} \quad (\text{A.36})$$

By the way equation (A.31) was derived, G_e can also be expressed as

$$G_e = P^T G P \quad (\text{A.37})$$

Equations (A.35) and (A.37) provide a straightforward way of making the attachment modes linearly independent of *kept* elastic normal modes. Since Λ_{ee}^{-1} is diagonal, G_e can be expanded in terms of kept and deleted elastic normal modes:

$$G_e = \Phi_k \Lambda_{kk}^{-1} \Phi_k^T + \Phi_d \Lambda_{dd}^{-1} \Phi_d^T \quad (\text{A.38})$$

The *residual flexibility matrix* G_d is defined as the flexibility of deleted elastic normal modes, or

$$G_d = \Phi_d \Lambda_{dd}^{-1} \Phi_d^T = G_e - \Phi_k \Lambda_{kk}^{-1} \Phi_k^T = P^T G P - \Phi_k \Lambda_{kk}^{-1} \Phi_k^T \quad (\text{A.39})$$

Conceptually, the first term on the right side, $P^T G P$, contains information on the flexibility of all modes while the second term, $\Phi_k \Lambda_{kk}^{-1} \Phi_k^T$, removes only the information of the kept normal modes. Note that to get G_d the deleted component normal modes need not be used.

The set of residual attachment modes that are linearly independent of rigid-body modes and kept elastic normal modes are given by

$$\Psi_a = G_d F \quad (\text{A.40})$$

For unconstrained components, equation (A.40) defines the set of *residual inertia relief*

attachment modes.

For constrained components, equation (A.40) defines the set of *residual attachment modes* and the following simplifications apply:

$$\begin{aligned} P &= I \\ G &= \begin{bmatrix} g_{ww} & g_{wa} \\ g_{aw} & g_{aa} \end{bmatrix} \\ F &= \begin{bmatrix} \mathbf{0}_{wa} \\ I_{aa} \end{bmatrix} \end{aligned} \tag{A.41}$$

and therefore G_d is simplified to

$$G_d = G - \Phi_k \Lambda_{kk}^{-1} \Phi_k^T \tag{A.42}$$

B. DERIVATION OF CONSTRAINT EQUATION (4.12)

Following is a derivation of an approximate constraint equation that is used by the Craig-Chang method. The derivation begins with the equation of motion for a component in physical coordinates:

$$m^p \ddot{u}^p + k^p u^p = f^p \quad (\text{B.1})$$

Writing equation (4.8) in the simpler form

$$u^p = [\Phi_k \ \Psi_r \ \Psi_d]^p \begin{Bmatrix} P_k \\ P_r \\ P_d \end{Bmatrix} \quad (\text{B.2})$$

and substituting it into equation (B.1) gives

$$m^p [\Phi_k \ddot{P}_k + \Psi_r \ddot{P}_r + \Psi_d \ddot{P}_d]^p + k^p [\Phi_k P_k + \Psi_r P_r + \Psi_d P_d]^p = f^p \quad (\text{B.3})$$

Premultiplying equation (B.3) separately by component p 's Φ_k^T , Ψ_r^T , and Ψ_d^T gives the three uncoupled equations of motion:

$$\left. \begin{aligned} \ddot{P}_k + \Lambda_{kk} P_k &= \Phi_k^T f \\ \ddot{P}_r &= \Psi_r^T f \\ \Psi_d^T m \Psi_d \ddot{P}_d + \Psi_d^T k \Psi_d P_d &= \Psi_d^T f \end{aligned} \right|_p \quad (\text{B.4})$$

Here an approximation is made: the inertia term in the third equation in (B.4) is neglected to yield

$$[\Psi_d^T k \Psi_d P_d = \Psi_d^T f]^p \quad (\text{B.5})$$

By definition, G_d is

$$G_d^p = [\Phi_d \Lambda_{dd}^{-1} \Phi_d^T]^p \quad (\text{B.6})$$

and since F only applies a unit force at one joint coordinate for each attachment mode, equation (4.9) can be written in the form

$$\Psi_d^p = [\Phi_d \Lambda_{dd}^{-1} \Phi_{jd}^T]^p \quad (\text{B.7})$$

This is easily seen by expanding Φ_d^T as were the modes in equation (4.8) and post multiplying it by F as given in equation (4.10). Substituting the equation (B.7) into equation (B.5) gives, since the forces are exerted only at the joints,

$$\left. \begin{aligned} \Psi_d^T k \Psi_d P_d &= \Psi_d^T f \\ \Phi_{jd} \Lambda_{dd}^{-1} \Phi_d^T k \Phi_d \Lambda_{dd}^{-1} \Phi_{jd}^T P_d &= \Phi_{jd} \Lambda_{dd}^{-1} \Phi_d^T f \\ \Phi_{jd} \Lambda_{dd}^{-1} \Phi_{jd}^T P_d &= \Phi_{jd} \Lambda_{dd}^{-1} \Phi_{jd}^T f_j \end{aligned} \right|_p \quad (\text{B.8})$$

and therefore

$$[\Phi_{jd} \Lambda_{dd}^{-1} \Phi_{jd}^T (P_d - f_j)]^p = 0 \quad (\text{B.9})$$

or

$$P_d^p = f_j^p \quad (\text{B.10})$$

Because of force compatibility at the joints (equation (3.3)), equation (B.10) is rewritten as, for a two component system,

$$P_d^a + P_d^b = 0 \quad (\text{B.11})$$

C. HMB-2R FLEXIBLE MODE SHAPES UP TO 50 HZ

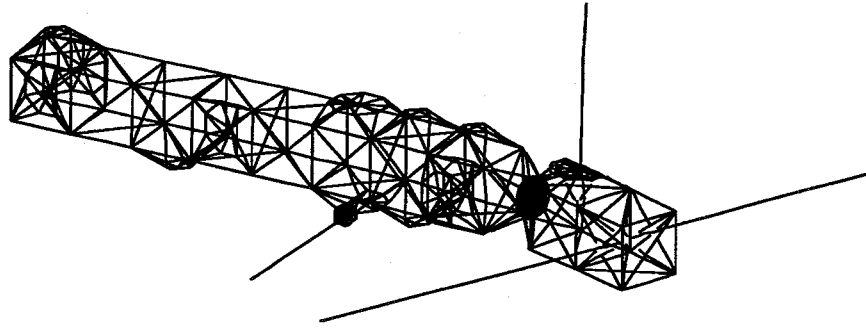


Figure C.1: HMB-2R mode shape one, 4.66 Hz.

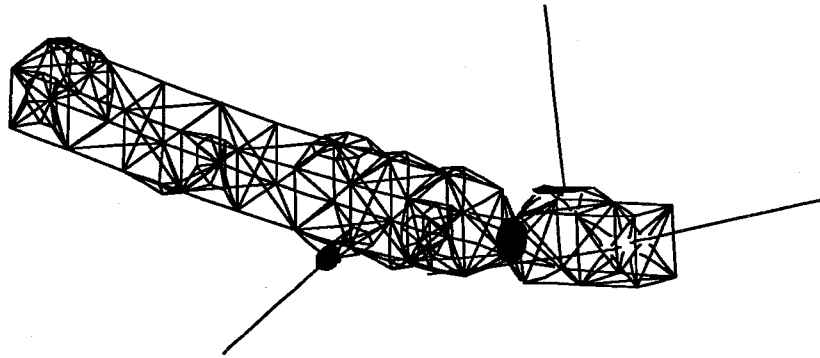


Figure C.2: HMB-2R mode shape two, 5.97 Hz.

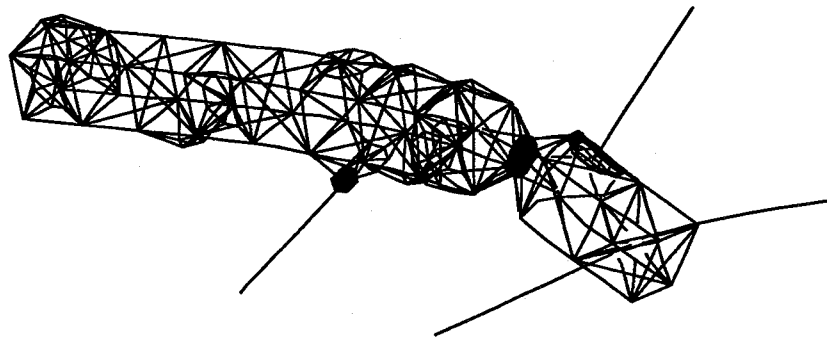


Figure C.3: HMB-2R mode shape three, 7.54 Hz.

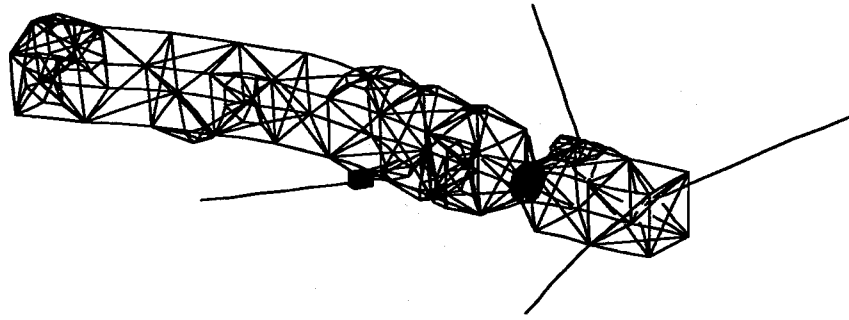


Figure C.4: HMB-2R mode shape four, 10.8 Hz.

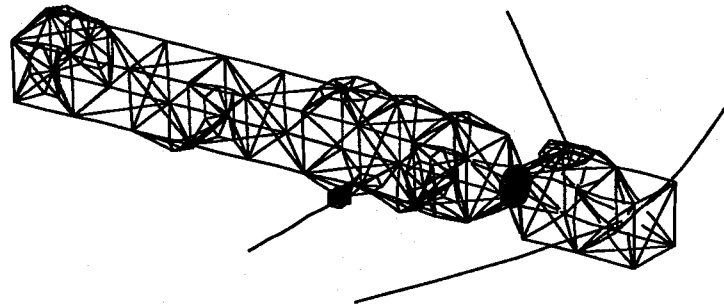


Figure C.5: HMB-2R mode shape five, 11.9 Hz.

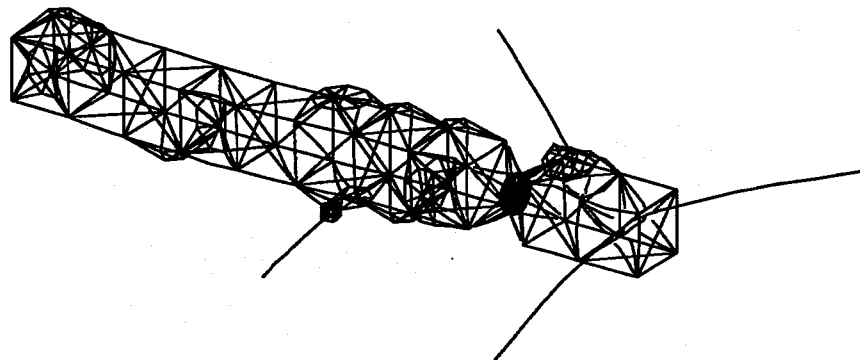


Figure C.6: HMB-2R mode shape six, 12.5 Hz.

©

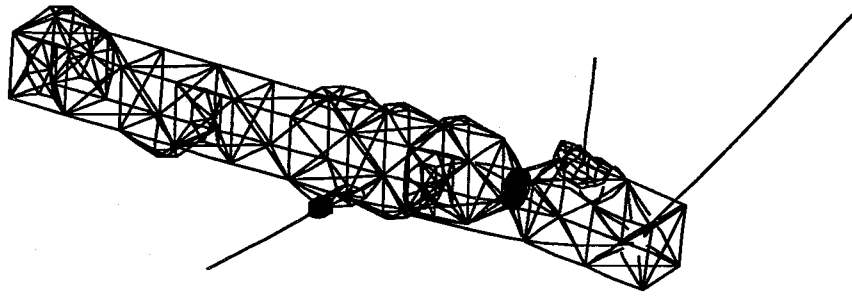


Figure C.7: HMB-2R mode shape seven, 13.2 Hz.

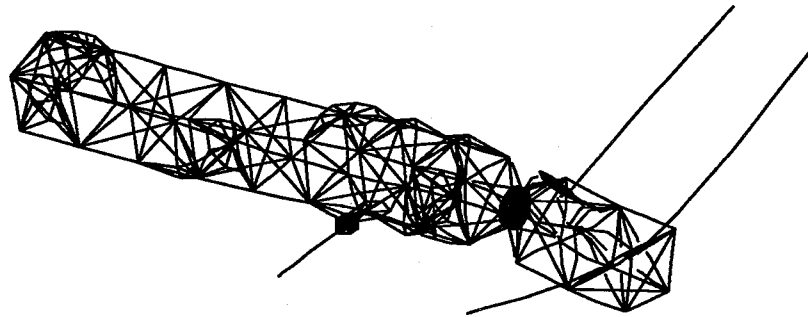


Figure C.8: HMB-2R mode shape eight, 13.8 Hz.

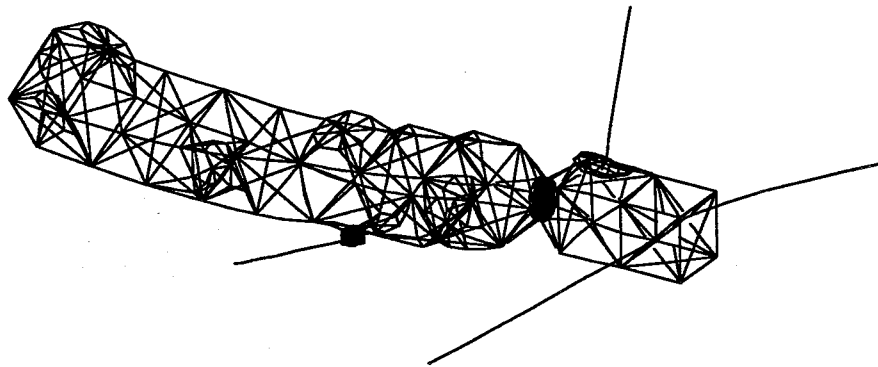


Figure C.9: HMB-2R mode shape nine, 14.3 Hz.

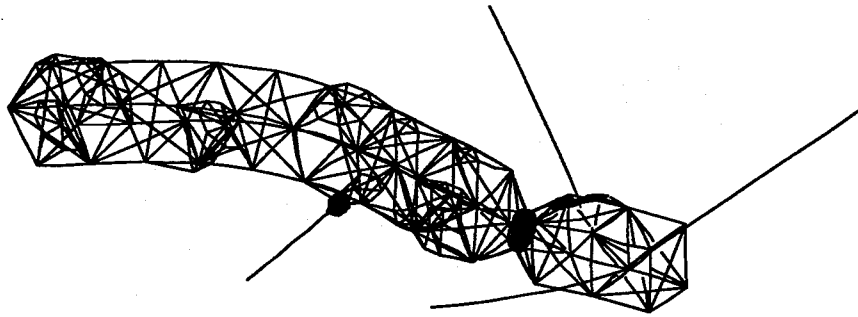


Figure C.10: HMB-2R mode shape ten, 15.5 Hz.

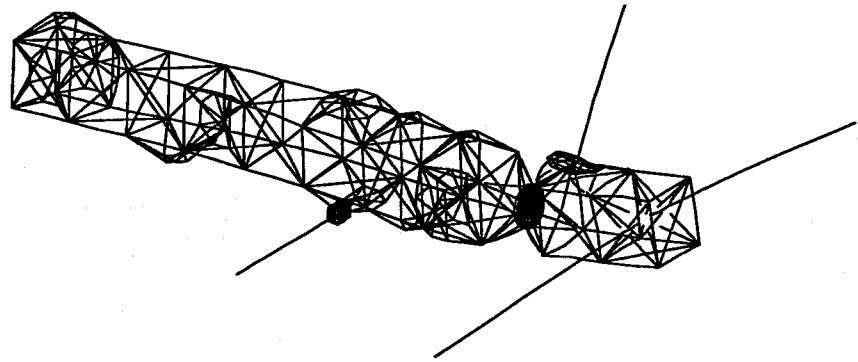


Figure C.11: HMB-2R mode shape eleven, 21.3 Hz.

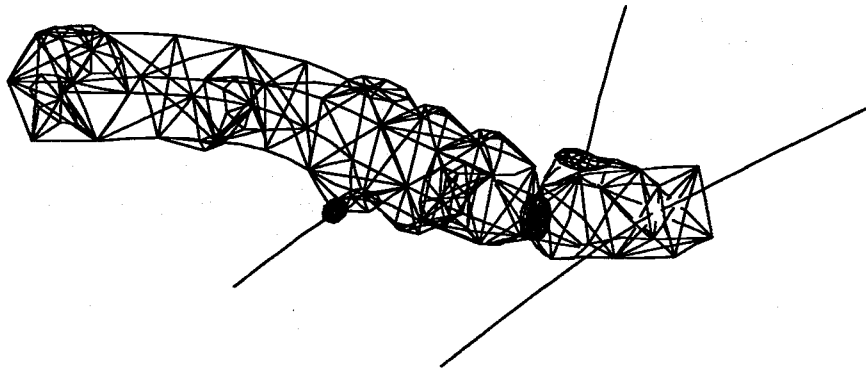


Figure C.12: HMB-2R mode shape twelve, 24.7 Hz.

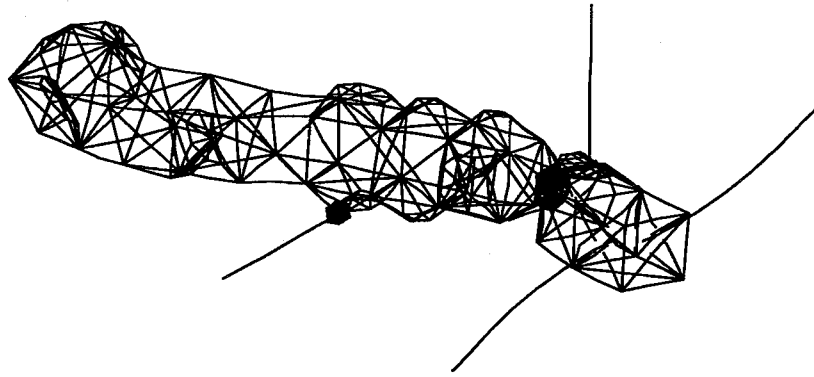


Figure C.13: HMB-2R mode shape thirteen, 27.0 Hz.

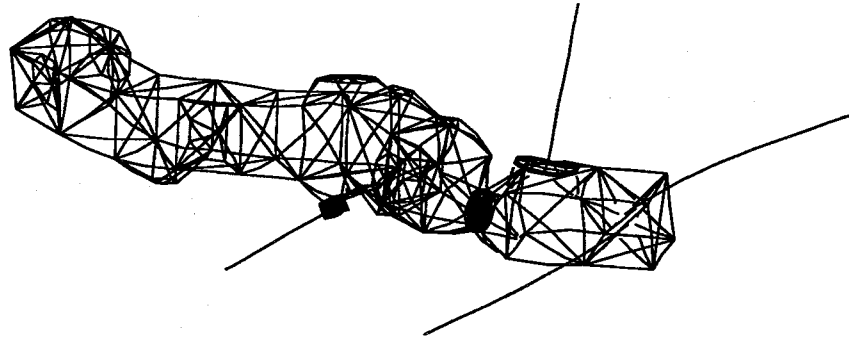


Figure C.14: HMB-2R mode shape fourteen, 33.7 Hz.

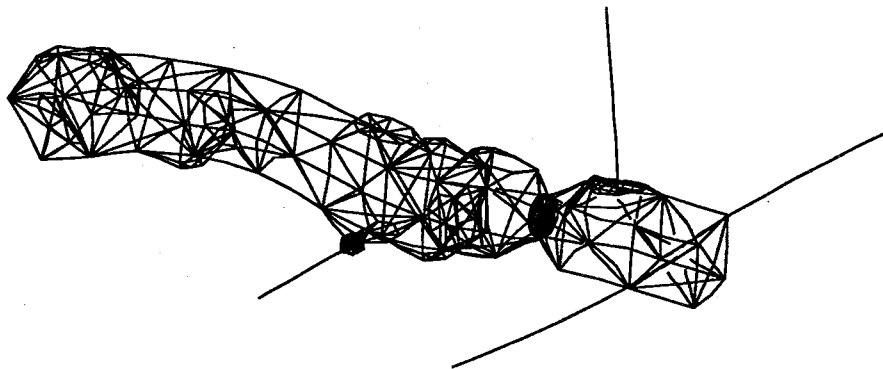


Figure C.15: HMB-2R mode shape fifteen, 38.2 Hz.

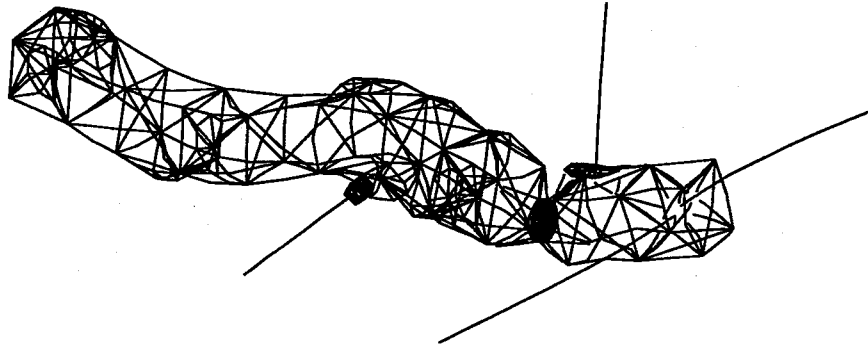


Figure C.16: HMB-2R mode shape sixteen, 40.2 Hz.

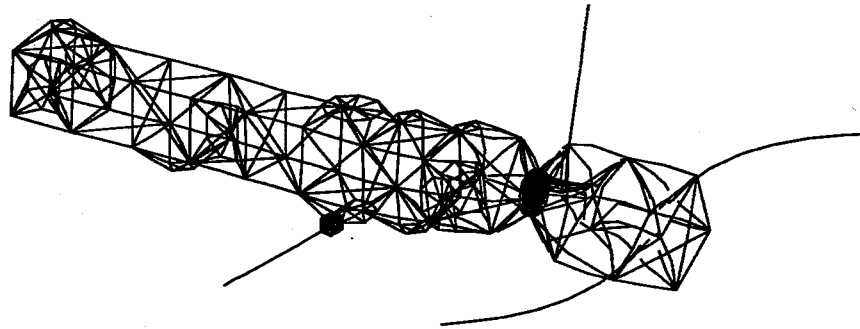


Figure C.17: HMB-2R mode shape seventeen, 43.1 Hz.

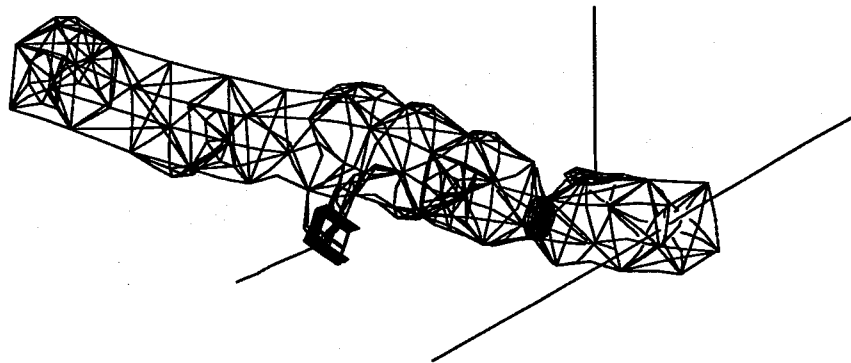


Figure C.18: HMB-2R mode shape eighteen, 49.7 Hz.

D. THE FINITE ELEMENT METHOD

Following is a very cursory look at the finite element approach of using this simple element to form the system mass and stiffness matrices. For more information, see Shames and Dym²⁴ or Przemieniecki²⁵.

The element used in the beam model is shown in Figure D.1. It has two translational degrees of freedom (in the x and y directions) and one rotational degree of freedom (about the z -axis).

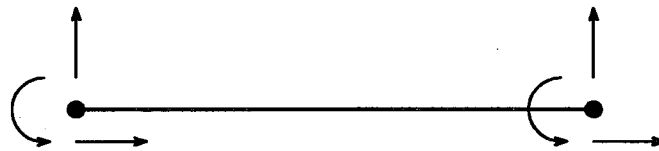


Figure D.1: The degrees of freedom for this finite element.

To form the system mass and stiffness matrices, the finite element approach first forms the mass and stiffness matrix for each element. These matrices are in “local” coordinates; that is, the origin is at the first node and the x -axis is along the element. In local coordinates, the mass and stiffness matrices for one element are given by equations (D.1) and (D.2). The order of the displacement coordinates for these matrices is: x , y , and $rot-z$ for node one and x , y , $rot-z$ for node two.

$$\mathbf{M}_l = \rho A L \begin{bmatrix} \frac{1}{3} & 0 & 0 & \frac{1}{6} & 0 & 0 \\ 0 & \frac{13}{35} & \frac{11L}{210} & 0 & \frac{9}{70} & -\frac{13L}{420} \\ 0 & \frac{11L}{210} & \frac{L^2}{105} & 0 & \frac{13L}{420} & -\frac{L^2}{140} \\ \frac{1}{6} & 0 & 0 & \frac{1}{3} & 0 & 0 \\ 0 & \frac{9}{70} & \frac{13L}{420} & 0 & \frac{13}{35} & -\frac{11L}{210} \\ 0 & -\frac{13L}{420} & -\frac{L^2}{140} & 0 & -\frac{11L}{210} & \frac{L^2}{105} \end{bmatrix} \quad (\text{D.1})$$

$$\mathbf{K}_l = \begin{bmatrix} \frac{AE}{L} & 0 & 0 & -\frac{AE}{L} & 0 & 0 \\ 0 & \frac{12EI}{L^3} & \frac{6EI}{L^2} & 0 & -\frac{12EI}{L^3} & \frac{6EI}{L^2} \\ 0 & \frac{6EI}{L^2} & \frac{4EI}{L} & 0 & -\frac{6EI}{L^2} & \frac{2EI}{L} \\ -\frac{AE}{L} & 0 & 0 & \frac{AE}{L} & 0 & 0 \\ 0 & -\frac{12EI}{L^3} & -\frac{6EI}{L^2} & 0 & \frac{12EI}{L^3} & -\frac{6EI}{L^2} \\ 0 & \frac{6EI}{L^2} & \frac{2EI}{L} & 0 & -\frac{6EI}{L^2} & \frac{4EI}{L} \end{bmatrix} \quad (\text{D.2})$$

where the element properties, ρ , A , L , E , and I , are respectively the material density, cross-sectional area, length, elastic modulus, and cross-sectional area moment of inertia.

The subscript l denotes *local*. Once these matrices are formed for an element they are then rotated to global coordinates via the transformation matrix

$$T = \begin{bmatrix} \cos(\theta) & \sin(\theta) & 0 & 0 & 0 & 0 \\ -\sin(\theta) & \cos(\theta) & 0 & 0 & 0 & 0 \\ 0 & 0 & 1 & 0 & 0 & 0 \\ 0 & 0 & 0 & \cos(\theta) & \sin(\theta) & 0 \\ 0 & 0 & 0 & -\sin(\theta) & \cos(\theta) & 0 \\ 0 & 0 & 0 & 0 & 0 & 1 \end{bmatrix} \quad (\text{D.3})$$

where θ is the angle between the local x-axis and the global x-axis. M_l and K_l are transformed to global coordinates by

$$M_g = T^T M_l T, \quad K_g = T^T K_l T \quad (\text{D.4})$$

These element matrices are then put into their respective positions in the system mass and stiffness matrices. Once the system matrices have been assembled, various types structural analysis can be performed.

E. BEAM MODEL FLEXIBLE MODE SHAPES UP TO 100 HZ

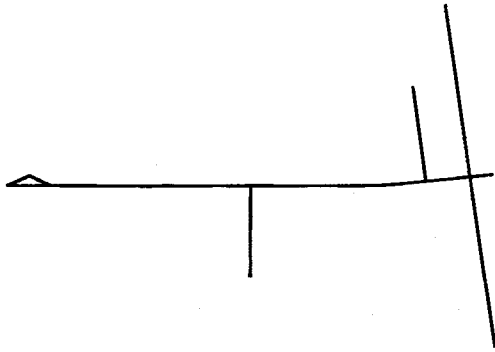


Figure E.1: Beam model mode shape one, 4.66 Hz.

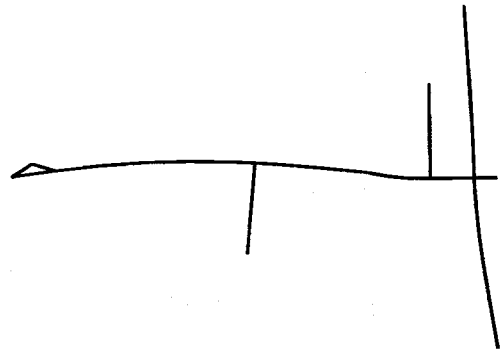


Figure E.2: Beam model mode shape two, 24.1 Hz.

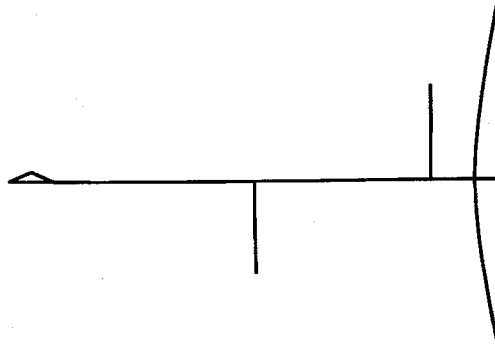


Figure E.3: Beam model mode shape three, 26.9 Hz.

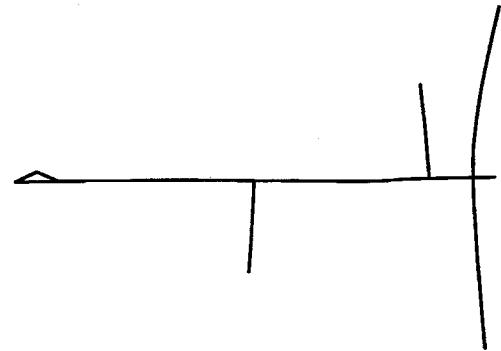


Figure E.4: Beam model mode shape four, 34.5 Hz.

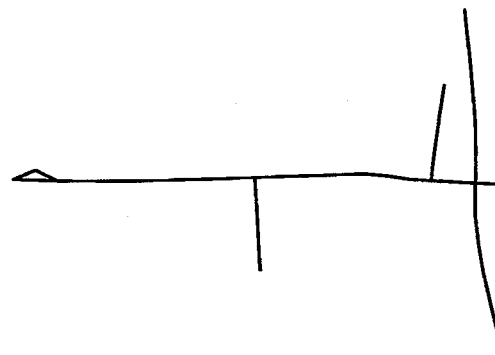


Figure E.5: Beam model mode shape five, 38.9 Hz.

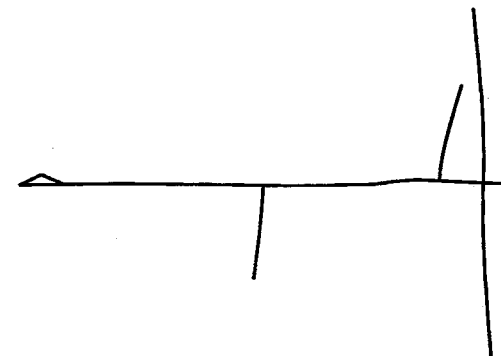


Figure E.6: Beam model mode shape six, 50.6 Hz.

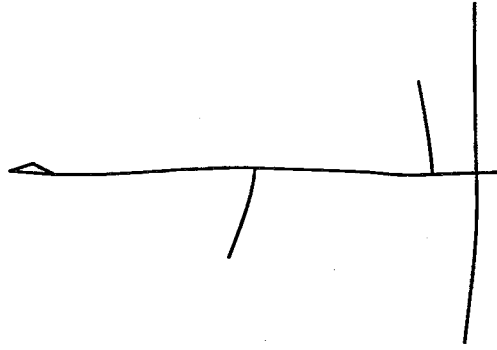


Figure E.7: Beam model mode shape seven, 58.6 Hz.

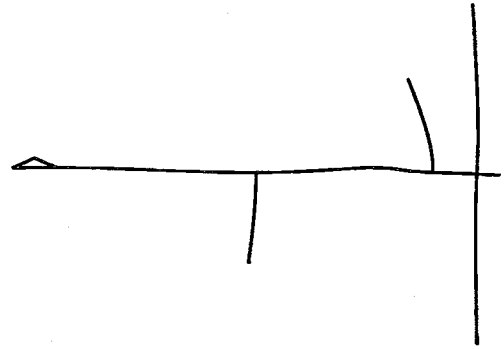


Figure E.8: Beam model mode shape eight, 70.5 Hz.

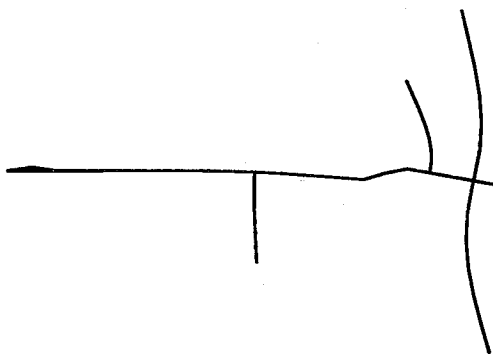


Figure E.9: Beam model mode shape nine, 93.8 Hz.

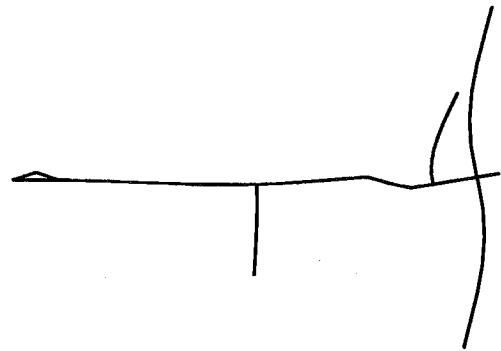


Figure E.10: Beam model mode shape ten, 95.5 Hz.

F. THE ANALYTICAL MODEL IMPROVEMENT METHOD¹⁸

The AMI Method is used for updating the mass and stiffness matrices of a structure so that they agree with test results.

After collecting frequency and mode shape data, the first step in the AMI method is to calculate the missing coordinates of the mode shapes. This is done by using the *existing* mass and stiffness matrix along with the measured frequencies and measured coordinates of the mode shapes. First, the eigenvalue problem for mode i is partitioned in the form

$$\left(\begin{bmatrix} \mathbf{K}_1 & \mathbf{K}_2 \\ \mathbf{K}_3 & \mathbf{K}_4 \end{bmatrix} - \omega_i^2 \begin{bmatrix} \mathbf{M}_1 & \mathbf{M}_2 \\ \mathbf{M}_3 & \mathbf{M}_4 \end{bmatrix} \right) \begin{Bmatrix} \phi_{mi} \\ \phi_{ci} \end{Bmatrix} = \mathbf{0} \quad (\text{F.1})$$

where m denotes the *measured* portion of the mode and c denotes the portion to be *calculated*. From equation (F.1), the formula for calculating the missing coordinates is

$$\phi_{ci} = -[\mathbf{K}_4 - \omega_i^2 \mathbf{M}_4]^{-1} [\mathbf{K}_3 - \omega_i^2 \mathbf{M}_3] \phi_{mi} \quad (\text{F.2})$$

Note that although the mode shapes must be full length for the rest of this procedure, the number of modes does not matter.

The next step is to update the mass matrix. The idea is to add the smallest changes to each element in the mass matrix that orthogonalize the modes. The approach used here is to minimize

$$\varepsilon = \left\| \mathbf{M}^{-\frac{1}{2}} (\mathbf{M}_{new} - \mathbf{M}) \mathbf{M}^{-\frac{1}{2}} \right\| \quad (\text{F.3})$$

subject to

$$\Phi^T \mathbf{M}_{new} \Phi = \mathbf{I} \quad (\text{F.4})$$

The result is

$$M_{new} = M + M\Phi m^{-1}(I - m)m^{-1}\Phi^T M \quad (\text{F.5})$$

where

$$m = \Phi^T M \Phi \quad (\text{F.6})$$

The final step is update the stiffness matrix by using a similar approach. It is desired to find the smallest changes of the elements in the stiffness matrix that satisfy orthogonality, the eigenvalue equation, and symmetry. This problem is solved by minimizing

$$\varepsilon = \left\| M_{new}^{-\frac{1}{2}} (K_{new} - K) M_{new}^{-\frac{1}{2}} \right\| \quad (\text{F.7})$$

subject to

$$\begin{aligned} \Phi^T K_{new} \Phi &= \Lambda \\ K_{new} \Phi &= M_{new} \Phi \Lambda \\ K_{new} &= K_{new}^T \end{aligned} \quad (\text{F.8})$$

The result is

$$K_{new} = K + \Delta + \Delta^T \quad (\text{F.9})$$

where

$$\Delta = \frac{1}{2} M_{new} \Phi (\Phi^T K \Phi + \Lambda) \Phi^T M_{new} - K \Phi \Phi^T M_{new} \quad (\text{F.10})$$





